Inhibitors of p53 and HIF-prolyl-4-hydroxylases provide mitochondrial protection in a model of oxytosis

Dissertation

zur

Erlangung des Doktorgrades

der Naturwissenschaften

(Dr. rer. nat.)

dem

Fachbereich Pharmazie (16)

der Philipps-Universität Marburg

vorgelegt von

Sandra Neitemeier

aus Beckum

Marburg/Lahn 2015

Erstgutachter: Prof. Dr. Carsten Culmsee

Zweitgutachter: Prof. Dr. Jens Kockskämper

Eingereicht am 13.05.2015

Tag der mündlichen Prüfung am 24.06.2015

Hochschulkennziffer: 1180

Meinen Eltern und meiner Schwester

ERKLÄRUNG

Ich versichere, dass ich meine Dissertation

„Inhibitors of p53 and HIF-prolyl-4-hydroxylases provide mitochondrial protection in a model of oxytosis“

selbständig ohne unerlaubte Hilfe angefertigt und mich dabei keiner anderen als der von mir ausdrücklich bezeichneten Quellen bedient habe. Alle vollständig oder sinngemäß übernommenen Zitate sind als solche gekennzeichnet.

Die Dissertation wurde in der jetzigen oder einer ähnlichen Form noch bei keiner anderen Hochschule eingereicht und hat noch keinen sonstigen Prüfungszwecken gedient.

Marburg, den 29.04.2015

.....

Sandra Neitemeier

Table of contents

1 Introduction 1

1.1 Regulated cell death in neurons 1

1.1.1 Oxytosis 6

1.1.2 Ferroptosis 8

1.1.3 p53 dependent cell death 9

1.2 Role of mitochondria in neuronal cell death 12

1.3 HIF-prolyl-4-hydroxylases 15

1.3.1 HIF-prolyl-4-hydroxylase 1 17

1.3.2 HIF-prolyl-4-hydroxylase 2 17

1.3.3 HIF-prolyl-4-hydroxylase 3 18

1.4 The HT-22 model system 19

1.5 Aims of the study 21

2 Materials and methods 23

2.1 Chemicals and reagents 23

2.1.1 Inducers of cell death 23

2.1.2 Inhibitors of cell death 23

2.1.3 Kits 25

2.1.4 Transfection reagents 26

2.1.5 Plasmid vectors 26

2.1.6 SiRNAs 26

2.1.7 Primary antibodies 26

2.1.8 Secondary antibodies 28

2.1.9 Transformation and preparation of plasmids 28

2.2 Cell culture material 29

2.3 Cell culture 29

2.3.1 Cultivation of HT-22 cells 29

2.3.2 Transfection protocols 31
2.4 Cell viability assays 32
2.4.1 Morphological cell viability analysis 32
2.4.2 MTT-assay 33
2.4.3 xCELLigence system 33
2.5 ATP assay 34
2.6 Measurements of oxygen consumption rate 35
2.7 Flow cytometric measurements 35
2.7.1 FITC Annexin V/Propidium iodide staining 35
2.7.2 Detection of lipid peroxides 36
2.7.3 Assessment of intracellular, soluble ROS 37
2.7.4 Measurement of mitochondrial ROS formation 37
2.7.5 Evaluation of mitochondrial membrane potential 38
2.8 Determination of glutathione levels 38
2.9 Immunocytochemistry 40
2.9.1 Staining of mitochondria 40
2.9.2 Evaluation of mitochondrial morphology 40
2.9.3 Immunocytochemistry 41
2.10 Analysis of p53 transcriptional activity 42
2.10.1 Cloning of p53-firefly-luciferase-plasmid 42
2.10.2 Measurement of p53 transcriptional activity by luminescence 43
2.11 RNA analysis 44
2.11.1 RNA sample preparation 44
2.11.2 Determination of RNA amount 44
2.11.3 Reverse transcriptase polymerase chain reaction 45
2.11.4 Agarose gel electrophoresis 52
2.12 Protein analysis 53
2.12.1 Protein sample preparation 53

2.12.2 Determination of protein amount 54
2.12.3 Gel electrophoresis and Western blot analysis 55
2.13 Statistical analysis 58
3 Results 59
3.1 Glutamate sensitivity of HT-22 cells 59
3.1.1 Mitochondrial demise in oxytosis 60
3.2 Inhibition of p53 provides neuroprotection 61
3.2.1 PFTα prevents glutamate-induced cell death 61
3.2.2 Mitochondrial integrity is preserved by PFTα 63
3.2.3 PFTα reduces lipid peroxidation 65
3.2.4 p53 gene silencing delays glutamate-induced cell death 66
3.2.5 Deficiency of p53 fails to preserve mitochondrial integrity 68
3.2.6 Knockdown of p53 is not able to abolish lipid peroxidation 70
3.2.7 p53 translocation to mitochondria is not involved in oxytosis 71
3.2.8 Effect of p53 inhibition on p53 transcriptional activity 73
3.2.9 PFTα acts independently of p53 inhibition 74
3.3 Silencing PHD1 mediates neuroprotection 77
3.3.1 Knockdown of PHD1 attenuates glutamate toxicity 77
3.3.2 PHD1 silencing restores mitochondrial integrity 80
3.3.3 Deficiency of PHD1 reduces lipid peroxidation 82
3.4 Pharmacological inhibition of PHDs provides neuroprotection 84
3.4.1 Structural diverse PHD-inhibitors prevent glutamate-induced cell death 84
3.4.2 Inhibition of PHDs restores mitochondrial morphology and function 88
3.4.3 PHD-inhibitors preserve mitochondrial respiration and abolish mitochondrial ROS formation 91
3.4.4 Lipid peroxidation is prevented by inhibition of PHDs 93
3.4.5 Glutamate-induced glutathione depletion is not restored by oxyquinoline 94

3.4.6 Oxyquinoline exhibits antioxidative properties 95
3.4.7 The eIF2α/ATF4 pathway is regulated by oxyquinoline 97
3.4.8 Oxyquinoline protects against oxytosis independent of ATF4 100
3.5 Inhibition of PHDs prevents ferroptosis 102
3.5.1 Erastin sensitivity of HT-22 cells 102
3.5.2 Targeting PHDs inhibits erastin-induced cell death 103
4 Discussion 105
4.1 Impact of mitochondrial demise in oxytosis 106
4.2 The role of p53 in glutamate-induced oxytosis 110
4.2.1 PFTα mediates mitochondrial protection 113
4.2.2 p53 silencing does not prevent mitochondrial demise 117
4.2.3 Differential effects of p53 gene silencing and pharmacological p53 inhibition 119
4.3 The role of PHDs in oxytosis 121
4.3.1 Different concepts of PHD inhibition provide neuroprotection 122
4.3.2 PHD-inhibition mediates neuroprotection upstream of mitochondria 125
4.3.3 PHD inhibition and the eIF2α/ATF4 pathway 127
4.4 PHD inhibition protects against ferroptosis 130
5 Summary 133
6 Zusammenfassung 135
7 Abbreviations 138
8 References 145
9 Publications 167
9.1 Original papers 167
9.2 Books 167
9.3 Poster presentations 167
10 Danksagung 169
11 Curriculum vitae 171

1 Introduction

There are many ways to die for whole organisms, but also for single cells. Therefore, while writing about cell death one has to distinguish between accidental and regulated cell death (RCD) independent of the species, tissue or cell type. Accidental cell death (ACD) occurs after serious injuries such as chemical forces or high temperature and pressure. Mechanical insults are also able to induce ACD. The harshness of ACD renders it typically inaccessible for pharmacological or genetic approaches[1]. In contrast, RCD could be either the result of intra- or extracellular stimuli and subsequent dysfunctions or physiological processes. Hence, RCD appears mostly in a delayed, but controlled fashion and accordingly, can be targeted by pharmacological or genetic interventions[2]. In former times, the term programmed cell death (PCD) instead of RCD was used for those cell death paradigms occurring in a self-regulated manner via molecular pathways[3].

1.1 Regulated cell death in neurons

Progressive, but regulated dysfunction and death of neurons are considered as major causes for impaired brain function in several neurodegenerative disorders like Alzheimer's (AD) and Parkinson's disease (PD)[4,5] and are, thus, assigned to the topic RCD[6].

Besides its major role in neuropathology, RCD also affects physiological processes. For example, during brain development the highly regulated death of neurons accounts for creating typical brain architecture and maintaining neuronal homeostasis in the post-embryonic state[5,7]. It was recently recommended to use the term PCD as a subtype of RCD exclusively for these physiological cell death patterns[1].

Since millions of people worldwide suffer from neurodegenerative diseases, it is of great interest to improve our understanding of the underlying mechanisms of RCD in neurons as they imply huge therapeutic potential. Distinct morphological and biochemical features of non-physiological cell death subroutines have been identified over the last decades, classified as apoptosis, necrosis and autophagy[8].

The term 'apoptosis' was first introduced in 1972 by Kerr *et al.* and used for a specific way of cell deletion which appeared in an actively regulated manner and was characterised by typical morphological alterations such as nuclear and cytoplasmic condensation, DNA fragmentation and the concluding formation of apoptotic bodies.

In 1972, the authors had already recognised the importance of apoptotic cell death for embryonic development and the maintenance of cellular homeostasis[9]. Later, additional biochemical investigations revealed two different apoptotic cascades: the extrinsic and the intrinsic or mitochondrial pathway which may occur in a caspase-dependent or caspase-independent manner[10].

Extrinsic apoptosis is induced by the extracellular binding of lethal ligands like FAS/CD95 ligand (FASL), tumor necrosis factor α (TNFα) and TNF-related apoptosis inducing ligand (TRAIL) to their particular death receptors FAS/CD95, TNFα receptor 1 (TNFR1) and TRAIL receptor (TRAILR) 1-2 (reviewed in[10]) which are located at the plasma membrane and comprise a death domain (DD)[11]. Upon ligand binding, receptors undergo conformational changes allowing for the assembly of their DD with other death domain containing adaptor proteins such as Fas-associated death domain (FADD) or TNF receptor-associated death domain (TRADD)[12]. The TNFα/TNFR1/TRADD complex further recruits FADD and receptor-interacting protein (RIP)[13]. FADD dimerises with pro-caspase-8 or -10 via the death effector domain (DED)[14] to form the so-called death inducing signalling complex (DISC) and to initiate the apoptotic machinery via auto-catalytic activation of procaspases-8 and -10. Activated initiator caspases -8 and -10 enable effector procaspase-3 whose activated form has been shown to play a central role during ischemic brain damage[15,16] since it splits caspase-activated DNase (CAD) from its inhibitor (ICAD) thereby inducing the final, irreversible steps of apoptotic death. Subsequently, CAD cuts chromosomal DNA causing chromatin condensation, a hallmark of apoptosis[17]. Caspase-3 also induces the formation of apoptotic bodies by disruption of the cytoskeleton and cleaves poly (ADP-ribose) polymerase (PARP), thereby inhibiting its DNA-repairing function which in turn leads to further DNA damage[18]. Generation of truncated Bid (tBid) from BH3 interacting-domain death agonist (Bid) by caspase-8[19,20] directly links extrinsic to intrinsic apoptosis[21] described below (Fig. 1).

Intrinsic apoptosis is primarily characterised by mitochondrial dysfunction due to the permeabilisation of the mitochondrial membrane[1,8] and represents the predominating death pathway in neurons. Therefore, intrinsic pathways of apoptosis were associated with progressive neuronal death in various neurodegenerative diseases. It is initiated for example by neurotrophic factor withdrawal, overstimulation of glutamate-receptors, intracellular Ca^{2+}-overload, and enhanced oxidative stress[5,22]. These apoptotic stimuli trigger, amongst others, activation of the family of mitogen-

activated protein kinases (MAPKs) composed of extracellular signal-related kinases (ERKs), c-jun NH_2-terminal kinases (JNKs) and p38 MAPKs leading to transactivation of pro-apoptotic Bcl-2-associated x protein (Bax)[23] and Bcl-2 antagonist/ killer 1(Bak)[24] and altered gene expression promoting either cell survival or death[25]. Normally the pro-apoptotic function of Bax and Bak is redundant, but in neurons Bax plays the predominant role compared to Bak, since full-length Bak is absent in these cells[26,27]. Transactivation of Bax and Bak, which can also be induced by direct interaction with the transcription factor p53 and the BH-3 only proteins Bid and Bcl-2-like protein 11 (Bim), leads to mitochondrial outer membrane permeabilisation (MOMP) since Bax and Bak form a channel permeable for proteins of the mitochondrial intermembrane space (IMS), finally resulting in mitochondrial membrane permeabilisation. At the inner mitochondrial membrane (IMM), the permeability transition pore complex (PTPC) is responsible for mitochondrial membrane permeabilisation[28,29]. The precise composition of this pore is still unknown, but cyclophilin D (CypD), voltage-dependent anion channel (VDAC) and adenine nucleotide translocase (ANT) are regarded as their main constituents[25,28]. Many proteins and enzymes are associated with the regulation of the PTPC such as hexokinase[30] or mitochondrial creatine kinase[31] displaying possible therapeutic targets. Recent studies also suggested a pivotal role for mitochondrial adenosine triphosphate (ATP) synthase in formation and the opening of the PTPC[32–34]. Under physiological conditions, the PTPC exhibits low conductance and assures exchange of metabolites between the mitochondrial matrix and the cytosol. Upon lethal stimuli like oxidative stress or intracellular Ca^{2+}-overload, PTPC opens leading to mitochondrial membrane permeabilisation with an unregulated influx of water and cytosolic components into the mitochondrial matrix.

Mitochondrial membrane permeabilisation either induced by MOMP or by opening of the PTPC results in a breakdown of the mitochondrial membrane potential (MMP) and subsequent banned ATP synthesis, uncoupling of the respiratory chain and following significant increases in production of reactive oxygen species (ROS) and release of toxic IMS proteins such as cytochrome c (Cyt c), endonuclease G (Endo G), apoptosis-inducing factor (AIF), high temperature acquired protein A2 (Omi/HrtA2) or second mitochondria-derived activator of caspases (Smac/Diablo) into the cytosol. Cyt c and Smac/Diablo are in charge of caspase-dependent execution of

intrinsic apoptosis, whereas Endo G and AIF promote caspase-independent pathways[8,25,28].

Cytosolic Cyt c forms the so called ‘apoptosome’ together with apoptosis-protease activating factor 1 (Apaf1) and deoxy-ATP, thereby activating pro-caspase-9 which subsequently initiates the caspase cascade by proteolytic maturation of pro-caspase-3[35,36] leading to caspase-dependent activation of CAD, DNA fragmentation and cell death as described before. Under physiological conditions, the members of the inhibitor of apoptosis (IAP) family prevent exaggerated activation of the caspase machinery, but release of Smac/Diablo and Omi/HrtA2 blocks the anti-apoptotic effect of IAPs by sequestration thereby triggering caspase-dependent cell death[28,37].

Growing evidence proposes a crucial role for a caspase-independent intrinsic pathway in differentiated neurons under pathological conditions such as neonatal cerebral hypoxia-ischemia[38]. In this model harlequin mice exhibiting reduced AIF expression levels were significantly protected against neuronal damage compared to wild-type littermates[39]. Upon release into the cytosol, AIF and Endo G translocate to the nucleus, where they induce lethal DNA fragmentation and chromatin condensation. Additionally, Omi/HrtA2 which besides its caspase activation functions as a serine protease, cleaves cytoskeletal proteins, thus contributing to caspase-independent cellular demise[21,29,40]. In combination with the bioenergetic failure due to dissipation of MMP, uncoupling of the respiratory chain and frozen ATP synthesis these events drive the cell into death independent of caspase activation.

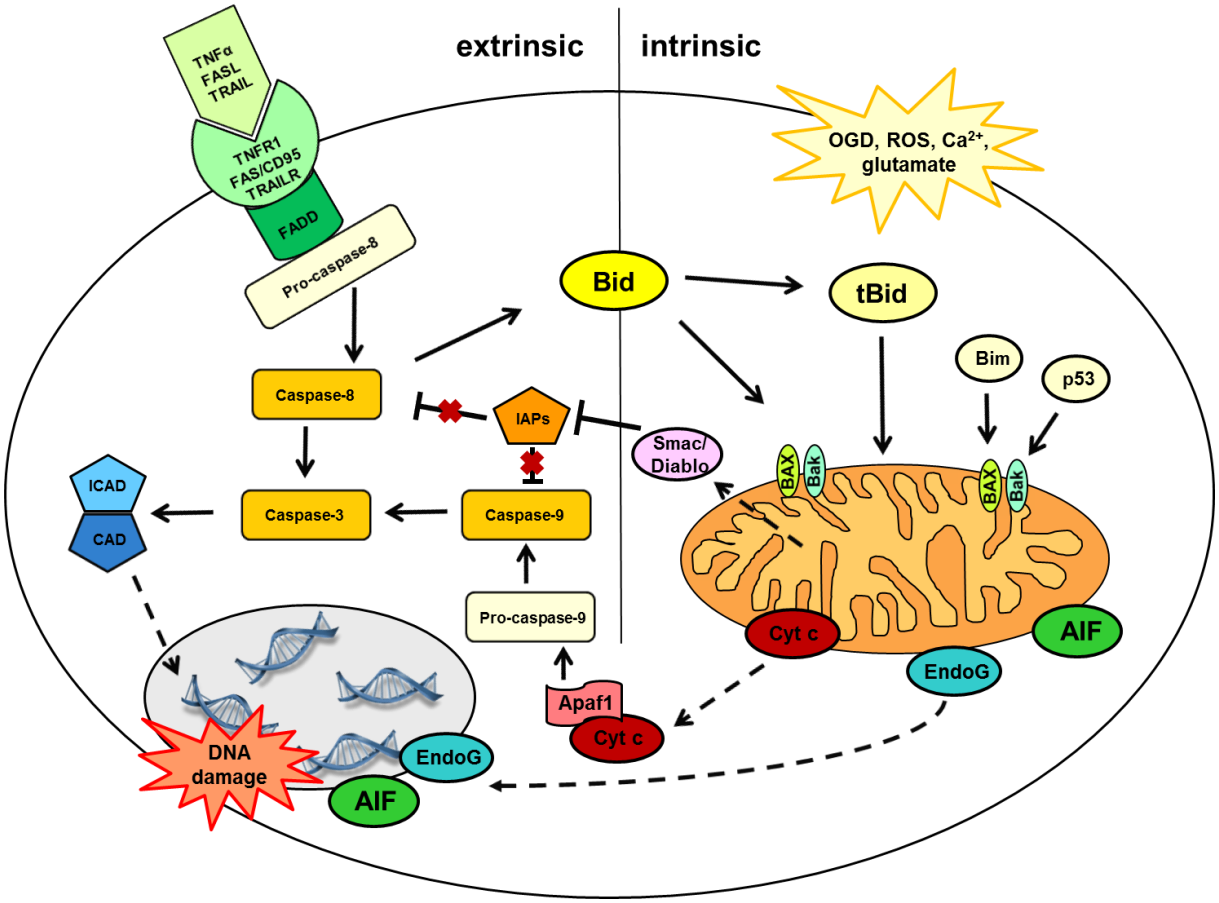

Figure 1: Schematic mechanism of extrinsic and intrinsic apoptotic pathways

Ligand binding to particular death receptors activates extrinsic apoptosis (left part) via the caspase cascade which in turn leads to the release of CAD from its inhibitor ICAD and subsequent DNA damage. The intrinsic, mitochondria dependent apoptotic pathway (right part) is initiated by ROS, OGD or Ca^{2+}-overload, thereby activating Bid, Bim or p53 which transactivate BAX and Bak leading to mitochondrial permeabilsation and release of Cyt c, Endo G and AIF. Cyt c together with Apaf1 forms the apoptosome further triggering caspase activation, whereas AIF and Endo G translocate to the nucleus and lead to DNA fragmentation (for details see 1.1).

1.1.1 Oxytosis

Oxytosis displays a prominent representative of caspase-independent cell death mechanisms in neurons induced by oxidative stress and high amount of ROS.

Neuronal cell death due to oxidative stress was first described in 1989 by Murphy and co-workers[41] and 12 years later, Tan *et al.* introduced the term 'oxytosis' for this specific caspase-independent intrinsic cell death paradigm whose key players are supposed to be Bid and AIF[42–44]. Blockage of cystine/glutamate antiporter system (X_c^-) composed of the specific xCT subunit and the 4F2 heavy chain[45] by glutamate, for example, initiates oxytosis by depleting cells of cystine which is required for the synthesis of glutathione (GSH)[46], the most important antioxidant in eukaryotic cells and especially in the brain[47]. Cystine uptake is the rate-limiting step of GSH synthesis in neurons since they are not able to produce cystine *de novo*[48]. The detrimental effect of GSH depletion can be reversed by replacing the missing antioxidant with trolox[49]. Loss of GSH is correlated with an increase in ROS due to enhanced lipid peroxidation by 12/15-lipoxygenases (LOX), since lack of GSH decreases glutathione peroxidase-4 (GpX4) activity, thereby suspending its inhibitory effect on 12/15-LOX[50]. Elevated levels of ROS induce translocation of several pro-apoptotic proteins such as Bid or dynamin-related protein 1 (DRP1) to the mitochondria[43,51] which subsequently produce a second burst of ROS up to 400-fold[46] of control levels and ultimately release Cyt c into the cytosol[44]. Despite Cyt c release, which can activate the caspase cascade via apoptosome formation[36], oxytosis is regarded to occur independently of caspases since caspase-inhibitors do not prevent induction of this oxidative form of cell death[43,44].

Besides lipid peroxides, 12-LOX also produces hydroxyeicosatetraenoic acids activating soluble guanylyl cylcase (sGC), thus increasing cGMP levels which in turn can stimulate Ca^{2+}-influx[52] leading to enhanced mitochondrial Ca^{2+}-levels further promoting ROS formation. Generation of mitochondrial ROS, however, conversely increases cytosolic Ca^{2+} as well, strongly suggesting mutual reinforcement of both processes promoting cell death. This conclusion is further confirmed by reduced ROS formation after inhibition of Ca^{2+} uptake and vice versa[46]. Elevated Ca^{2+}-levels are a hallmark of many cell death pathways in neurons and trigger neuronal demise e.g. via activation of caspases or calpains. In oxytosis, calpains were activated and shown to play a central role while caspases do not[53]. The kinetics of calpain activation correlate well with ROS formation and can mediate cleavage of Bid which

upon mitochondrial localisation accounts for the release of AIF from the mitochondria[54] and its subsequent translocation to the nucleus[43] where it can induce detrimental DNA fragmentation compassing cell death. However, DNA fragmentation was not consistently observed in oxytosis throughout the literature[44,53,55]. Additionally, nuclear AIF translocation can also be induced by PARP[56].

Furthermore, activation of the MAP kinase family composed of ERK, JNK and p38 by 12-LOX metabolites[57] is involved in neuronal demise due to oxytosis[44] indicated by the neuroprotective effects of their particular inhibitors and genetic approaches, respectively[44,57–60]. How MAP kinase activation interferes with ROS induced oxidative stress is not fully understood, but they are considered to be important signal transducers from the cell surface to the nucleus[61].

Regarding the aforementioned cell death cascade, it is comprehensible that targeting the main enzymes and proteins of this pathway like for example 12/15-LOX or Bid displays a powerful strategy to prevent oxidative stress induced cell death[49,51,62–64]. Moreover, overexpression of the anti-apoptotic protein Bcl-2[65], activation of small conductance calcium-activated potassium channels (SK2/K_{Ca}2.2)[66] and inhibition of macromolecular synthesis[55,67], the tumor suppressor protein p53[68] or serine proteases[55,69] have been shown to attenuate oxytosis. However, the underlying mechanisms of oxytosis are not entirely elucidated and require further investigations. The previous findings suggested that the oxidative machinery leading to cell death is highly complex and involves many more players than identified so far.

In summary, oxytosis is characterised by cell shrinkage[55], enhanced formation of ROS[46,70], severe mitochondrial damage[51,70–72] and ultimately, DNA fragmentation without chromatin condensation[44,55,67]. Furthermore, this cell death paradigm on the one hand is independent of caspase activation, but on the other hand is mediated via Bid and AIF[43,53]. Taking these hallmarks together, one cannot assign oxytosis to apoptosis or necrosis, which is characterised by cellular leakage, swelling of organelles and the condensation of chromatin into small patches[73], since oxytosis exhibits common features of both apoptosis and necrosis[42,44]. Therefore, oxytosis is regarded as a specialised form of regulated necrosis[73] and overall, falls under the category of RCD, a cell death mechanism involved in the pathology and progression of several neurodegenerative disorders like AD and PD[4,5].

1.1.2 Ferroptosis

More recently, another specialised form of regulated necrosis termed ferroptosis was identified[73]. This term was first introduced in 2012 by Dixon and colleagues and defined as an iron-dependent form of non-apoptotic cell death in RAS-transformed cancer cells “morphologically, biochemically, and genetically distinct from apoptosis, necrosis, and autophagy” and heavily depending on the formation of soluble and lipid ROS induced by the small molecule erastin or treatment with sulfasalazine[74]. This massive ROS production is supposed to originate from the Fenton reaction or other iron-dependent enzymatic reactions mediated by lipoxygenases, xanthin oxidases, NADPH oxidase or catalase[75] rather than from the mitochondrial electron transport chain (ETC), although erastin treatment alters mitochondrial appearance[74,76]. The crucial role of lipid peroxides in ferroptosis was further confirmed by the requirement of the fatty acid metabolism regulators acyl-CoA synthetase family member 2 (ACSF2) and citrate synthase (CS) for the induction of ferroptosis. Erastin inhibits the X_c^--transporter[74,77] and thereby, depletes cells of GSH which is necessary for the toxicity of erastin[78]. The missing link between erastin-induced GSH depletion and enhanced formation of lipid ROS is the regulation of GpX4, which is inhibited by reduced GSH levels and accordingly triggers lipid peroxidation[78]. Furthermore, erastin has been shown to act independently of caspase activation[79] and to directly interact with VDAC 2 and 3, thereby changing the permeability of the outer mitochondrial membrane (OMM) which induces alterations of the mitochondrial morphology and possible detrimental metabolic effects[76].

Iron dependency of ferroptosis was demonstrated by the use of the well-known iron chelators deferoxamine (DFO) and ciclopirox (CPO) which attenuated erastin-induced cell death[74,80]. Furthermore, simultaneous administration of iron and erastin potentiated its cytotoxicity[74], but this effect was also observed for oxidative glutamate toxicity[70].

The mechanisms underlying erastin toxicity in cancer cells are reminiscent of the aforementioned concept of oxytosis in neurons, although mitochondrial damage seems not to be involved in the ferroptosis of cancer cells. But the fact that the ferroptosis-inhibitor ferrostatin-1 reduces glutamate-induced neurotoxicity in organotypic hippocampal slice cultures[74] and protects HT-22 cells against glutamate exposure[70] also suggests a similarity between both pathways or at least a contribution of ferroptotic mechanisms to glutamate toxicity in paradigms of oxytosis.

Thus, it is not surprising that since the first description of ferroptosis in RAS-transformed cancer cells, this cell death paradigm was further observed in a neuronal context. Ferrostatin-1 prevented cell death in models of both Huntington's disease (HD) and periventricular leukomalacia (PVL)[81] and also attenuated erastin toxicity in neuronal HT-22 cells[70]. Moreover, features of ferroptotic cell death have been observed in kidney cells[82,83], overall suggesting an emerging role of ferroptosis in the paradigms of RCD.

1.1.3 p53 dependent cell death

The transcription factor p53 is regarded as the guardian of the genome, since the majority of organisms with loss of function or mutations of p53 are prone to cancer development[84,85]. But p53 does not only act as a tumor suppressor, it is also involved in the regulation of a large variety of other cellular processes, such as differentiation[86], longevity, aging[87], glycolysis[88,89], autophagy[90] and apoptotic responses via both the extrinsic and the intrinsic cell death pathway[91].

A variety of stimuli can induce p53 such as nutrient deprivation, hypoxia, DNA damage and oncogene activation leading not only to apoptosis, but also to cell-cycle arrest, DNA repair or senescence depending on the nature and extent of the insult[85]. Hence, p53 plays a pivotal, but dual role for cellular maintenance since it can on the one hand trigger cell-cycle arrest via the induction of p21 expression[92] and on the other hand apoptosis via enhanced expression of e.g. Bax and p53 upregulated modulator of apoptosis (PUMA)[4,93]. These effects are mostly mediated via the transcriptional regulation of gene expression, but also transcriptional independent mechanisms are described[91].

In neurons, a wide range of insults such as DNA damage and oxidative stress result in increased p53 levels indicating its involvement in various neurodegenerative diseases such as stroke[93], traumatic brain injury (TBI)[94], AD[4,95,96], PD[95] and HD[97]. Salutary effects by genetic deletion or inhibition of p53 in models of those disorders[94,98,99] further supported the pivotal function of p53 in neuronal death, but observations where $p53^{+/-}$ mice were protected against cerebral ischemia compared to $p53^{-/-}$ mice[100,101] indicated a divergent role of p53 and underline the importance of a precisely-controlled p53 action.

Oxidative DNA damage indicated by the accumulation of DNA double-strand breaks is a common result of all aforementioned insults by which they are able to activate

p53 via the induction of post-translational modifications e.g. phosphorylation[93,102]. These modifications are performed by several different kinases such as ataxia telangiectasia mutated (ATM) kinase[103] and its downstream effectors including checkpoint kinases (Chk) 1 and 2[104], cyclin-dependent kinases (CDK) 4 and 6[105] and MAP kinases JNK or p38[106] depending on the stimulus inducing DNA damage which in that way transduce the primary stress signal to p53-dependent cell death.

As described before, p53 mainly mediates cell death at the transcriptional level. Here, it is able to both induce and repress gene expression[107]. The most important transcriptional effect of p53 in neuronal cell death is the induction of Bax[108], a Bcl-2 family protein involved in the breakdown of the MMP and subsequent Cyt c release (for details see 1.1), thereby triggering mainly caspase-independent cell death. Other important pro-apoptotic targets of p53 are the BH3-only proteins Bid, PUMA and Noxa[4,85,93,109,110]. Via enhanced expression of Apaf1, p53 also influences formation of the apoptosome and subsequent caspase-dependent neuronal death[111]. Since p53 activation is a key point during neuronal demise, it is no wonder that transcriptional effects of p53 also play a role in death receptor-mediated neuronal cell death, where upregulation of Fas has been observed to occur in a p53-dependent manner[112]. Besides the induction of pro-death proteins and pathways, p53 can also mediate cell death via repression of pro-survival mechanisms such as the NF-κB-pathway[98] or the anti-apoptotic protein Bcl-2[113].

Transcription-independent induction of apoptosis by p53 was first demonstrated in cancer cells expressing a mutant p53 without transcriptional activity[114]. To date there is growing evidence that transcription-independent effects of p53 contribute to the induction of cell death[115,116], and also in neurons. Here, the localisation, whether it is cytosolic or mitochondrial, determines how p53 performs its apoptotic function[116]. Translocation of cytosolic p53 to the mitochondria upon stress, where it directly interacts with and thereby, activates the pro-apoptotic Bcl-2 family proteins Bax and Bak or liberates them from their inhibitory counterparts such as B-cell lymphoma-extra large (Bcl-xL) is a common way leading to MOMP, subsequent Cyt c release and caspase activation and finally apoptosis[116]. This mode of action of p53 reminiscent of a BH3-only protein was for instances observed in rat hippocampal neurons after transient global cerebral ischemia[117,118] and also in C6 glioma cells p53 translocates to the mitochondria upon oxidative stress followed by Cyt c release and caspase activation. Blocking p53 transcriptional activity was insufficient to prevent

cell death in this setting[119]. Moreover, pifithrin-μ (PFTμ) which inhibits translocation of p53 to mitochondria and its interaction with Bcl-xL[120] protected rats against hypoxic-ischemic brain damage[121] further supporting the hypothesis of transcription-independent mechanisms mediating cell death through activation of cytosolic p53 and independent of nuclear transactivation and transcriptional activities.

For mitochondrial p53, accumulation in the mitochondrial matrix after oxidative stress and subsequent complex formation with CypD have been shown to directly trigger the opening of the PTPC in mouse embryo fibroblast (MEF), thereby inducing necrosis in a transcription- and also Bax-/Bak-independent manner. Complex formation was also observed in mice after ischemia/reperfusion injury and abolished in $p53^{+/-}$ mice[101]. Findings of mitochondrial dysfunction and death in synaptosomes of wild-type mice in response to oxidative and excitotoxic stress and restored mitochondrial function and viability in p53-deficient mice[122] further underline the crucial role of transcriptional-independent mechanisms of p53 in mitochondrial damage and neuronal death.

1.2 Role of mitochondria in neuronal cell death

Thousands of mitochondria can be found in almost every aerobic eukaryotic cell not only assuring cellular energy demand, but also influencing development, signalling cascades and cell death[123].

Mitochondria with their own circular mitochondrial DNA (mtDNA), RNA and protein synthesis are regarded as semi-autonomous organelles. They are surrounded by two membranes: the inner and the outer mitochondrial membrane (OMM) enclosing the IMS. The IMM is highly folded forming so-called mitochondrial cristae. The mitochondrial matrix carries the mtDNA that encodes 37 mitochondrial genes including 13 protein subunits of the respiratory complexes I-V which build the mitochondrial ETC located in the cristae and allowing mitochondria to produce >90% of intracellular ATP. Therefore, mitochondria are known as the powerhouse of the cell[123–125].

ATP is the final product of aerobic respiration also known as oxidative phosphorylation. Reducing equivalents nicotinamide adenine nucleotide (NADH) and flavine adenine dinucleotide ($FADH_2$) derived from the tricarboxylic acid (TCA) cycle which is also located in the matrix provide electrons which run through the ETC, thereby enabling mitochondrial complexes I, III and IV to pump protons via the IMM into the IMS creating a proton gradient. Finally, electrons are transferred to O_2 generating H_2O and then, ATP synthase (complex V) utilises the resulting electrochemical gradient to generate ATP[125].

In order to adapt to consistently changing energy demands and metabolic processes mitochondria are highly-dynamic organelles undergoing continuously fission and fusion, a tightly controlled process. Recruitment of DRP1 and mitochondrial fission 1 protein (Fis1) to the outside of mitochondria initiates fission, while mitochondrial fusion is mainly regulated by the GTPases Mitofusin (Mfn) 1 and 2 located in the OMM and the IMS protein Optic atrophy 1 (Opa1) that is associated with the IMM[123]. Thus, mitochondrial appearance varies from elongated, tubular-like mitochondria building an interconnected network to small rounded ones separated from each other and correlates with mitochondrial function[71,126]. Knockout of any protein of the fusion machinery results in embryonic lethality and mutations of Mfn2 or Opa1 cause the inherited neurodegenerative diseases Charcot-Marie-Tooth type 2A and dominant optic atrophy, respectively[127]. Furthermore, cells lacking Opa1 or Mfns display, besides abrogated fusion, severe mitochondrial dysfunctions and disturbed cellular

respiration[128]. Accordingly, overexpression of Mfn2 increases glucose metabolism and maintains MMP[129]. In contrast knockout or inhibition of the fission machinery in form of Drp1 prevents loss of MMP and reduces infarct volume after transient focal cerebral ischemia[51], highlighting the importance of well-controlled fission and fusion both for mitochondrial appearance and function.

Not only congenital diseases, but also the most prevalent age-related neurodegenerative disorders such as AD and PD are associated with disturbed mitochondrial function.

In AD, direct interactions of amyloid precursor protein (APP) and amyloid beta (Aβ) with the mitochondria have been reported[130]. For example, APP can inhibit the mitochondrial protein import machinery[131] and Aβ can interact with the serine protease Omi/HrtA2[132,133]. In models of PD, α-synuclein mutant A53T which is associated with early-onset PD was predominantly located in degenerating mitochondria[134]. Although the pathophysiological relevance of those interactions remains to be fully determined, they seem to be linked to mitochondrial dysfunction.

Even though the pathologies of AD and PD are not fully understood and their causes and progression are distinct from each other, mitochondrial demise due to oxidative stress is a common feature and regarded as a main trigger in both diseases[124,130]. ROS are a toxic by-product of oxidative phosphorylation and since mitochondria emit around 2% of their consumed oxygen as ROS they are their main source[135,136]. A minor part is derived from other enzymes such as 2-oxoglutarate dehydrogenase (OGDH) and pyruvate dehydrogenase (PDH)[137]. Due to its spatial proximity to the ETC, mtDNA is prone to damage by ROS which leads to the disruption of electron transport, MMP and subsequent altered ATP production. Furthermore, oxidative stress induces mutations of mtDNA contributing to aging and related mitochondrial modifications which are linked to neurodegeneration[130]. Mitochondria-generated ROS can also directly initiate cell death by oxidation of cardiolipin, thereby triggering the release of Cyt c and opening of the PTPC[136]. This disruption of the mitochondrial membrane determines the cell fate and marks the so-called ‘point of no return’[25], at which mitochondria and accordingly cells are beyond remedy.

In order to cope with ROS physiologically developing during oxidative phosphorylation, mitochondria own a variety of enzymatic antioxidant mechanisms. For instances, superoxide dismutases such as manganese (MnSOD) or copper and

zinc (CuZnSOD) superoxide dismustases detoxify superoxides, whereas catalases and peroxiredoxins remove hydrogen peroxide. GpX4 is the main enzyme protecting lipid membranes against oxidative attacks and GSH the most important non-enzymatic antioxidant[135,136]. In neurons, GSH depletion and down regulation of GpX4 are associated with enhanced formation of lipid peroxides[50], while overexpression of MnSOD prevents glutamate-induced mitochondrial dysfunction and cell death[138]. However, not only too high but also too low amounts of mitochondrial ROS can cause mitochondrial impairment and severe damage[139] further emphasising the pivotal role of well-controlled ROS metabolism for the maintenance of cellular signalling and survival.

Besides detrimental ROS formation, Ca^{2+} overload and the activation of specific Bcl-2 family proteins are further reasons for mitochondrial and subsequent neuronal damage. Upon apoptotic stimuli, Bax and Bak insert into the mitochondrial membrane forming a channel and thereby, permeabilising the OMM. Additional binding of Bid and Bim can further enhance Bax-/Bak-induced membrane permeabilisation. Bax and Bak itself are further capable of augmenting opening of the PTPC. Under physiological conditions, the pro-apoptotic function of Bax and Bak is controlled by anti-apoptotic Bcl-2 family proteins like Bcl-xL and Bcl-2 which form stable complexes with Bax and Bak, respectively, thus inhibiting their detrimental pore-forming function[25,28,140]. Notably, in neurons Bak only enhances the pro-apoptotic function of Bax, since there is no full-length Bak[26,27] in neurons as aforementioned.

The essential functions of mitochondria during development, cellular signalling and metabolism and the here described mechanisms leading to perturbed mitochondrial function and their unfavourable consequences for the whole brain, highlight the importance of mitochondria and expose mitochondrial protection as a promising strategy in combating and treating neurodegenerative diseases.

1.3 HIF-prolyl-4-hydroxylases

The family of HIF-prolyl-4-hydroxylases (PHDs) consisting of the three isoforms of PHD1, PHD2 and PHD3 was first described in 2001 as a family of dioxygenases depending on 2-oxoglutarate, iron and oxygen which regulates expression levels of hypoxia-inducible factor (HIF) via hydroxylation and subsequent proteasomal degradation by von-Hippel-Lindau protein (VHL)[141].

HIF is a heterodimeric transcription factor composed of a constitutively expressed β-subunit and a hypoxia-regulated α-subunit which in mammals, can be further subdivided into HIF-1, 2 and 3. HIF-1α is widely expressed in almost every cell type, while expression of HIF-2α and HIF-3α is more restricted[142–144]. HIF-1α mainly induces transcription of glycolytic enzymes such as pyruvate dehydrogenase kinase in response to acute hypoxia[145,146], whereas HIF-2α is rather activated under conditions of chronic oxygen deficiency and thereby, controls renal erythropoietin (EPO) production[142,143,147]. Furthermore, HIF-2α regulates various genes involved in neurological diseases and cancer[144]. To date, the function of HIF-3α is less well studied and remains fairly elusive[143].

Under normoxic conditions, PHDs hydroxylate HIF-α protein at one or both proline residues P564 and P402 in its oxygen degradation domains (ODD) enabling binding of VHL, a E3 ubiquitin ligase which leads to polyubiquitination and consequent proteasomal degradation[148]. During hydroxylation one oxygen atom of a dioxygen molecule is transferred to the respective prolyl residue of HIF-α, while the other one is incorporated into 2-oxoglutarate yielding succinate and CO_2. This reaction requires an Fe^{2+} ion in the catalytic domain of PHDs[149]. In order to prevent oxidation of Fe^{2+} to Fe^{3+} the presence of reducing agents such as ascorbate or GSH is also necessary for proper PHD function[143]. Since PHDs need oxygen as a cofactor, their activity is greatly reduced under hypoxic conditions resulting in enhanced levels of HIF-α protein and subsequent transcription of its target genes such as EPO, lactate dehydrogenase or vascular endothelial growth factor (VEGF). Therefore, PHDs are regarded as major oxygen sensors in aerobic eukaryotes[150], but are also dependent on the tight regulation of iron homeostasis[149]. Furthermore, TCA cycle intermediates as succinate and pyruvate can also inhibit PHD activity, because then less 2-oxoglutarate, another essential cofactor, is available[142].

Nowadays, the concept of HIF-stabilisation via inhibition of PHDs is also used as therapeutic intervention. For example the PHD-inhibitor Molidustat is tested in clinical

phase II for the treatment of anaemia[151] and also in models of ischemic, arterial and gastrointestinal disorders salutary effects of PHD-inhibitors have been observed[143]. In these settings, PHD-inhibition is achieved via iron chelation or application of 2-oxoglutarate analogues, but more specific inhibitors are under way[143,152].

Since pharmacological inhibition of PHDs provides protection in a wide set of neurodegenerative diseases such as stroke[153–155], PD[156,157] and AD[158,159] this approach represents a promising strategy to accomplish neuroprotection. Indeed, these effects are not exclusively explainable by upregulation of HIF-target genes, but more and more HIF-independent functions of PHD-inhibitors have been reported indicated for instances by DFO, ethyl-3,4-dihydroxybenzoate (DHB) and DMOG mediated protection against oxidative stress induced cell death in neuronal cells depleted of HIF-1α[160,161]. Furthermore, PHD inhibition prevents activation of the mammalian target of rapamycin complex 1 by amino acids in a HIF-independent manner[162].

Apart from effects in response to overall PHD-inhibition also HIF-independent mechanisms have been discovered which are partly isoform specific[158,160]. For instance, in human clear renal carcinoma cells PHD1 and PHD2 but not PHD3 have been shown to interact with the large subunit of RNA polymerase II (Rpb1). However, PHD1 catalyses hydroxylation of Rpb1 upon oxidative stress which is a prerequisite for its phosphorylation and subsequent degradation, whereas interaction of PHD2 with Rpb1 inhibits its hydroxylation[163]. Thus, PHDs or their inhibition are capable of regulating transcription independent of HIF. Furthermore, depletion of PHD1 is accompanied by a decrease of cyclin D1 levels and suppression of mammary gland proliferation *in vivo*, thereby reducing tumor growth[164]. Moreover, in lung, brain and hematopoietic cancer cell lines knockdown of PHD1 revealed salutary effects[164]. Activating transcription factor 4 (ATF4) represents another mutual HIF-independent target of PHD1 and PHD3. Both isoforms regulate and interact with ATF4[165,166], a transcription factor displaying both anti-apoptotic[167,168] and pro-apoptotic properties[169,170] depending on the cellular system. Thereby, PHD1 and PHD3 can directly influence cellular survival and death, respectively.

Since these isoform specific HIF-independent properties of particular PHDs have been identified in non-neuronal settings, their relevance in terms of neurodegeneration remains elusive and the underlying mechanisms of HIF-independent neuroprotection need further investigation.

1.3.1 HIF-prolyl-4-hydroxylase 1

PHD1 is a 43.9 kDa protein which is also known as egg-laying defective nine homolog-2 (EGLN2) or HPH3[171]. It is constitutively expressed with high amounts in the testis and lower in kidney, heart, brain and liver and localised in the nucleus[172,173]. PHD1 hydroxylates similarly both proline residues P564 and P402 of HIF-1α and HIF-2α[174]. Under normoxic conditions, it preferentially acts on HIF-2α and it is not induced by hypoxia[141,143]. Alternative translation initiation can result in two PHD1 isoforms with a size of 43 and 40 kDa, respectively not differing in their activity[174].
Mice lacking PHD1 are viable and do not exhibit a particular phenotype[175]. Indeed, in skeletal muscle fibres of PHD1$^{-/-}$ mice formation of oxidative stress upon ischemia was reduced and mitochondrial function preserved. These metabolic adaptations primarily rely on HIF-2α[176]. Increased tolerance to hypoxia after knockout of PHD1 was also observed in models of focal cerebral ischemia[177] and ischemia/reperfusion injury in heart[178] and liver[179]. These results are further confirmed by *in vitro* studies revealing increased levels of PHD1 in the aged rat brain[180] and protection of selective PHD1, but not PHD2 or PHD3 gene silencing in cortical neurons against oxidative stress[160] suggesting PHD1 as a promising target treating oxidative stress related neurodegenerative diseases.

1.3.2 HIF-prolyl-4-hydroxylase 2

In contrast to PHD1, regulation of PHD2, a 46 kDa protein also known as EGLN1 or HPH2[171], is mediated by hypoxia or pharmacological inhibition of PHD activity[141,173]. PHD2 localised in the cytoplasm can be found in almost every tissue, but with particular high amounts in the heart and moderate expression in the brain[172,173]. It hydroxylates both proline residues P564 and P402 of HIF-1α and HIF-2α, but predominantly influences HIF-1α degradation[181]. Unlike knockdown of PHD1 and PHD3, selective silencing of PHD2 leads to accumulation of HIF-1α emphasising the pivotal role of PHD2 in HIF-1α regulation[150] which was further confirmed in mice with conditional knockout of PHD2[182,183]. Furthermore, these mice show enhanced vascular growth and polycythemia revealing a central function of PHD2 for angiogenesis and blood cell production[182,184]. Due to placental and cardiac defects global knockout of PHD2 is embryonic lethal[175,182]. In contrast, additional investigations exposed a protective effect of PHD2 silencing in models of cardiac and cerebral hypoxia. For example, siRNA-mediated PHD2 silencing reduced the infarct

size of hearts subjected to ischemia/reperfusion injury[185] and neuron-specific deletion of PHD2 resulted in reduced infarct size after transient cerebral ischemia[186]. Moreover, PHD2$^{+/-}$ mice displayed improved functional outcome after middle cerebral artery occlusion (MCAO) compared to wild-type littermates[177] exposing also the regulation of PHD2 as a possible way to combat neurodegenerative diseases associated with oxidative stress.

1.3.3 HIF-prolyl-4-hydroxylase 3

With a size of 27.3 kDa PHD3 which is also known as EGLN3 or HPH1[171] is the smallest PHD isoform, because it lacks the N-terminal domain which is present in PHD1 and PHD2, whereas the C-terminus is highly conserved throughout the PHD family. PHD3 located in both the nucleus and cytoplasm is greatly expressed in heart and liver and to less extent in the brain and kidney[172,173]. Interestingly, PHD3 expression increases with age[180,187].

Two alternative splice variants with a size of 17 and 24 kDa have been found of which only the bigger one retains its hydroxylase activity[188]. As opposed to the other PHD isoforms, PHD3 only performs hydroxylation of proline P564[141,181]. Similar to PHD2, PHD3 is inducible by hypoxia and hypoxia mimetics like DFO, but in contrast PHD3 primarily hydroxylates HIF-2α[181].

Mice lacking PHD3 are viable[175], but show changes in CNS innervations regarding sympathoadrenal regulation leading amongst others to reduced plasma catecholamine levels and blood pressure[189]. Similar to findings for PHD1 and PHD2 knockouts, also PHD3$^{-/-}$ mice are protected against myocardial ischemia/reperfusion injury[190] and show improved cardiac function after myocardial infarction[191]. In contrast, PHD3 knockout was not able to prevent neuronal damage due to MCAO[177] which in turn stands in sharp contrast to studies, where overexpression of PHD3 induced apoptosis in PC12 cells and also enhanced expression of SM-20, the rat orthologue of PHD3 promoted cell death in PC12 cells[192] and sympathetic neurons[193]. Furthermore, sympathetic neurons of PHD3$^{-/-}$ mice are protected against the withdrawal of nerve growth factor (NGF)[194], overall suggesting a rather pro- than anti-apoptotic function of PHD3 in neuronal cells *in vitro*.

1.4 The HT-22 model system

In order to investigate the role of p53 and PHDs in terms of oxidative stress in a neuronal setting, HT-22 cells were used, a mouse hippocampal cell line selected for glutamate sensitivity and immortalised by using a temperature-sensitive SV-40 T antigen[195,196]. These cells do not express ionotropic glutamate receptors[197], but a cystine/glutamate antiporter system (X_c^-) which exchanges under physiological conditions intracellular glutamate against extracellular cystine, thereby ensuring GSH synthesis. In HT-22 cells, high extracellular glutamate concentrations in the millimolar range inhibit the X_c^--transporter thereby leading to impaired GSH synthesis resulting in a rapid drop of GSH levels and subsequent formation of ROS via reduced GpX4 and enhanced 12/15-LOX activity[49,50]. Upon oxidative stress attributed to lipid peroxidation, pro-apoptotic proteins like Bid, Bax and DRP1 translocate to the mitochondria[43,51] where they induce loss of mitochondrial integrity indicated by enhanced fission, breakdown of the MMP and subsequent loss of ATP triggering a second, much more pronounced burst of ROS which is accompanied by an increase in intracellular Ca^{2+}-levels[46,49,71]. Finally, AIF is released from the mitochondria to the nucleus where it induces DNA fragmentation as a hallmark of the final steps of cell death[43]. Although HT-22 cells lack ionotropic glutamate receptors, they exhibit common features of apoptosis and necrosis observed in neurodegenerative diseases. Since disturbed GSH metabolism[48] and enhanced ROS formation[4,130,198] are associated with neurodegeneration in neurological diseases, this model system (Fig. 2) is a useful and suitable tool to study the effects of oxidative stress and to identify underlying molecular mechanisms of resulting RCD in neuronal cells.

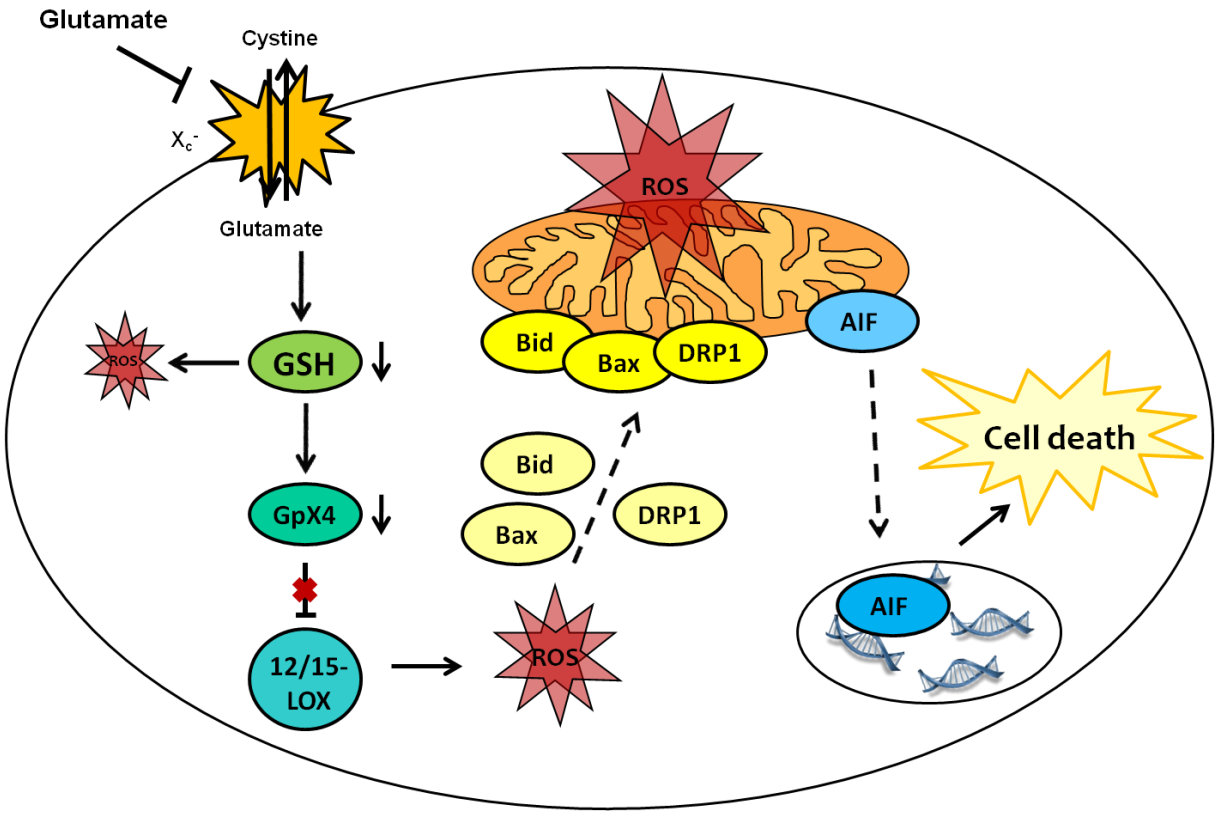

Figure 2: Mechanisms of glutamate-induced oxidative stress and cell death in neuronal HT-22 cells
Inhibition of the cystine/glutamate antiporter system (X_C^-) leads to a drop of glutathione (GSH) levels in the HT-22 cells resulting in formation of soluble reactive oxygen species (ROS) and a decline in glutathione peroxidase-4 (GpX4). This results in the loss of the inhibitory function of GpX4 on 12/15-lipoxygenases (12/15-LOX) which in turn create a first pronounced burst of ROS. Upon this ROS formation the pro-apoptotic proteins Bid, Bax and DRP1 translocate to the mitochondria where they induce a second wave of ROS leading to the translocation of the apoptosis-inducing factor (AIF) to the nucleus. In the nucleus, AIF mediates DNA fragmentation as a hallmark of the final steps of regulated cell death (RCD) in this model system of oxytosis.

1.5 Aims of the study

Oxidative stress and subsequent mitochondrial demise causing neuronal impairment and death are common features of many neurodegenerative diseases, although they widely differ in their pathogenesis and symptoms. Growing evidence shows the importance of mitochondria in various cell death paradigms, since it is well established that the mitochondrial fate also accounts for the whole cell. Therefore, the strategy of mitochondrial protection is pursued in many models of neurological disorders and comprises hope for future therapeutic strategies.

The p53-inhibitor PFTα has been extensively studied in different models of neuronal impairment and its neuroprotective potential has been associated with mitochondrial protection, also in paradigms of oxidative stress and excitotoxicity. Furthermore, mitochondrial localisation of p53 upon oxidative stress suggests a link between p53 and mitochondrial demise in neurons. In order to investigate the role of p53 regarding mitochondria in glutamate-induced oxytosis the effects of PFTα on cell viability and mitochondrial function were compared to selective down regulation of p53 by siRNA approaches and transcriptional effects were examined to further elucidate the underlying mechanisms of mitochondrial protection.

Since some reports about p53-independent effects of PFTα questioned the selectivity of this particular p53-inhibitor, the second aim of this study was to explore whether PFTα-mediated protection of HT-22 cells and in particular of mitochondria was p53-dependent. Therefore, the neuroprotective potential of PFTα was in turn determined in p53 silenced HT-22 cells.

The second part of this thesis focused on PHDs, since salutary effects of PHD-inhibition against various insults associated with neuronal demise have been shown over the last years, but very little is known about their impact on mitochondria. So far it is also not clear whether all three isoforms of the PHD family similarly influence neuronal cell death or if one exceeds the others. Thus, first PHD isoform 1 was silenced by siRNA transfections and cell viability and various mitochondrial parameters were assessed. In order to compare these effects with the broad inhibition of PHDs and to answer the question whether all three isoforms are of similar importance, in a second part the PHD-inhibitors DFO, CPO, DHB and oxyquinoline (Oxy) were used to examine cell viability and mitochondrial integrity. To extend the results and identify underlying mechanisms of protection the effects of

oxyquinoline on the eIF2α/ATF4 pathway were investigated because recent studies linked PHDs with ATF4 transcriptional activity.

Since recent reports suggested a connection between PHD1 and ferroptosis, the last part of this thesis aimed to characterise this relationship in ferroptosis of HT-22 cells using broad PHD-inhibitors and siRNA approaches selectively targeting PHD1.

2 Materials and methods

2.1 Chemicals and reagents

All standard chemicals were obtained from Sigma-Aldrich (Taufkirchen, Germany) or Roth (Karlsruhe, Germany), if not otherwise declared. All buffers and solutions were prepared using demineralised, ultrapure water which was produced with the SG Ultra Clear UV plus pure water system (VWR, Darmstadt, Germany) and autoclaved with a steam autoclave (Systec V-40, Systec GmbH, Wettenberg, Germany).

2.1.1 Inducers of cell death

A 1 M stock solution of glutamate was prepared dissolving L-glutamic acid monosodium salt hydrate (Sigma-Aldrich, Taufkirchen, Germany) in Dulbeccos's modified Eagle's medium (DMEM; Sigma-Aldrich, Taufkirchen, Germany) and stored at -20 °C. For induction of cell death, working solutions of 3-7 mM were used and HT-22 cells were harvested or analysed 3-24 h later.

For H_2O_2-induced cell death, a stock solution of 30% hydrogen peroxide (H_2O_2; Fluka, Taufkirchen, Germany) was diluted with DMEM to 700-900 µM.

A stock solution of erastin (Calbiochem, Darmstadt, Germany) with a concentration of 10 mM was prepared dissolving erastin in dimethyl sulfoxide (DMSO) and stored at -20 °C. For induction of ferroptosis, erastin stock solution was diluted with DMEM to a concentration of 1-2 µM.

2.1.2 Inhibitors of cell death

Pifithrin-α (PFTα; Sigma-Aldrich, Taufkirchen, Germany) was dissolved in DMSO to a stock concentration of 13.6 mM (Fig. 3) and used in a final concentration range from 2 to 10 µM diluted in DMEM for application to HT-22 cells. The stock solution was stored at -20 °C.

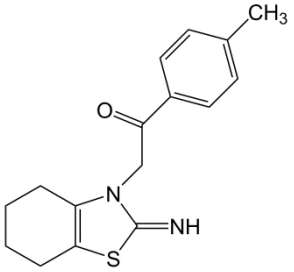

Figure 3: The chemical structure of PFTα

Pifithrin-μ (PFTμ; Sigma-Aldrich, Taufkirchen, Germany) was dissolved in DMSO to a stock concentration of 20 mM (Fig. 4) and stored at -20 °C. PFTμ was used in a final concentration range from 2 to 10 μM in DMEM.

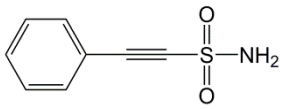

Figure 4: The chemical structure of PFTμ

PHD-inhibitor oxyquinoline (Oxy; Calbiochem, Darmstadt, Germany) was dissolved in DMSO to a concentration of 100 mM (Fig. 5) and stored at -20 °C. Oxyquinoline was applied to HT-22 cells in a final concentration range from 0.5 to 20 μM diluted in DMEM.

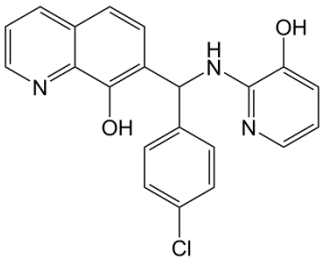

Figure 5: The chemical structure of oxyquinoline

Deferoxamine (DFO), ethyl-3,4-dihydroxybenzoate (DHB) and ciclopirox (CPO) were a kind gift from Prof. Ratan. DFO (Fig. 6) and DHB (Fig. 7) were dissolved in DMSO to a stock concentration of 100 μM and used in a concentration range from 0.1 to 100 and 50 μM, respectively. CPO (Fig. 8) was also dissolved in DMSO and used in a concentration range from 1 to 20 μM diluted in DMEM.

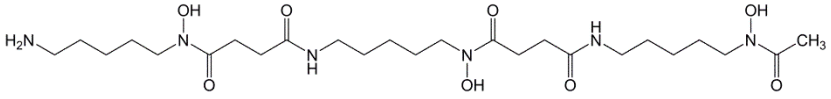

Figure 6: The chemical structure of DFO

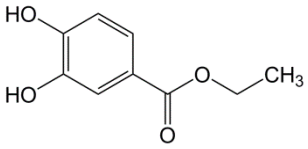

Figure 7: The chemical structure of DHB

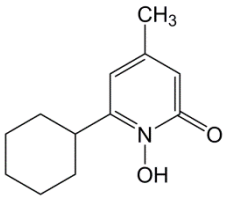

Figure 8: The chemical structure of CPO

2.1.3 Kits

The following kits were used in the present work according to manufacturer's protocol. Changes in the protocol are declared in the relevant sections:

Table 1: Kits

Kit	**Company**
Annexin-V-FITC Detection Kit	Promokine, Heidelberg, Germany
Bodipy (581/591 C11)	Invitrogen, Karlsruhe, Germany
CM-H2DCFDA	Invitrogen, Karlsruhe, Germany
Dual-Luciferase® Assay Kit	Promega, Madison, USA
Glutathione Assay Kit	Cayman Chemical Company, Ann Arbor, USA
InviTrap® Spin Universal RNA Mini Kit	Stratec Molecular GmbH, Berlin, Germany
MitoPT™ ΔΨm	ImmunoChemistry Technologies, Bloomington, USA
MitoSOX™ Red	Life Technologies, Darmstadt, Germany
Pierce® BCA Protein Assay Kit	Perbio Science, Bonn, Germany
QIAGEN Plasmid Plus Midi Kit	Qiagen, Hilden, Germany
SuperScript III One Step RT-PCR System with Platinum® Taq	Invitrogen, Karlsruhe, Germany
ViaLight™ Plus Cell Proliferation and Cytotoxicity BioAssay Kit	Lonza, Verviers, Belgium
XF Cell Mito Stress Test Kit	Seahorse Bioscience, Copenhagen, Denmark

2.1.4 Transfection reagents

For DNA and siRNA transfections Opti-MEM I (Invitrogen, Karlsruhe, Germany) was used as basal antibiotic free medium.

DNA containing plasmids were transfected using Attractene transfection reagent (Qiagen, Hilden, Germany).

Formation of siRNA complexes was performed with Lipofectamine® RNAiMAX transfection reagent (Invitrogen, Karlsruhe, Germany).

2.1.5 Plasmid vectors

For analysis of p53 transcriptional activity a p53-Luc-reporter plasmid was generated as described in 2.10.1. Renilla-vector was obtained from Promega (Madison, USA).

Transformation and amplification of plasmid vectors is described in 2.1.9.

2.1.6 SiRNAs

For selective silencing of p53 one single siRNA sequence 5'-CCACUUGAUGGAGAGUAUU-3' (Eurofins MWG Operon, Ebersberg, Germany) and an ON-TARGETplus SMARTpool consisting of four target sequences 5'-GUAAACGCUUCGAGAUGUU-3', 5'-AAAUUUGUAUCCCGAGUAU-3', 5'-GAGGA GUCACAGUCGGAUA-3' and 5'-CAGUCUACUUCCCGCCAUA-3' (Dharmacon, Bonn, Germany) were used referred to as "si p53" and "si p53 smart".

Specific knockdown of PHD1 was achieved by following siRNA sequences from Sigma-Aldrich (Taufkirchen, Germany): 5'-CAGUGUGGCUGGCGGUCAU-3' (siPHD1 II, Mm01_00154010) and 5'-GCCAUCACUGUCUGGUAUU-3' (siPHD1 I, Mm02_00337792).

ATF4 was targeted by siATF4 with following sequence: 5'-AUCGA AGUCAAACUCUUUCUU-3' (Eurofins MWG Operon, Ebersberg, Germany).

Non-functional scrambled siRNA (siScr) 5'-UAAUGUAUUGGAACGCAUA-3' was obtained from Dharmacon (Bonn, Germany).

2.1.7 Primary antibodies

All primary antibodies used for Western blot analysis in the present work are listed in table 2. They were diluted either in Tris-buffered saline (TBS) containing 0.05%

Tween® 20 (TBST) and 5% nonfat skim milk powder or TBST containing 5% BSA or TBS containing 0.1% Tween® 20 and 0.2% I-BLOCK™ (Tropix, Bedford, USA).
For immunocytochemistry, p53 antibody (Cell Signaling, Danvers, USA) was diluted 1:100 in phosphate buffered saline (PBS) containing 3% horse-serum (Invitrogen, Karlsruhe, Germany) and phospho-p53 antibody (Cell Signaling, Danvers, USA) 1:100 in PBS containing 3% goat-serum (Invitrogen, Karlsruhe, Germany).

Table 2: Antibodies

Primary antibody	Secondary antibody	Dilution	Company
Actin Clone C:4	Mouse	1:10 000 in 5% milk in TBST	MP Biomedicals, Illkirch Cedex, France
CREB-2 (C19) = ATF4	Goat	1:500 in I-BLOCK	Santa Cruz, Santa Cruz, USA
eIF2α	Rabbit	1:1 000 in 5% BSA in TBST	Cell Signaling, Danvers, USA
p53	Mouse	1:1 000 in 5% milk in TBST	Cell Signaling, Danvers, USA
PHD1	Rabbit	1:1 000 in I-BLOCK	Novus Biologicals, Littleton, USA
Phospho-eIF2α	Rabbit	1:500 in 5% BSA in TBST	Cell Signaling, Danvers, USA
Phospho-p53	Rabbit	1:100 in 3% goat serum	Cell Signaling, Danvers, USA
Superoxide dismutase 2 = MnSOD	Rabbit	1:1 000 in 5% milk in TBST	Novus Biologicals, Littleton, USA
xCT	Rabbit	1:1 000 in 5% milk in TBST	Abcam, Cambridge, UK
XIAP	Mouse	1:1 000 in 5% milk in TBST	BD Transduction Laboratoires™, Heidelberg, Germany

2.1.8 Secondary antibodies

For Western blot analysis, horse radish peroxidase (HRP) labelled secondary antibodies targeting mouse IgG, rabbit IgG or goat IgG (Vector Labs, Burlingame, USA) were diluted 1:2 500 in 5% milk in TBST.

For immunocytochemistry, biotinylated anti-mouse-IgG (Vector Labs, Burlingame, USA) was diluted 1:200 in PBS containing 3% horse-serum (Invitrogen, Karlsruhe, Germany) and biotinylated anti-rabbit-IgG (Vector Labs, Burlingame, USA) 1:200 in PBS containing 3% goat-serum.

2.1.9 Transformation and preparation of plasmids

For amplification of plasmids, vectors were transformed in competent E.coli. First, competent E.coli were thawed on ice and meanwhile, 20 µl 5x KCM buffer (Tab. 3), 4 µl vector (500 ng/µl) and 76 µl bidest H_2O were mixed and incubated for 20 min on ice. Afterwards, 100 µl E.coli were added and the mixture was incubated for 10 min at room temperature (RT) followed by addition of 1 ml LB-medium (Tab. 4) and shaking at 850 rpm at 37 °C for 50 min (Thermomixer compact, Eppendorf, Hamburg, Germany). The preparation was diluted in 100 ml LB-medium containing particular antibiotic for selection (see below) and further shaken at 37 °C with 850 rpm overnight. For the preparation of Renilla-luciferase-plasmid and p53-firefly-luciferase reporter plasmid ampicillin was used at a concentration of 100 mg/ml. Plasmid purification from bacterial cultures was performed with QIAGEN Plasmid Plus Midi Kit (Qiagen, Hilden, Germany) according to manufacturer's protocol. Concentration of plasmids was determined with NanoPhotometer™ (Implen, Munich, Germany).

Table 3: 5x KCM buffer

1 M KCl	5 ml
1M $CaCl_2$	1.5 ml
1 M MgCl	2.5 ml
Bidest H_2O	ad 10 ml

Table 4: LB-medium

LB-medium powder Lennox (AppliChem, Darmstadt, Germany)	20 g
Bidest H_2O	ad 1 l

2.2 Cell culture material

All sterile plastic ware used in this work is listed in table 5.

Table 5: Sterile plastic ware

Plastic material	Company
T75 flasks	Greiner, Frickenhausen, Germany
T175 flasks	Greiner, Frickenhausen, Germany
6-well plates	Greiner, Frickenhausen, Germany
24-well plates	Greiner, Frickenhausen, Germany
96-well plates	Greiner, Frickenhausen, Germany
96-well E-plates	Roche, Penzberg, Germany
8-well ibidi slides	Ibidi, Munich, Germany
15 ml tubes	Sarstedt, Nümbrecht, Germany
50 ml tubes	BD Bioscience, Durham, USA
0.5 ml, 1 ml, 2 ml tubes	Sarstedt, Nümbrecht, Germany
Cell Scraper	Sarstadt, Nümbrecht, Germany
0.22 µm Sterile filter	GE Healthcare, Buckinghamshire, UK
1 ml, 5 ml, 10 ml Injekt®	Braun, Melsungen, Germany

2.3 Cell culture

2.3.1 Cultivation of HT-22 cells

HT-22 cells were originated from HT4 cells based on glutamate sensitivity[196] and obtained from Gerald Thiel (Homburg/ Saar, Germany). This cell line is immortalised from mouse hippocampal neurons using a temperature-sensitive SV-40 T antigen[195]. HT-22 cells were cultured in Dulbecco's modified Eagle's medium (DMEM; Sigma-Aldrich, Taufkirchen, Germany) with the addition of 10% heat-inactivated fetal calf serum (FCS, Biochrom, Berlin, Germany), 100 U/ml penicillin (Biochrom, Berlin,

Germany), 100 µg/mL streptomycin (Biochrom, Berlin, Germany), 20 mM HEPES-Buffer (Sigma-Aldrich, Taufkirchen, Germany) and 2 mM L-Alanyl-L-glutamine (Biochrom, Berlin, Germany) (Tab. 6). For standard cultivation cells were kept in 75 cm^2 flasks in a humidified incubator at 37 °C with 5% CO_2. Stock cells were split twice a week in a ratio of 1:10-1:20 depending on the cell density. Therefore, culture medium was removed, cells were washed one time with 5 ml PBS (Tab. 7) and then incubated with 2 ml Trypsin-EDTA (1x TE, Tab. 8) for 2-4 min to detach cells from the culture dish. Trypsinisation was stopped by the addition of 5-8 ml culture medium. The cell suspension was transferred to a 50 ml tube and centrifuged for 5 min at 1 000 rpm. Afterwards, supernatant was discarded and cells were resuspended in fresh culture medium. One-tenth of the cell suspension was put in a new flask containing 10 ml fresh culture medium for continuing stock cultivation. In case of following siRNA transfections, cells were resusupended in antibiotic free culture medium. For cell culture experiments, the number of cells in the cell suspension was determined by counting cells in a Neubauer-Zählkammer (Brand, Wertheim, Germany). Respective number of cells were seeded in specific culture dishes as listed in Tab. 9 or indicated for particular experiments. Normally, treatment with inducers and inhibitors of apoptosis was performed 24 h after seeding, if not otherwise declared.

Table 6: Culture medium for HT-22 cells

FCS	50 ml
HEPES-Buffer (1 M)	10 ml
Penicillin (10 000 U/ml)/ Streptomycin (10 000 µg/ml)	5 ml
L-Alanyl-L-glutamine	5 ml
DMEM	ad 500 ml

Table 7: Phosphate buffered saline (PBS), pH 7.4

NaCl	9 g
Na_2HPO_4	0.527 g
KH_2PO_4	0.144 g
HCl	qs for pH adjustment
Bidest H_2O	ad 1 l

Table 8: Trypsin-EDTA (1x TE)

Trypsin (7500 U/mg)	100 mg
EDTA	40 mg
PBS	ad 200 ml

Table 9: Cell numbers and volumes in culture dishes

Culture dish	Cell number per well	Total volume per well
75 cm^2 flask	1.5 mio	10 ml
175 cm^2 flask	3-3.5 mio	25 ml
6-well plate	120 000-200 000	2 ml
24-well plate	20 000-60 000	900 µl
96-well plate	8 000-10 000	100 µl
96-well E-plate	4 000-8 000	100 µl
8-well ibidi slides	17 000-20 000	200 µl

2.3.2 Transfection protocols

2.3.2.1 DNA transfection

For transfection of DNA containing plasmids Attractene transfection reagent (Qiagen, Hilden, Germany) was used. One day prior to transfection, HT-22 cells were seeded at a density of 30 000 cells/well for the assessment of p53 transcriptional activity in 24-well plates. Transfection mix was prepared as listed in Tab. 10 and incubated for 20 min at RT. In the meantime, the cell culture medium was changed. Thereafter, 60 µl of transfection mix were added dropwise to each well and carefully mixed by pipetting.

Table 10: Transfection of p53-firefly-luciferase-reporter plasmid and renilla-luciferase-plasmid per well

p53-firefly-luciferase-reporter plasmid	108 ng
Renilla-luciferase-plasmid	17 ng
Attractene	1.5 µl
Opti-MEM I	ad 60 µl

2.3.2.2 siRNA transfection

For siRNA transfection, Lipofectamin® RNAiMAX (Invitrogen, Karlsruhe, Germany) was used. Therefore, particular siRNAs were diluted in Opti-MEM I (Invitrogen, Karlsruhe, Germany) and 1.2 µl Lipofectamin® RNAiMAX were added per 100 µl transfection mix. Precise amounts of Lipofectamin® RNAiMAX and Opti-MEM I for each well in different culture dishes are listed in Tab. 11. The solution was shortly vortexed and incubated for 20 min at RT to allow complex formation. Afterwards, siRNA mixture was transferred into the culture dish and cell suspension in antibiotic free medium was added to achieve a final siRNA concentration of 10-80 nM. Cells were grown for two days before treatment or analysis. In order to control for effects of the transfection reagents, control cells were treated with a mixture of Lipofectamin® RNAiMAX and Opti-MEM I, exclusively referred to as “vehicle” in the present work. An unspecific scrambled siRNA was used as control for transfection effects.

Table 11: siRNA transfection protocols

	6-well plate	**24-well plate**	**96-well plate**	**8-well ibidi slide**
siRNA	qs	qs	qs	qs
Lipofectamin® RNAiMAX	4.8 µl	1.2 µl	0.24 µl	0.48 µl
Opti-MEM I	ad 400 µl	ad 100 µl	ad 20 µl	ad 40 µl

2.4 Cell viability assays

2.4.1 Morphological cell viability analysis

Induction of cell death was confirmed via analysis of morphological changes of HT-22 cells detected by transmission light microscopy using Leica DM IL LED microscope (Leica, Wetzlar, Germany) which was equipped with a Lumenera Infinity 2 digital camera (Lumenera Corporation, Ottawa, Canada). Light was collected through a 10x objective and images were acquired using phase contrast. Digital image recording was conducted with INFINITY ANALYZE software (Lumenera Corporation, Ottawa, Canada).

2.4.2 MTT-assay

3-(4,5-Dimethylthiazol-2-yl)-2,5-diphenyltetrazolium bromide is a yellow tetrazolium salt which is reduced to an insoluble purple formazan mainly by NAD(P)H-dependent enzymes of the endoplasmic reticulum, but also by mitochondrial enzymes[199]. The absorbance of this formazan correlates with the metabolic activity of the cells and was therefore used to determine cell viability in this study.

HT-22 cells were seeded in 96-well plates and 24 h later treated with glutamate, erastin or H_2O_2 to induce cell death. After 12-18 h, depending on the cell morphology, 20 µl of MTT-solution (2.5 mg/ml in PBS) were added to the culture medium (final concentration: 0.5 mg/ml). In case of H_2O_2 treatment, the culture medium was replaced by PBS before addition of MTT to avoid disturbance of the redox reaction. Cells were incubated at 37 °C for 1 h before the reaction was stopped by complete removal of the medium. After storage at -80 °C for at least 1 h, the formazan was dissolved in 70-100 µl DMSO, depending on the colour intensity. Absorbance was measured at 570 nm with FluoStar OPTIMA (BMG Labtech, Offenbach, Germany) after incubation for another hour at 37°C on a shaker, background signals at 630 nm were subtracted. Absorbance of control conditions was set as 100% and cell viability was displayed relatively as % of controls. All experiments were repeated at least three times with n=6-8.

2.4.3 xCELLigence system

The xCELLigence system (Roche, Penzberg, Germany) is a cell-based assay which records cellular events in real-time by measuring changes in electrical impedance via microelectrodes integrated in the bottom of the culture plate: E-plate (Roche, Penzberg, Germany). The impedance rises with an increasing number of cells and correlates well with cell proliferation and morphological alterations. Therefore, the system is able to detect cell growth, kinetics of cell proliferation, but also cell death accompanied by altered cellular morphology and attachment properties. The changes in impedance are depicted as cell index (CI) as function of time by RTCA Software 1.2 (Roche Diagnostics, Penzberg, Germany)[200].

Before seeding HT-22 cells in 96-well E-plates at a density of 8 000 cells/well, background measurement was performed with 100 µl/well growth medium. For siRNA transfections 3 000 cells/well were used. When a CI of ~1 was reached, cells were treated with glutamate or erastin and different cell death inhibitors. To grade

differences in proliferation the CI was normalised before analysis. All experiments were repeated at least three times.

After the experiments E-plates were recycled by removing the medium and cleaning with bidest H_2O, followed by incubation with 1x TE for 15 min. After removal of 1x TE wells were again washed three times with bidest H_2O. Finally, the E-plate was put under UV light for 30 min to ensure sterility.

2.5 ATP assay

Adenosine triphosphate (ATP) is one of the most important energy carriers in living cells. Since ATP is required for survival of every cell and cytoplasmic levels drop in response to cellular damage, measurement of ATP levels can be used for analysis of cell proliferation and cytotoxicity.

In the present study, ATP levels were determined via bioluminescent measurements. Luciferase enzyme catalyses the formation of light from luciferin in an ATP-dependent reaction as follows:

$$\text{ATP} + \text{Luciferin} + O_2 \xrightarrow[Mg^{2+}]{\text{Luciferase}} \text{AMP} + \text{Oxyluciferin} + PP_i + CO_2 + \text{Light}$$

The amount of emitted light is directly proportional to the ATP content of the sample. For detection of luminescence, HT-22 cells were seeded in white 96-well plates (8 000 cells/well) and challenged with glutamate and particular inhibitors of cell death 24 h later. For evaluation of p53 and PHD1 specific silencing, cells were transfected with respective siRNA sequences (3 500 cells/well) 48 h prior to glutamate exposure. The first row of each plate was only filled with culture medium for background analysis. At indicated time points ATP analysis was performed using the ViaLight^{TM} plus Kit (Lonza, Verviers, Belgium) according to manufacturer's protocol. After bringing all reagents and the cell culture plate at RT, 50 µl cell lysis reagent was given to growth medium and incubated for 10 min to release the ATP from the cells. Next, 100 µl ATP monitoring reagent was added and luminescence was recorded after two more minutes of incubation with FluoStar OPTIMA (BMG Labtech, Offenbach, Germany). Emission intensity of control cells was set to 100%. All data were correct for background luminescence and experiments were repeated at least three times with n=4-8.

2.6 Measurements of oxygen consumption rate

To elucidate the mitochondrial respiration the cellular oxygen consumption rate (OCR) was examined with the Seahorse XF96 system (Bioscience, Copenhagen, Denmark) using the XF Cell Mito Stress Test Kit. HT-22 cells were seeded in special XF96-well microplates at a density of 8 000 cells/well and cultured overnight. After 15 h of glutamate exposure and treatment with particular PHD-inhibitors culture medium was replaced by ~180 µl of assay medium (with 4.5 g/l glucose as the sugar source, 2 mM glutamine, 1 mM pyruvate, pH 7.35) and cells were incubated at 37 °C for 1 h. Three baseline measurements were performed before applying the compounds for metabolic analysis. First, 20 µl oligomycin were injected in Port A at a final concentration of 3 µM. Oligomycin inhibits the ATP synthase by blocking its proton channel causing an increase in the proton gradient and a retarded electron transport decreasing the oxygen consumption. Next, 22.5 µl carbonyl cyanide-4-(trifluoromethoxy)phenylhydrazone (FCCP) was added in Port B at a concentration of 0.4 µM. FCCP acts as an uncoupler of the mitochondrial respiratory chain leading to a decreased proton gradient and breakdown of the MMP which is reflected by an immediate increase in the OCR. Finally, a combination of rotenone and antimycin A (25 µl) was applied in Port C at a concentration of 1 µM. Rotenone is an inhibitor of mitochondrial complex I and antimycin A blocks the function of complex III resulting in a complete deactivation of the mitochondrial respiration indicated by a decline in the OCR. Three measurements were performed after the addition of each compound (4 min mixing followed by 3 min measuring). Measurements were performed by Amalia Dolga and repeated three times with n=6.

2.7 Flow cytometric measurements

2.7.1 FITC Annexin V/Propidium iodide staining

The fluorescent dyes FITC conjugated Annexin V (AV) and propidium iodide (PI) are commonly used to visualise cell death. Their fluorescence correlating with the extent of cell death can be quantified by flow cytometric measurements. AV is a Ca^{2+}-dependent phospholipid-binding protein unable to enter intact cells. In living cells, phospholipid phosphatidylserine (PS) is located at the inner leaflet of the plasma membrane. Upon induction of apoptotic cell death, PS translocates to the outer leaflet of the intact plasma membrane, where AV can bind to it. Therefore, AV

staining shows early stages of apoptosis. To distinguish between apoptotic and necrotic cells AV staining is combined with a vital dye, like PI which is excluded by vital cells with intact plasma membranes. Late apoptosis and necrosis induce a loss of plasma membrane integrity whereupon PI can stain the cells. Accordingly, viable cells are AV and PI negative whereas early apoptotic cells appear only AV positive and late apoptotic and necrotic AV and PI positive[201]. In this work the amount of early and late apoptotic cells (AV and AV/PI positive cells) was depicted as bar graphs and representative dot plots.

For analysis of cell death, HT-22 cells were seeded in 24-well plates and after 24 h treated as indicated. When cell death was detectable under the microscope, cells were harvested with 1x TE, washed 1x with PBS and stained with 2 µl each AV and PI/sample. After incubation for 5 min in the dark samples were put on ice and analysed by flow cytometric measurements using Guava EasyCyte™ Flow Cytometer (Merck Millipore, Darmstadt, Germany). Annexin-V-FITC was excited at 488 nm and emission was detected through a 525/30 band pass filter. Propidium iodide was excited at 488 nm and fluorescence emission was detected using a 690/50 band pass filter. Data were collected from 10 000 cells from at least three wells per condition. All experiments were repeated at least three times.

2.7.2 Detection of lipid peroxides

BODIPY 581/591 C11 is a lipophilic fluorescent dye undergoing a shift from red (~590 nm) to green (~510 nm) fluorescent emission upon oxidation by free radicals. Therefore, it can be used as a sensor for oxidation of lipids and membranes. To analyse lipid peroxidation, HT-22 cells were seeded in 24-well plates at a density of 55 000 cells/well followed 24 h later by glutamate challenge and co-treatment with particular inhibitors of cell death. For evaluation of siRNA effects, cells were transfected with respective siRNA sequences (20 000 cells/well) and treated with glutamate 48 h later. After induction of cell death, cells were stained with BODIPY 581/591 C11 for 1 h at 37 °C in culture medium at a final concentration of 2 µM. Next, cells were harvested with 1x TE, centrifuged at 200 x g for 5 min and washed once with PBS. After resuspension in the appropriate amount of PBS, cells were analysed with Guava EasyCyte™ Flow Cytometer (Merck Millipore, Darmstadt, Germany). Excitation was performed at 488 nm and emission was recorded with a 525/30 band pass filter (green) and a 690/50 band pass filter (red). Data were

collected from 10 000 cells from at least three wells per condition. All experiments were repeated at least three times.

2.7.3 Assessment of intracellular, soluble ROS

CM-H_2DCFDA (DCF) is a sensor detecting intracellular, soluble ROS upon oxidation. After passive diffusion into cells, acetate groups are cleaved by intracellular esterases trapping the dye inside the cells. Intracellular ROS oxidise the deacetylated form of CM-H_2DCFDA yielding a green fluorescent product. For detection of intracellular, soluble ROS in HT-22 cells, cells were seeded in 24-well plates (55 000 cells/well). After particular treatment with glutamate or transfection with siRNA, culture medium was removed and cells loaded with 2.5 µM CM-H_2DCFDA in serum-free medium to avoid deacetylation of the dye by esterases of the serum. After incubation for 30 min at 37 °C, followed by incubation for another 30 min at 37 °C without dye in serum containing fresh medium cells were trypsinised with 1x TE, centrifuged at 200 x g for 5 min and washed once with PBS. For detection of green fluorescence with Guava EasyCyte™ Flow Cytometer (Merck Millipore, Darmstadt, Germany) samples were resuspended in the appropriate amount of PBS. Excitation was performed at 488 nm and emission was recorded with a 525/30 band pass filter. Data were collected from 10 000 cells from at least three wells per condition. All experiments were repeated at least three times.

2.7.4 Measurement of mitochondrial ROS formation

MitoSOX™ Red (Life Technologies, Darmstadt, Germany) is a live-cell permeable dye selectively targeted to mitochondria. Oxidation by superoxides leads to enhanced red fluorescence. To evaluate the formation of mitochondria-derived ROS, HT-22 cells were seeded in 24-well plates (55 000 cells/well) and after 24 h, treated with glutamate and respective inhibitors. SiRNA transfection (22 000 cells/well) was performed 48 h prior to glutamate challenge. After indicated time of treatment cells were loaded with 2.5 µM MitoSOX red in culture medium and incubated for 30 min at 37 °C. Afterwards, cells were harvested with 1x TE, centrifuged at 200 x g for 5 min and washed once with PBS. Red fluorescence of samples resuspended in PBS was analysed with Guava EasyCyte™ Flow Cytometer (Merck Millipore, Darmstadt, Germany). MitoSOX red was excited at 488 nm and emission was recorded using a

690/50 band pass filter. Data were collected from 10 000 cells from at least three wells per condition and the experiments were performed minimum three times.

2.7.5 Evaluation of mitochondrial membrane potential

For the evaluation of the MMP in HT-22 cells the Mito PT™ ΔΨm Kit (Immunochemistry Technologies, Hamburg, Germany) containing the potentiometric fluorescent dye tetramethylrhodamine ethyl ester (TMRE) was used. Due to its positive charging TMRE accumulates inside healthy mitochondria with an intact membrane potential as mitochondria are negatively charged resulting in red fluorescence. In cells with disrupted MMP TMRE is distributed in the cytosol indicated by a loss of red fluorescence. To assess the MMP in HT-22 cells after glutamate challenge, cells were seeded in 24-well plates at a density of 55 000 cells/well and treated as indicated after 24 h. For siRNA experiments cells were transfected at a density of 22 000 cells/well 48 h prior to glutamate challenge. After 11-15 h, cells were harvested with 1x TE and stained with TMRE dissolved in culture medium at a final concentration of 200 nM followed by an incubation at 37 °C for 20 min. Subsequently, cells were centrifuged at 200 x g for 5 min, washed once with PBS and resuspended in the appropriate amount of 1x assay buffer provided by the manufacturer. Changes in the MMP were examined by analysis of red fluorescence with Guava EasyCyte™ Flow Cytometer (Merck Millipore, Darmstadt, Germany). 10 000 cells from at least three wells per condition were excited at 488 nm and emission was recorded using a 690/50 band pass filter. All measurements were performed at least three times.

2.8 Determination of glutathione levels

To determine GSH levels, HT-22 cells were seeded in 6-well plates (180 000 cells/well). After treatment with glutamate and oxyquinoline for the indicated amount of time two wells per condition were harvested by scratching, centrifuged at 200 x g for 5 min and washed 1x with PBS. Pellets were stored at -80 °C for further experiments or directly used. GSH measurements were performed using Glutathione Assay Kit (Cayman Chemical Company, Ann Arbor, USA) following manufacturer's protocol. Before starting the assay all reagents were equilibrated to RT. Briefly, cells were resuspended in 100 µl MES-buffer (0.4 M 2-(N-mopholino)ethanesulphonic acid, 0.1 M phosphate, 2 mM EDTA, pH 6.0) and homogenised by sonification.

Insoluble fragments were removed by centrifugation at 10 000 x g for 15 min at 4 °C. 80 µl of the supernatant were deproteinated by addition of an equal volume of metaphosphoric acid (1.25 M). The remaining supernatant was analysed for protein content using the BCA assay as described in 2.12.2. After incubation for 5 min at RT the mixture was centrifuged at 17 000 x g for 10 min. The supernatant was stored at -20 °C or directly mixed with 8 µl of a 4 M solution of triethanolamine to increase the pH. For calibration purposes different dilutions of provided GSH standards were prepared. After transfer of 50 µl of each sample and standard into a 96-well plate, 150 µl of freshly-prepared assay cocktail composed of provided MES-buffer, the cofactors $NADP^+$ and glucose-6-phosphate, the enzymes glutathione reductase and glucose-6-phosophate dehydrogenase and Ellman's reagent (5,5'-dithio-bis-(2-nitrobenzoic acid): DTNB) were added. GSH reacts via its sulfhydryl group with DTNB and forms yellow 5-thio-2-nitrobenzoic acid (TNB). This mixed disulfide is reduced by the glutathione reductase discharging GSH which subsequently can generate more TNB. The glutathione reductase requires $NADPH/H^+$ as a cofactor which is recycled via oxidation of glucose-6-phosphate by glucose-6-phosphate dehydrogenase (Fig. 9).

Absorbance of TNB measured at 405 nm after 30 min of incubation with EL_X808 Ultra Microplate Reader (Bio-Tek Instruments, Bad Friedrichshall, Germany) correlates with the host of GSH in the samples. Total GSH amount was determined via standard curve calculation and normalised to protein content. Data were depicted in % of control and experiment was performed four times for statistical analysis.

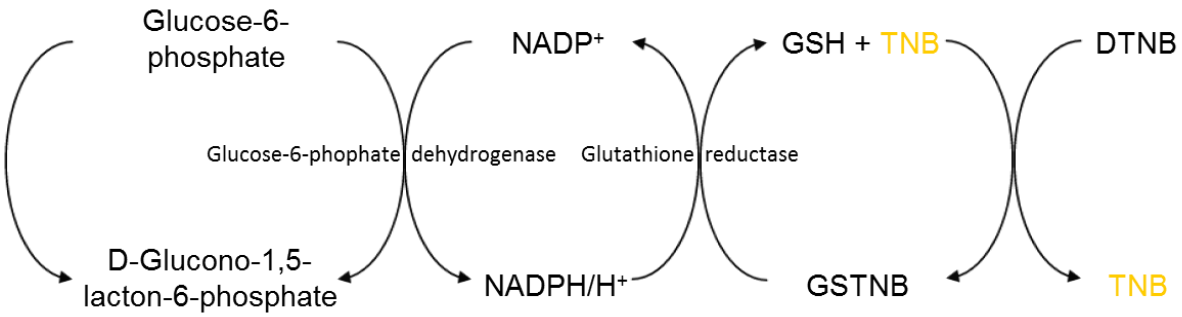

Fig. 9 Reaction of glutathione assay

2.9 Immunocytochemistry

2.9.1 Staining of mitochondria

For visualisation of glutamate-induced changes in the mitochondrial morphology of HT-22 cells, MitoTracker® Deep Red FM (Invitrogen, Karlsruhe, Germany) was used which is a red-fluorescent dye selectively staining mitochondria in living cells. MitoTracker® Deep Red was dissolved in DMSO to a stock concentration of 50 µM and stored at -20 °C in the dark. A working solution with a concentration of 200 nM in cell culture medium was freshly prepared for every experiment.

For morphological analyses, cells were seeded in 8-well ibidi slides (17 000 cells/ well) and stained with MitoTracker® Deep red for 20 min at 37 °C. Furthermore, a counterstaining of the nuclei was performed with 1 µg/ml 4′,6-diamidin-2-phenylindol (DAPI; Sigma-Aldrich, Taufkirchen, Germany), a dye emitting blue fluorescence after binding to AT regions of the DNA. Next, medium was removed, cells washed once with culture medium and then treated with glutamate and particular inhibitors. After appropriate time, cells were washed carefully with 1x PBS and fixed with 4% paraformaldehyde (PFA) for 30 min at RT. Afterwards, PFA was removed and cells carefully washed three times with 1x PBS. Samples were stored in PBS at 4 °C until analysis or used for immunocytochemistry (s. 2.9.3). Images were acquired with an epifluorescence microscope DMI6000B (Leica, Wetzlar, Germany) or confocal laser scanning microscope (Axiovert 200, LSM Image Software, Carl Zeiss, Jena, Germany) with a 63 x 1.4 NA oil immersion objective. Fluorescence of MitoTracker® Deep red was excited at 633 nm (band pass filter) and emission was detected at 670 nm (long pass filter). DAPI fluorescence was analysed with an epifluorescence microscope exciting with 360 nm band pass filter and recording emission 470 nm band pass filter.

2.9.2 Evaluation of mitochondrial morphology

To evaluate mitochondrial alterations, mitochondria were stained with MitoTracker® Deep Red prior to particular treatment as described in 2.9.1. Cells were divided into three categories as previously defined[71]. Category I represented predominantly by healthy cells is characterised by elongated mitochondria organised in a tubular network. Cells of category II exhibit large round mitochondria which appear as dots and are spread all over the cytosol. Category III predominantly found in severely

damaged cells represents totally fragmented mitochondria surrounding the nucleus. For quantification, at least 500 cells per condition were counted blinded to treatment using epifluorescence microscope DMI6000B (Leica, Wetzlar, Germany). For statistical analysis, experiments were performed at least three times.

2.9.3 Immunocytochemistry

For visualisation of changes in the location of p53 and phospho-p53 during glutamate challenge, HT-22 cells were seeded in 8-well ibidi slides at a density of 17 000 cells/ well. After staining with MitoTracker® Deep Red, cells were challenged with glutamate (3 mM) for 3 and 6 h, respectively. Next, culture medium was removed, cells were carefully washed twice with 1x PBS and fixed with 4% PFA for 25 min at RT in the dark. Afterwards, cells were washed again twice with 1x PBS and permeabilised with a solution of 0.4% Triton® X-100 (Sigma-Aldrich, Taufkirchen, Germany) in PBS for 5 min at RT followed by a further washing step with 1x PBS. To avoid unspecific binding of the p53 antibody, blocking was performed with a solution of 3% horse-serum (Invitrogen, Karlsruhe, Germany) in PBS for 30 min at RT. For samples stained with phospho-p53 antibody, blocking was performed with a solution of 3% goat-serum (Invitrogen, Karlsruhe, Germany). Subsequently, p53 antibody diluted 1:100 in 3% horse-serum or phospho-p53 antibody diluted 1:100 in 3% goat-serum was applied and incubated overnight at 4 °C followed by 2 h at RT the next day. In order to remove unbound antibody, cells were washed three times with 1x PBS and then corresponding secondary biotinylated anti-mouse antibody diluted 1:200 in 3% horse-serum or secondary biotinylated anti-rabbit antibody diluted 1:200 in 3% goat-serum was added for 1.5 h at RT, respectively. Afterwards, cells were again washed three times with 1x PBS and stained with Streptavidin Oregon green (Invitrogen, Karlsruhe, Germany) for 40 min at RT in the dark. For removal of surplus dye, cells were again washed three times with 1x PBS and then stored at 4 °C in the dark in PBS or directly analysed. Images were obtained using confocal laser scanning microscope (Axiovert 200, LSM Image Software, Carl Zeiss, Jena, Germany). Light was collected through a 63 x 1.4 NA oil immersion objective. MitoTracker® Deep red was excited at 633 nm and emission was detected at 670 nm. Fluorescence of Streptavidin Oregon green was excited at 488 nm and emission was detected at 505 nm. To control for specificity of p53 antibody binding, emission of negative controls lacking incubation with primary p53 antibody was

recorded. For digital analysis of fluorescence intensity the software LSM Image Browser 4.2.0 (Carl Zeiss, Jena, Germany) was used.

2.10 Analysis of p53 transcriptional activity

2.10.1 Cloning of p53-firefly-luciferase-plasmid

To analyse the effects of p53 siRNA on p53 transcriptional activity a p53-firefly-luciferase reporter plasmid was generated containing six consensus p53 DNA binding elements[202] with the following sequences: sense 5'-CTAGCAGACATGCCTA GACATGCCTAGACATGCCTAGACATGCCTAGACATGCCTAGACATGCCTCGA-3' and anti-sense 5'-GATCTCGAGGCATGTCTAGGCATGTCTAGGCATGTCTAGG CATGTCTAGGCATGTCTAGGCATGTCTG-3'. Both oligonucleotides were flanked by restriction sites for the enzymes Nhe1 and Bgl2. First, both oligonucleotides were phosphorylated in separate reactions for 1 h at 37 °C:

Antisense/ sense oligonucleotide (100 µM)	1 µl
10x T4 ligase buffer	2 µl
T4 polynucleotide kinase	1.5 µl
H_2O	15.5 µl

Afterwards, phosphorylated oligonucleotides were annealed in a water bath at 95 °C for 5 min and slowly cooled down to RT:

Phosphorylated sense oligonucleotide	2 µl
Phosphorylated antisense oligonucleotide	2 µl
Annealing buffer (10 mM Tris, 50 mM NaCl, 1 mM EDTA)	46 µl

p53-firefly-luciferase reporter plasmid was generated via ligation of annealed oligonucleotides and pTAL-Luciferase (Luc) reporter plasmid using the Nhe1 and Bgl2 restriction sites. pTAL-Luc vector contains a TATA-like promoter region from the herpes simplex virus thymidine kinase (HSV-TK) promoter driving the firefly luciferase expression upon p53 binding to its enhancer element. The p53-firefly-luciferase-reporter plasmid was transformed in E.coli and prepared as described in 2.1.9.

2.10.2 Measurement of p53 transcriptional activity by luminescence

For analysis of p53 transcriptional activity, HT-22 cells were transfected with p53 siRNA in 24-well plates at a density of 30 000 cells/well and grown overnight. After transfection with 17 ng renilla-luciferase-plasmid and 108 ng p53-firefly-luciferase reporter plasmid/well as described in 2.3.2.1 and growing for 24 h more, cells were challenged with glutamate. After the appropriate time, medium was removed, cells once washed with 1x PBS and luciferase activity measured with Dual-Luciferase® Assay Kit (Promega, Madison, USA) according to manufacturer's protocol. Briefly, 100 µl lysis buffer were applied and cells lysed for 30 min at 37 °C. Afterwards, 2 µl of lysate were transferred into a white 96-well plate. Next, 25 µl Luciferase Assay Substrate reconstituted in Luciferase Assay Buffer II were added and luminescence of firefly luciferase which directly correlates with p53 transcriptional activity was recorded with FluoStar OPTIMA (BMG Labtech, Offenbach, Germany). The luminescence resulted from the following reaction:

$$\text{Luciferin} + \text{ATP} + O_2 \xrightarrow[Mg^{2+}]{\text{Firefly luciferase}} \text{Oxyluciferin} + \text{AMP} + PP_i + CO_2 + \text{Light}$$

In order to control for differences in transfection efficiency luminescence of co-transfected renilla-luciferase-plasmid was determined. Therefore, 25 µL Stop & Glow® Reagent diluted 1:100 with Stop & Glow® Buffer were added to stop the reaction of firefly luciferase and initiate the following reaction of renilla luciferase:

$$\text{Colenterazine} + O_2 \xrightarrow{\text{Renilla luciferase}} \text{Colenteramide} + CO_2 + \text{Light}$$

Emitted light was again detected with FluoStar OPTIMA (BMG Labtech, Offenbach, Germany). Luminescence generated by firefly luciferase was normalised to luminescence produced by renilla luciferase and values of control cells were set to 100%. Data were depicted as bar graphs. For statistical analysis, experiments were repeated three times with n=4.

2.11 RNA analysis

2.11.1 RNA sample preparation

For RNA analysis cells were seeded in 6-well plates at a density of 160 000-180 000 cells/well. 24 h later, cells were treated with glutamate and particular inhibitors of cell death. SiRNA transfections were performed with 120 000 cells/well and if needed, glutamate was applied two days later. After the appropriate time of treatment, culture medium was collected, cells were scratched in 1x PBS and centrifuged at 200 x g for 5 min. After washing once with 1x PBS, pellet was resuspended in 350 µl Lysis Solution TR containing 1% β-mercaptoethanol and immediately frozen in liquid nitrogen. RNA extraction was performed with InviTrap® Spin Universal RNA Mini Kit (Stratec Molecular GmbH, Berlin, Germany) according to manufacturer's protocol. Briefly, lysates and any precipitates were directly pipetted onto the provided DNA-Binding Spin Filter and incubated for 1 min. After centrifugation for 2 min at 11 000 x g DNA-Binding Spin Filter was disposed and 250 µl 70% ethanol was added to the flow-through. The mixture was then transferred onto a RNA-RTA-Spin Filter, incubated for 1 min and centrifuged at 11 000 x g for 1 min. Now, the flow-through was discarded and 600 µl provided Wash Buffer R1 applied. After another centrifugation step at 11 000 x g for 1 min, flow-through was again disposed and 700 µl Wash Buffer R2 put on the RNA-RTA-Spin Filter which was removed by centrifugation. This step was repeated once, followed by 4 min centrifugation at maximum speed to fully eliminate any remaining ethanol. For elution of total RNA, RNA-RTA-Spin Filter was transferred into special RNase-free Elution Tubes, incubated with 60 µl Elution Buffer R for at least 2 min and centrifuged for 1 min at 11 000 x g. RNA samples were stored at -80 °C until usage.

2.11.2 Determination of RNA amount

For determination of total RNA amount absorbance at 260 nm was measured with the NanoPhotometer™ (Implen, Munich, Germany). In order to evaluate the purity of the extracted RNA the ratio of absorbance at 260 nm and 280 nm was used. A ratio of ~2.0 is commonly accepted as pure.

2.11.3 Reverse transcriptase polymerase chain reaction

To analyse RNA expression levels, isolated RNA of particular interest has to be amplified. For this purpose, the reverse transcriptase polymerase chain reaction (RT-PCR) is used. RT-PCR consists of two reactions. First, RNA is transcribed by reverse transcriptase into complementary DNA which is in a next step amplified by DNA-polymerase via PCR.

In the present work, the SuperScript III One Step RT-PCR System with Platinum® Taq (Invitrogen, Karlsruhe, Germany) was used to perform RT-PCRs. Primers were obtained from Eurofins (Eurofins MWG Operon,Ebersberg, Germany) and are listed in table 12.

Table 12: Primer sequences for RT-PCR

Primer	Sequence
AIF forward	5'-GCGTAATACGACTCACTATAGGGAGATCCAGGCAACTTGTTCCAGC-3'
AIF reverse	5'-CGTAATACGACTCACTATAGGGAGACCTCTGCTCCAGCCCTATCG-3'
ATF4 forward	5'-CGGGTGTCCCTTTCCTCT-3'
ATF4 reverse	5'-CAGGCACTGCTGCCTCTAAT-3'
Bid forward	5'-GGGA ACTGCCTGTGCAAGCTTAC-3'
Bid reverse	5'-CAGTGAGGFCCTTGTCTCTGAA-3'
DRP1 forward	5'-ACAGGAGAAGAAAATGGAGTTTGAAGCAG-3'
DRP1 reverse	5`-AACAAATCCTAGCACCACGCAT-3`
GAPDH forward	5'-AGGCCGGTGCTGAGTAT-3'
GAPDH reverse	5'-TGCCTGCTTCACCACC TTCT-3'
MDM2 forward	5'-CCAGCTTCGGAACAAGAGAC-3'
MDM2 reverse	5'-ACACAAT GTGCTGCTGCTTC-3'
MnSOD forward	5'-GCGGTCGTGTAAACCTCAAT-3'
MnSOD reverse	5'-CCAGAGCCTCGTGGTACTTC-3'
PHD1 forward	5'-TTGCCTGGGTAGAAGGTCAC-3'
PHD1 reverse	5'-GCTCGATGTTGGCTACCACT-3'
PHD2 forward	5'-AGCCATGGTTGCTTGTTACC-3'
PHD2 reverse	5'-CTCGCTCATCTGCATCAAAA-3'
PHD3 forward	5'-TCAACTTCCTCCTGTCCCTCATC-3'
PHD3 reverse	5'-GCGAACATAACCTGTCCCATTTC-3'
p21 forward	5'-GCAGATCCACAGCGATATCC-3'
p21 reverse	5'-CAACTGC TCACTGTCCACGG-3'
p53 forward	5'-GACCGCCGTACAGAAGAAGA-3'
p53 reverse	5'-GCCCCACTTTCTTGACC-3'
PUMA forward	5'-CAGACTGTGAATCCTGTGCT-3'
PUMA reverse	5'-ACAGTATCTTACAGGCTGGGG-3'

The RT-PCR reactions were prepared as listed in Tab. 13-15.

Table 13: Sample preparation for RT-PCR of AIF, ATF4, Bid, DRP1, MDM2, MnSOD, PHD1, PHD2, p21, p53 and PUMA

RNA	300-500 ng
2x Reaction Mix	12.5 µl
Forward primer (5 µM)	1 µl
Reverse Primer (5 µM)	1 µl
Taq polymerase	1 µl
RNase free H_2O	ad 25 µl

Table 14: Sample preparation for RT-PCR of GAPDH

RNA	300-500 ng
2x Reaction Mix	12.5 µl
Forward primer (5 µM)	1 µl
Reverse primer (5 µM)	1 µl
Taq polymerase	0.5 µl
RNase free H_2O	ad 25 µl

Table 15: Sample preparation for RT-PCR of PHD3

RNA	500 ng
2x Reaction Mix	12.5 µl
$MgSO_4$ (5 mM)	4.5 µl
Forward primer (5 µM)	1 µl
Reverse primer (5 µM)	1 µl
Taq polymerase	1 µl
RNase free H_2O	ad 25 µl

Following RT-PCR cycler programmes were used:

Table 16: RT-PCR cycler programme for AIF

60 °C	30 min	
95 °C	2 min	
95 °C	30 s	34x
57 °C	1 min	
70 °C	2 min	
70 °C	10 min	
4 °C	∞	

Table 17: RT-PCR cycler programme for ATF4

60 °C	30 min	
95 °C	2 min	
94 °C	30 s	28x
60 °C	1 min	
72 °C	1 min	
72 °C	10 min	
4 °C	∞	

Table 18: RT-PCR cycler programme for Bid

60 °C	30 min	
95 °C	2 min	
95 °C	30 s	27x
53 °C	1 min	
70 °C	2 min	
70 °C	10 min	
4 °C	∞	

Table 19: RT-PCR cycler programme for DRP1

60 °C	30 min	
95 °C	2 min	
95 °C	30 s	26x
57 °C	1 min	
70 °C	2 min	
70 °C	10 min	
4 °C	∞	

Table 20: RT-PCR cycler programme for GAPDH

60 °C	30 min	
95 °C	2 min	
95 °C	30 s	25x
57 °C	1 min	
70 °C	2 min	
70 °C	10 min	
4 °C	∞	

Table 21: RT-PCR cycler programme for MDM2

60 °C	30 min	
95 °C	2 min	
95 °C	30 s	30x
48 °C	1 min	
70 °C	2 min	
70 °C	10 min	
4 °C	∞	

Table 22: RT-PCR cycler programme for MnSOD

60 °C	30 min	
95 °C	2 min	
95 °C	30 s	25x
56 °C	1 min	
70 °C	2 min	
70 °C	10 min	
4 °C	∞	

Table 23: RT-PCR cycler programme for PHD1

60 °C	30 min	
95 °C	2 min	
95 °C	30 s	27x
55 °C	30 s	
70 °C	30 s	
70 °C	10 min	
4 °C	∞	

Table 24: RT-PCR cycler programme for PHD2

60 °C	30 min	
95 °C	2 min	
95 °C	30 s	25x
52 °C	30 s	
70 °C	30 s	
70 °C	10 min	
4 °C	∞	

Table 25: RT-PCR cycler programme for PHD3

60 °C	30 min	
95 °C	2 min	
95 °C	30 s	30x
53 °C	1 min	
70 °C	1 min	
70 °C	10 min	
4 °C	∞	

Table 26: RT-PCR cycler programme for p21

60 °C	30 min	
95 °C	2 min	
95 °C	30 s	30x
52 °C	1 min	
70 °C	2 min	
70 °C	10 min	
4 °C	∞	

Table 27: RT-PCR cycler programme for p53

60 °C	30 min	
95 °C	2 min	
95 °C	30 s	26x
54.5 °C	30 s	
68 °C	30 s	
68 °C	5 min	
4 °C	∞	

Table 28: RT-PCR cycler programme for PUMA

60 °C	30 min	
95 °C	2 min	
95 °C	30 s	25x
54 °C	1 min	
70 °C	2 min	
70 °C	10 min	
4 °C	∞	

2.11.4 Agarose gel electrophoresis

RT-PCR products were visualised via agarose gel electrophoresis and ethidium bromide staining, a fluorescent dye intercalating with DNA. Therefore, 1.5% agarose gels were prepared suspending 1.5 g agarose (Sigma Aldrich, Taufkirchen, Germany) in 100 ml 1x TAE buffer (Tab. 29) and carefully warmed in a microwave to dissolve the agarose. After putting the solution in a gel frame 2 µl ethidium bromide solution (10 mg/ml; Sigma-Aldrich, Taufkirchen, Germany) was added and equally distributed. RT-PCR products were mixed with 2.8 µl 10x loading dye (Tab. 30) and 15 µl were transferred on the solid gel. For analysis of product size 5 µl of GeneRuler 100 bp Plus DNA Ladder (Thermo Scientific, Dreieich, Germany) was placed next to the samples on the gel. Electrophoresis was performed at 80 V for 30-45 min. DNA products were visualised under UV light with Chemidoc-XRS Imaging System (Bio-Rad, Munich, Germany) and quantified with the Quantity One software (Bio-Rad, Munich, Germany).

Table 29: 50x TAE buffer pH 8.5

Tris base	242 g
0.5 M EDTA	100 ml
Acetic acid	57.1 ml
HCl	qs for pH adjustment
Bidest H_2O	ad 1l

Table 30: 10x Loading dye

Glycerol	20 ml
EDTA	186.1 mg
Tris	60.57 mg
Orange G	125 mg
Bidest H_2O	ad 50 ml

2.12 Protein analysis

2.12.1 Protein sample preparation

For Western blot analysis, cells were seeded in 6-well plates at a density of 160 000-180 000 cells/well. 24 h later, cells were treated with glutamate and particular inhibitors of cell death. SiRNA transfections were performed with 120 000 cells/well and if needed, glutamate was applied two days later. After the appropriate time of treatment, culture medium was removed, cells were washed once with 1x PBS and harvested by scratching in 70-100 µl protein lysis buffer (Tab. 31). All steps were performed on ice. For the complete disruption of membranes, samples were immediately frozen in liquid nitrogen. After storage at -80 °C for at least 1 h, lysates were centrifuged at 10 000 x g for 15 min at 4°C to remove insoluble fragments. Supernatant was transferred into new Eppendorf Cups and kept on ice for the determination of protein content and subsequent Western blot analysis.

Table 31: Stock solution of protein lysis buffer pH 7.8

D-Mannitol	4.56 g
Tris base	0.788 g
EDTA	0.038 g
EGTA	0.038 g
Bidest H_2O	ad 100 mL

This stock mix was stored in aliquots of 10 ml at -20 °C. Prior to use, following substances were added:

100 mM DTT	100 µl
Triton® X-100	100 µl
Complete Mini Protease Inhibitor Cocktail	1 tablet
PhosSTOP	1 tablet

Complete Mini Protease Inhibitor Cocktail and PhosSTOP were obtained from Roche (Penzberg, Germany). Completed lysis buffer was stored at 4 °C and used for the maximum of one week.

2.12.2 Determination of protein amount

Protein amount of cell lysates was determined using bicinchoninic acid assay (BCA). This assay is based on a colorimetric reaction. First, Cu^{2+} is reduced to Cu^{+} by the peptide bonds of the proteins analysed with this assay. This step is proportional to the available amount of proteins and proceeds in a temperature-dependent manner. Therefore, the assay is performed at 60 °C. Second, Cu^{+} forms a purple complex chelating with two molecules of bicinchoninic acid which can be quantified by measuring absorption.

In the present work the Pierce® BCA Protein Assay Kit (Perbio Science, Bonn, Germany) was used according to manufacturer's protocol. Briefly, 2.5 µl cell lysate or protein standard were mixed with 100 µl of a 1:50 solution of reagent B and reagent A. After shaking with 650 rpm at 60 °C for 30 min, samples and standards were centrifuged for 20 s at maximum speed and 100 µl each transferred into a 96-well plate. Absorption was measured with FluoStar OPTIMA (BMG Labtech, Offenbach, Germany) at 562 nm. Protein amount of each sample was calculated via a protein standard curve including 0-200 µg/100 µl bovine serum albumin (Perbio Science, Bonn, Germany).

2.12.3 Gel electrophoresis and Western blot analysis

For Western blot analysis it is necessary to separate the proteins of cell lysates. To this end sodium dodecyl sulfate polyacrylamide gel electrophoresis (SDS-PAGE) was used. By this method proteins are separated by their molecular weight in an electric field.

Following solutions and buffers were used for SDS-PAGE and subsequent Western blot analysis:

Table 32: 1.5 M Tris pH 8.8

Tris-HCl	23.6 g
HCl	qs for pH adjustment
Bidest H_2O	ad 100 ml

Table 33: 0.5 M Tris pH 6.8

Tris-HCl	7.88 g
HCl	qs for pH adjustment
Bidest H_2O	ad 100 ml

Table 34: 10% Sodium dodecyl sulfate (SDS)

SDS	1 g
Bidest H_2O	ad 10 ml

Table 35: 10% Ammonium persulfate (APS)

APS	1 g
Bidest H_2O	ad 10 ml

Table 36: 3.5% Stacking gel

0.5 M Tris pH 6.8	2.5 ml
10% SDS	0.1 ml
30% Acrylamid/ 0.8% Bisacrylamid solution 37.5:1	1.2 ml
10% APS	0.05 ml
TEMED	0.02 ml
Bidest H_2O	ad 10 ml

Table 37: 12.5% Separation gel

1.5 M Tris pH 8.8	2.5 ml
10% SDS	0.1 ml
30% Acrylamid/ 0.8% Bisacrylamid solution 37.5:1	4 ml
10% APS	0.05 ml
TEMED	0.01 ml
Bidest H_2O	ad 10 ml

Table 38: 10x Electrophoresis buffer

Tris base	30 g
SDS	10 g
Glycine	144 g
Bidest H_2O	ad 1 l

For SDS-PAGE 10x electrophoresis buffer was diluted 1:10 with bidest H_2O.

Table 39: 5x SDS-sample buffer

1.5 M Tris-HCl pH 6.8	4 ml
Glycerol	10 ml
SDS	2 g
β-Mercaptoethanol	5 ml
1% Bromphenol blue	1 ml

Table 40: 10x Transfer buffer pH 8.3

Tris base	30 g
Glycine	144 g
HCl	qs for pH adjustment
Bidest H_2O	ad 1l

10x transfer buffer was diluted 1:10 prior to use with bidest H_2O and 20% methanol was added.

Table 41: 10x TBS pH 7.5

NaCl	292 g
Tris base	24.2 g
HCl	qs for pH adjustment
Bidest H2O	ad 1 l

Table 42: 1x TBST

10x TBS	100 ml
Tween® 20	0.5 ml
Bidest H_2O	ad 1l

Table 43: 5% Blocking buffer

Skim milk powder	25 g
TBST	ad 500 ml

Table 44: Stripping buffer pH 2.2

Glycine	15 g
SDS	1 g
Tween® 20	10 ml
HCl	qs for pH adjustment
Bidest H_2O	ad 1l

According to the proteins to be detected, 30-70 µg protein amount was loaded onto the SDS-gel. Gels composed of 3.5% stacking (Tab. 36) and 12.5% separation gel (Tab. 37) were prepared with BIO-RAD (Munich, Germany) gel casting stand and casting frames. Protein samples were mixed with 5x SDS-sample buffer (Tab. 39), brought to equal volume by addition of bidest H_2O and heated up to 96 °C for 10 min while continuously shaking at 650 rpm. Subsequently, samples were put on the gel. For the identification of particular molecular weight, 5 µl of PageRuler^{TM} Plus Prestained Ladder (Fermentas, St. Leon-Rot, Germany) were also loaded on the gel. Gel electrophoresis was initially performed at 60 V. When the samples reached the separation gel, voltage was switched to 125 V until the desired separation was achieved. Thereafter, separated proteins were blotted onto a polyvinylidene fluoride

(PVDF) membrane. To this end, PVDF membrane was activated by incubation in methanol for 1 min, followed by 1x transfer buffer for 10 min. Meanwhile, SDS-gel and filter papers were also incubated in 1x transfer buffer. For Western blotting, a Mini Trans-Blot® Electrophoretic Transfer Cell (Bio-Rad, Munich, Germany) was used. The transfer was performed with 20 mA per gel for 21 h at 4 °C. After the transfer, the membrane was washed for 5 min with 1x TBS, followed by blocking with 5% blocking buffer for 1 h at RT. Subsequent incubation with particular primary antibody (Tab. 2) was performed overnight at 4 °C. The next day, incubation was continued for 1 h at RT and then the membrane was washed for 5 min with TBST (Tab. 42) before the corresponding secondary antibody was applied for one more hour at RT. In order to reduce background signalling, membrane was washed three times with TBST for 15 min. Afterwards, the membrane was put in a chemiluminescent substrate solution HRP-Juice (PJK GmbH, Kleinblittersdorf, Germany) for 1-2 min and Western blot signal was detected with semi-automated Chemidoc-XRS Imaging System (Bio-Rad, Munich, Germany) and quantified with the Quantity One software (Bio-Rad, Munich, Germany). For reprobing membrane with further primary antibodies, the membrane was washed briefly with TBST and then stripped with stripping buffer (Tab. 44) for 10 min, followed by 2x washing with 1x PBS and 2x with TBST for 5 min each. Next, the same procedure as previously described was executed beginning with blocking the membrane.

2.13 Statistical analysis

All data are given as means + standard deviation (SD). Statistical comparison between treatment groups was performed by analysis of variance (ANOVA) followed by Scheffé's post hoc test. Calculations were executed with Winstat standard statistical software (R. Fitch Software, Bad Krozingen, Germany).

3 Results

3.1 Glutamate sensitivity of HT-22 cells

HT-22 cells are immortalised mouse hippocampal neurons lacking NMDA-receptors[197]. High extracellular concentrations of glutamate induce oxidative stress through inhibition of the cystine/glutamate-antiporter (X_C^-) and GSH depletion, thereby causing a form of cell death termed oxytosis that is characterised by typical morphological and metabolic alterations[42,203]. Under control conditions, HT-22 cells exhibit spindle shaped morphology. Upon glutamate exposure, cells shrink, round up and finally, detach from the bottom of the culture dish (Fig. 10A). These changes were also reflected in a loss of cell viability in the MTT assay which appeared in a dose-dependent manner (Fig. 10A). An increase in AV and AV/PI positive cells after glutamate challenge (Fig. 10B) suggests a continuum of apoptotic and necrotic cell death paradigms induced by glutamate in this model system. The sensitivity of HT-22 cells towards glutamate varies depending on passage number and cell density. Consequently, in the present work 3-7 mM glutamate was used for the induction of cell death and particular analysis performed after 10-18 h of treatment.

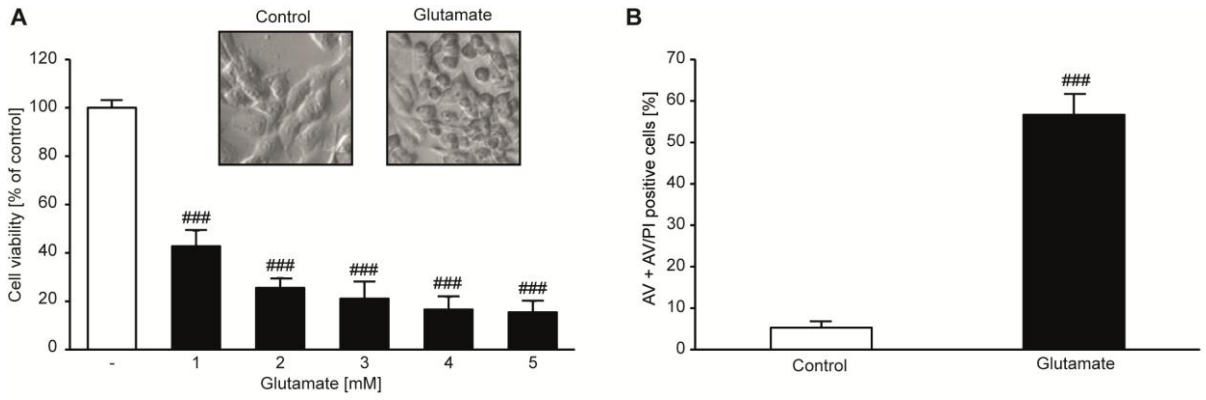

Figure 10: Glutamate sensitivity of HT-22 cells

A: Photomicrographs (100x magnification) showed glutamate-induced morphological alterations of HT-22 cells (3 mM, 14 h). MTT assay revealed dose-dependent loss of cell viability after glutamate exposure (16 h). Data are shown as mean + SD (n=6). $^{###}p<0.001$ compared to untreated control (ANOVA, Scheffé's test). **B:** FACS analysis detected glutamate-induced (3 mM, 12 h) increase in AV and AV/PI positive cells. Data are shown as mean + SD (n=4). $^{###}p<0.001$ compared to untreated control (ANOVA, Scheffé's test).

3.1.1 Mitochondrial demise in oxytosis

As described before, glutamate exposure induced lipid peroxidation and subsequent damage of mitochondria in the present model system of oxytosis[49]. This mitochondrial demise is characterised by distinct changes of mitochondrial morphology and function. In order to analyse and quantify these alterations in the present study, cells were divided into three categories depending on their mitochondrial appearance as previously established[71]. In healthy cells of category I, mitochondria mainly appear elongated and distributed all over the cell. Increasing oxidative stress leads to mitochondrial fission indicated by dotted, but still equally distributed mitochondria in category II cells. Severely damaged cells of category III already show morphological changes and mainly contain mitochondria which are highly fragmented and located in the vicinity of the nucleus (Fig. 11A). Quantification of these categories revealed a significant increase in cells of category III after the glutamate challenge (Fig. 11B).

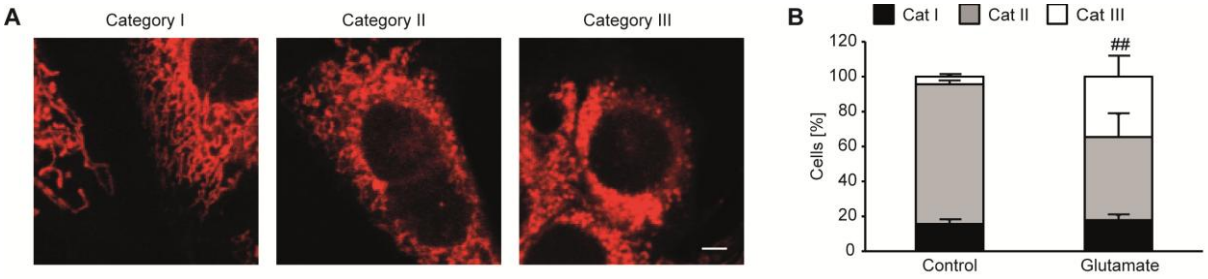

Figure 11: Glutamate induces changes in mitochondrial morphology

A: Confocal pictures (63x objective) showed mitochondrial categories. Category I: tubular, elongated; Category II: intermediate; Category III: fragmented. Scale bar: 10 µm. **B:** Quantification of 500 cells per condition counted without knowledge of treatment history revealed enhanced fragmentation upon glutamate challenge. Data are shown as mean + SD (n=4). $^{\#\#}p<0.01$ compared to Cat III of untreated control (ANOVA, Scheffé's test).

These morphological alterations were accompanied by a loss of MMP, another hallmark of oxytosis, detected by reduced TMRE fluorescence (Fig. 12A). Intact MMP is also required for proper ATP synthesis and thereby neuronal function[22]. Accordingly, ATP levels significantly decreased after application of glutamate (Fig. 12B) further confirming disturbed mitochondrial function and underlining the pivotal role of mitochondrial demise in this model of oxytosis.

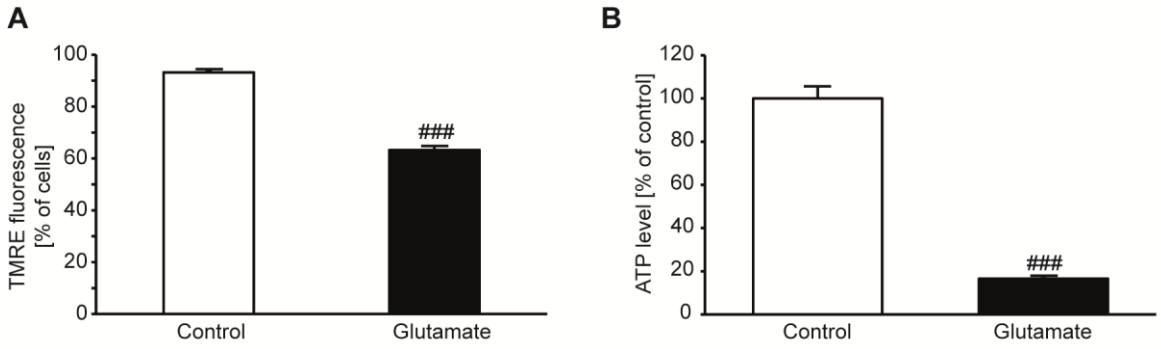

Figure 12: Glutamate disturbs mitochondrial function

A: FACS analysis revealed a loss of MMP indicated by reduced TMRE fluorescence upon glutamate challenge (3 mM, 12.5 h). Data are shown as mean + SD (n=4). ###p<0.001 compared to untreated control (ANOVA, Scheffé's test). **B:** Glutamate (7 mM, 14.5 h) induced a decrease of ATP levels. Data are shown as mean + SD (n=8). ###p<0.001 compared to untreated control (ANOVA, Scheffé's test).

3.2 Inhibition of p53 provides neuroprotection

Over the last years, many pharmacological and genetic studies showed the relevance of p53 in neurodegenerative processes *in vitro*[98,204] and *in vivo*[94,99,100,205]. Although several groups demonstrated beneficial effects of both genetic and pharmacological inhibition of p53 in different models of neurodegenerative diseases, these observations were not consistent throughout the literature[121,206]. In addition to transcriptional effects of p53, also direct detrimental effects at the level of mitochondria have been postulated[101,115,121]. In order to elucidate the effects of p53 on mitochondrial integrity and function in oxytosis, the p53-inhibitor PFTα[207] and a siRNA selectively targeting p53 were used in the present study.

3.2.1 PFTα prevents glutamate-induced cell death

First, the effect of PFTα on cell viability in oxytosis was investigated. To this end HT-22 cells were simultaneously treated with glutamate and PFTα or PFTα alone to rule out substance-related toxicity. Glutamate induced typical morphological signs of cell death such as shrinking and rounding of the cells. PFTα itself did not alter cell morphology and completely preserved HT-22 cells despite incubation with glutamate (Fig. 13A). These morphological observations were also confirmed in the MTT assay indicating the protection of cell viability by PFTα. The protective effect occurred in a dose dependent manner starting at a concentration of 5 µM, and almost full protection was achieved at a concentration of 10 µM PFTα. Therefore, this

concentration was used for further experiments, as it also did not exhibit any toxicity (Fig. 13B). In order to verify the beneficial effect of PFTα on cell viability, an AV/PI staining with subsequent FACS analysis was performed. Glutamate led to a dramatic increase in AV/PI positive cells shown in a shift of the cloud from the lower left quadrant to the upper right in dot plots derived from FACS analysis. This shift was strongly abolished by co-treatment with PFTα (Fig. 13C).

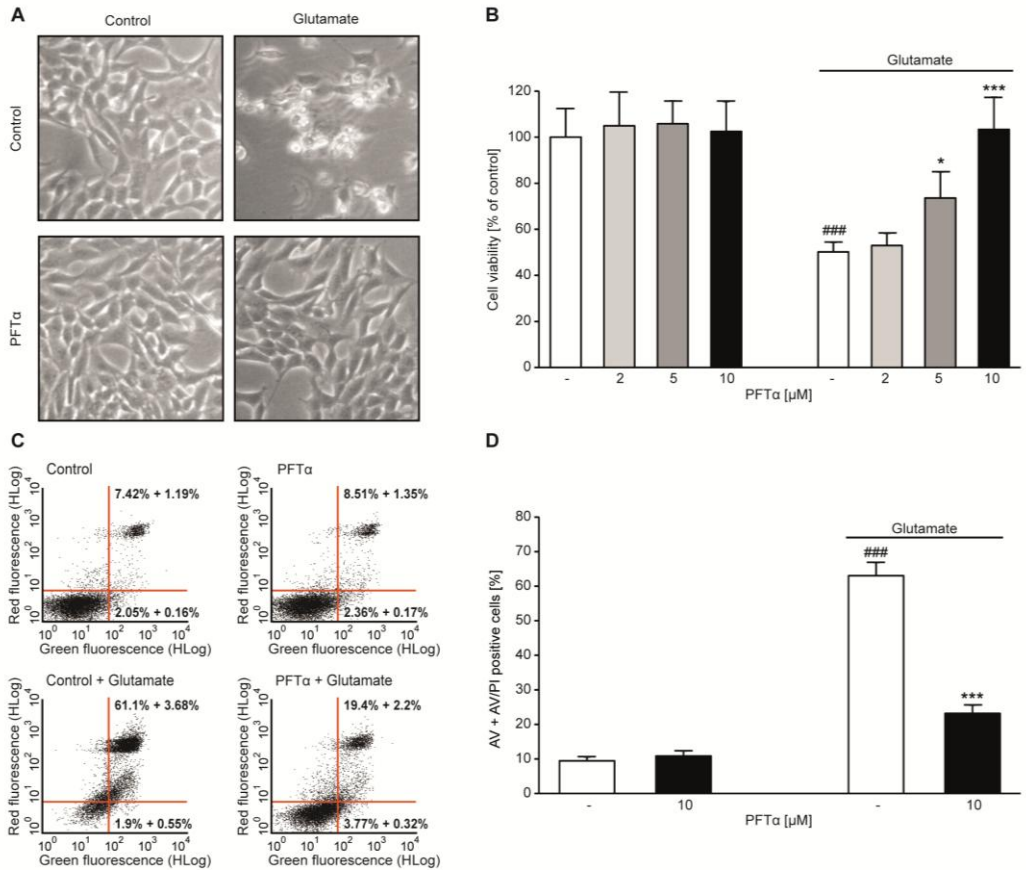

Figure 13: PFTα prevents glutamate-induced cell death

A: Photomicrographs (100x magnification) depicted glutamate (3 mM, 14 h) induced morphological alterations of HT-22 cells which were prevented by co-treatment with PFTα (10 µM). **B:** MTT assay showed concentration-dependent protective effect of PFTα against glutamate toxicity (7 mM, 16 h). Data are shown as mean + SD (n=8). $^{###}$p<0.001 compared to untreated control; *p<0.05 and ***p<0.001 compared to glutamate treated control (ANOVA, Scheffé's test). **C, D:** AV/PI staining and subsequent FACS analysis revealed protection of PFTα against glutamate exposure (4 mM, 14.5 h); representative dot plots (C) and quantification (D). Data are shown as mean + SD (n=4). $^{###}$p<0.001 compared to untreated control; ***p<0.001 compared to glutamate treated control (ANOVA, Scheffé's test).

The effect was also mirrored by corresponding quantification where the values for AV positive cells reflecting early apoptotic cell death and AV/PI positive cells reflecting late apoptotic and necrotic cell death were combined to determine total cell death.

PFTα significantly reduced the percentage of dead cells, but could not fully prevent glutamate-induced cell death (Fig. 13D). To further characterise the effects of PFTα, its neuroprotective potential under post-treatment conditions was investigated. HT-22 cells were seeded in 96-well E-plates and challenged with glutamate. Two, 4 and 6 h after the onset of glutamate exposure PFTα was applied and cell death was recorded over time using the xCELLigence system. A post-treatment with PFTα up to 4 h after glutamate exposure significantly reduced cell death, but both 2 h and 4 h of post-treatment were not as effective as the simultaneous administration of PFTα and glutamate (Fig. 14A, B).

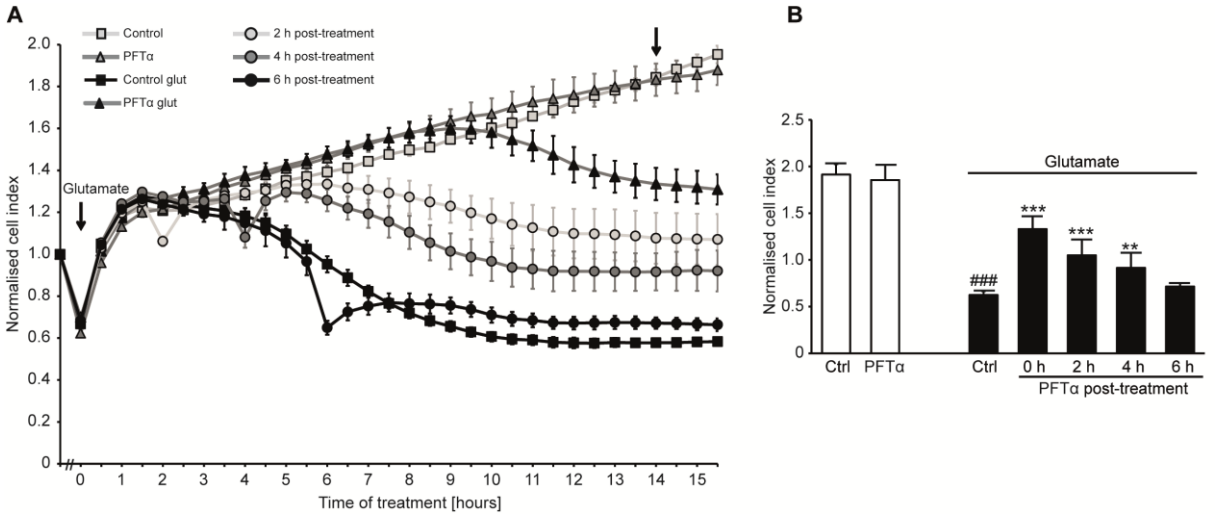

Figure 14: Post-treatment with PFTα protects HT-22 cells against glutamate-induced oxytosis

A: Impedance reflecting cell viability was measured using the xCELLigence system under post-treatment conditions when PFTα (10 µM) was added 2, 4 and 6 h after the onset of glutamate (4 mM). PFTα attenuated cell death compared to glutamate treated controls when applied up to 4 h after the onset of glutamate. **B:** Bar graph evaluation of the 14 h time point from the xCELLigence recordings of A (right black arrow). Data are given as mean + SD (n=7). $^{###}$p<0.001 compared to untreated control; **p<0.01 and ***p<0.001 compared to glutamate treated control (ANOVA, Scheffé's test).

3.2.2 Mitochondrial integrity is preserved by PFTα

Mitochondrial integrity was analysed to further clarify the role of p53 at the level of mitochondria during oxytosis and to check whether PFTα mediated neuroprotection was associated with mitochondrial protection. To this end, changes in MMP upon glutamate and PFTα treatment were analysed via TMRE staining and subsequent FACS analysis. PFTα alone did not affect MMP, while glutamate-induced depolarisation of the mitochondrial membrane as indicated by a leftward shift of the

FACS curve caused by a loss of TMRE fluorescence. This breakdown of MMP was fully abolished by co-treatment with PFTα (Fig. 15A).

Another parameter to assess mitochondrial function is the analysis of ATP levels. Unfortunately, evaluation of ATP content for PFTα was not possible, because the ATP assay used in the present work relies on ATP dependent firefly luciferase activity which is directly inhibited by PFTα at concentrations higher than 1 µM[208].

Hence, HT-22 cells were stained with MitoSOX™ Red after glutamate exposure to further examine mitochondrial ROS production. FACS analysis revealed a fourfold increase in mitochondrial ROS due to glutamate toxicity. PFTα entirely prevented enhanced formation of mitochondrial ROS (Fig. 15B). In addition, PFTα also inhibited glutamate-induced mitochondrial fission and preserved mitochondrial morphology as previously shown by Sebastian Diemert in our laboratory[68,209]. Taken together, these data suggest that PFTα acts at the level of mitochondria.

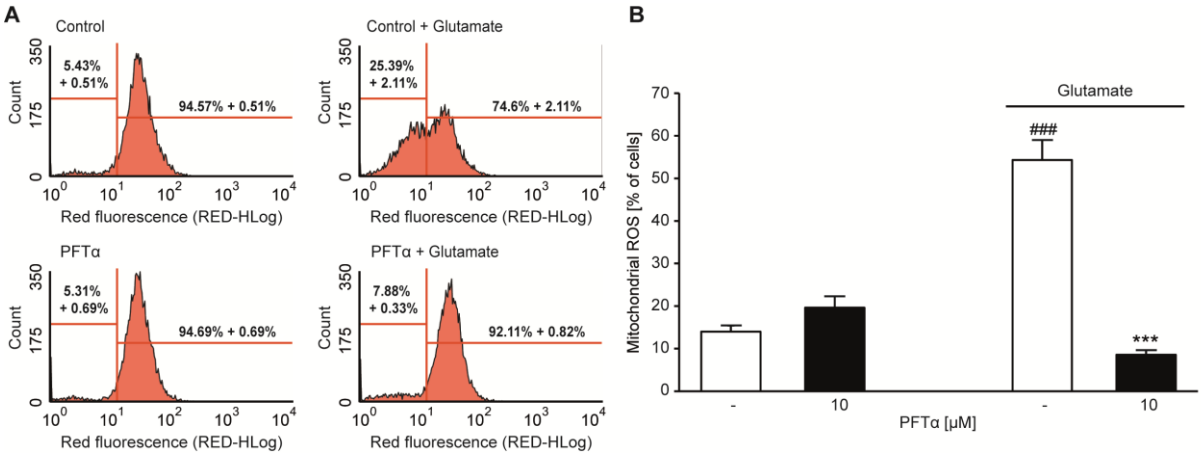

Figure 15: PFTα preserves mitochondrial integrity

A: Representative plots showed reduced TMRE fluorescence after glutamate exposure (3 mM, 14 h) which was fully prevented by co-treatment with PFTα (10 µM). **B:** PFTα (10 µM) abolished glutamate-induced (4 mM, 14.5 h) increase in mitochondrial ROS. Data are given as mean + SD (n=4). ###p<0.001 compared to untreated control; ***p<0.001 compared to glutamate treated control (ANOVA, Scheffé's test).

3.2.3 PFTα reduces lipid peroxidation

Lipid peroxidation is a main trigger mechanism of mitochondrial demise in oxytosis. In HT-22 cells, lipid peroxidation due to glutamate toxicity occurs in two steps: a first small increase and a second, much more pronounced one leading to mitochondrial fragmentation and dysfunction[46,49]. The effect of PFTα on formation of lipid peroxides was thus examined at 7 and 15 h after the onset of glutamate.

For this purpose, cells were stained with BODIPY 581/591 C11 and analysed by FACS. Representative FACS plots revealed a strong shift from red to green fluorescence after glutamate challenge for 7 h indicating enhanced lipid peroxidation which was reduced by PFTα in a dose dependent manner (Fig. 16A) according to the previous findings of the MTT assay (Fig. 13B). After 15 h of glutamate treatment, PFTα was still able to diminish formation of lipid peroxides (Fig. 16B) to a similar level as after 7 h of exposure. Notably, PFTα could not fully block glutamate-induced lipid peroxidation proposing that PFTα probably acts downstream of the first, but upstream of the second burst of ROS, at the level of mitochondria.

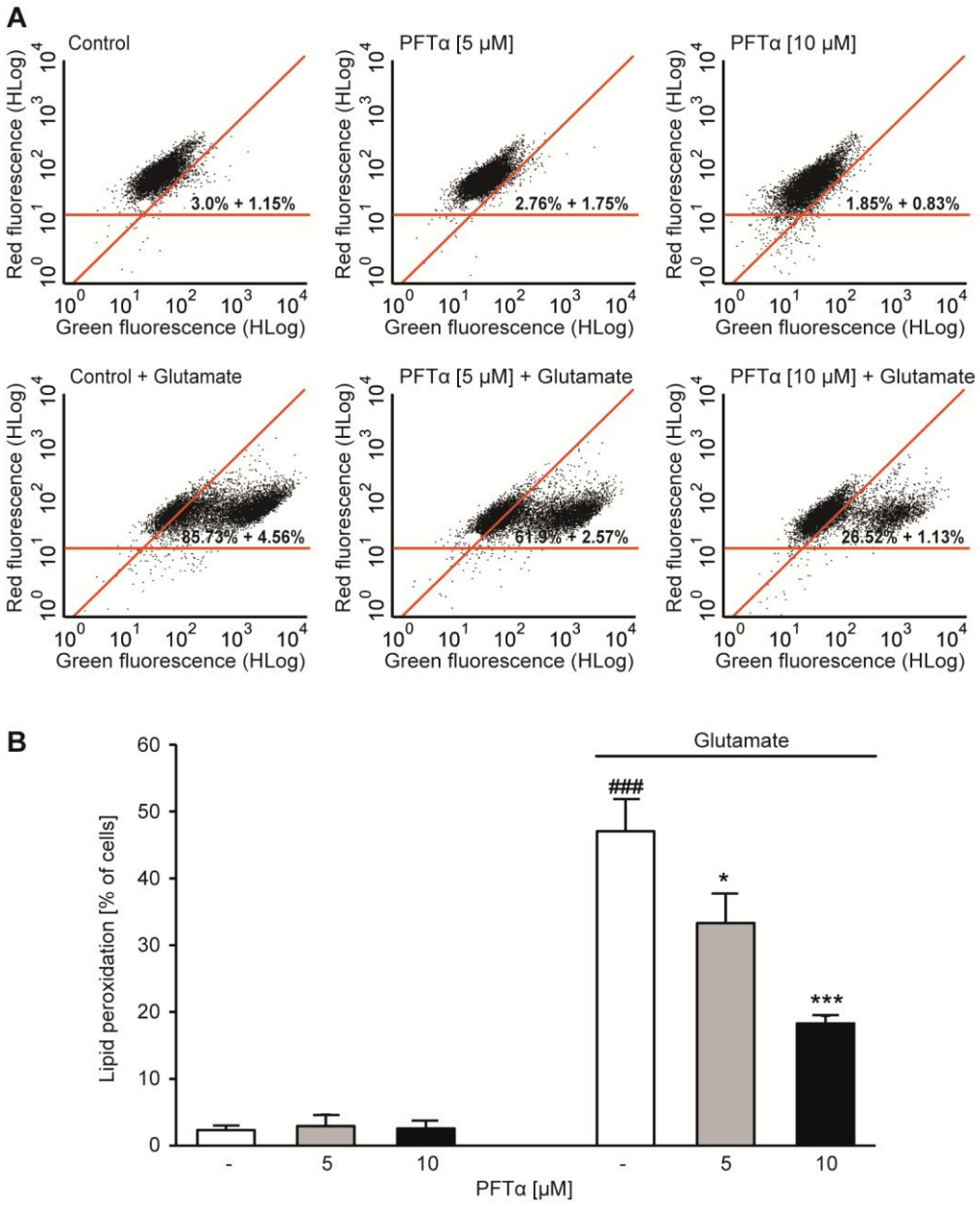

Figure 16: PFTα attenuates lipid peroxidation

A: Representative FACS plots revealed enhanced formation of lipid peroxides after 7 h of glutamate (7 mM) treatment which was attenuated by co-treatment with PFTα in a dose dependent manner. **B:** PFTα diminished lipid peroxidation in a dose dependent manner also 15 h after the onset of glutamate (7 mM). Data are given as mean + SD (n=4). ###p<0.001 compared to untreated control; *p<0.05 and ***p<0.001 compared to glutamate treated control (ANOVA, Scheffé's test).

3.2.4 p53 gene silencing delays glutamate-induced cell death

The previous results suggested a pivotal role of p53 in glutamate-induced mitochondrial dysfunction and subsequent cell death. To confirm this assumption the effects of down regulation of p53 on cell viability and mitochondrial function were studied in the model of oxytosis. Knockdown of p53 was achieved by siRNA approaches and confirmed at mRNA and protein levels by RT-PCR and Western blot

analysis, respectively (Fig. 17A). p53 silencing did not affect cell viability at control conditions, but significantly attenuated glutamate-induced cytotoxicity. Remarkably, simultaneous treatment of glutamate challenged cells with PFTα was much more effective than p53 gene silencing alone as shown by the MTT assay (Fig. 17B).

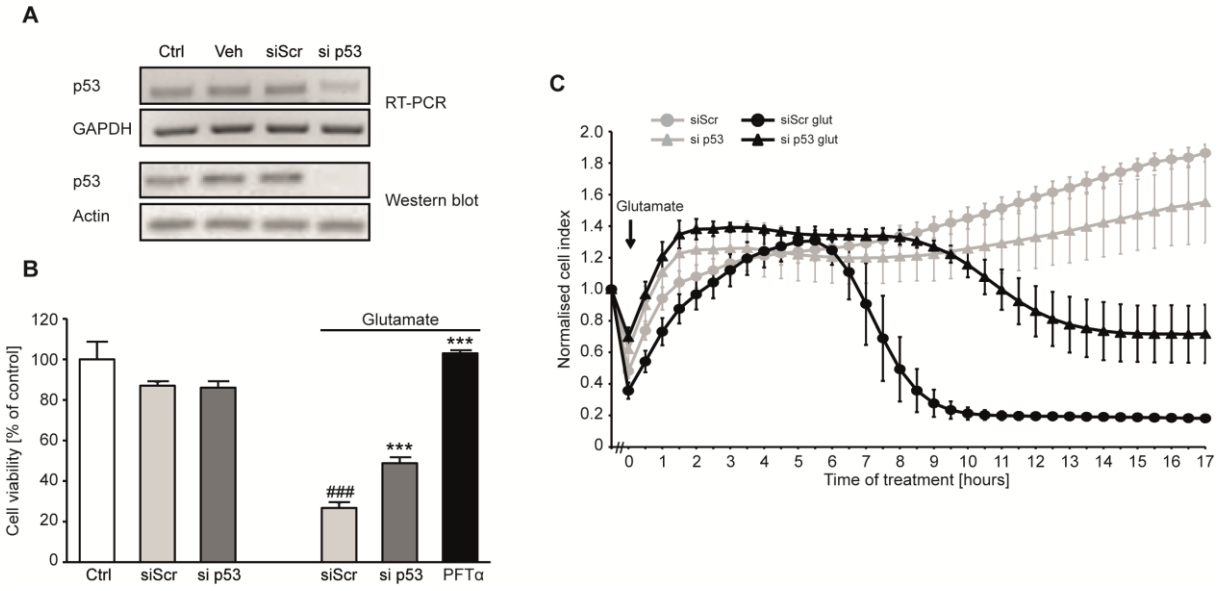

Figure 17: p53 gene silencing delays glutamate-induced cell death

A: Knockdown of p53 by siRNA (si p53, 20 nM) was verified by RT-PCR and Western blot analysis 48 h after transfection. **B:** MTT assay showed increased cell viability of cells transfected with si p53 (20 nM) compared to cells transfected with scrambled control siRNA (siScr, 20 nM) 48 h prior to glutamate challenge (3 mM, 14 h). PFTα (10 µM) was used as positive control for protection. Data are given as mean + SD (n=4). $^{###}$p<0.001 compared to untreated siScr; ***p<0.001 compared to glutamate treated siScr (ANOVA, Scheffé's test). **C:** xCELLigence real-time measurements revealed that cells transfected for 48 h with p53 siRNA (20 nM) were transiently protected against treatment with 3 mM glutamate (glut) compared to cells transfected with scrambled siRNA.

Since the MTT assay just provided information for one particular time point, next the xCELLigence system was used to study kinetics of cell death in cells transfected with a p53 siRNA (si p53) compared to cells transfected with a scrambled control siRNA (siScr). Down regulation of p53 delayed cell death after glutamate exposure for about 2 h (Fig. 17C). These findings explain well the less pronounced protection by si p53 versus PFTα treatment observed in the MTT assay, since PFTα has been shown before to delay cell death for about 5-6 h (Fig. 14A). In order to confirm the effects of si p53 a siRNA smart pool specifically targeting p53 (si p53 smart) was used in additional experiments to silence p53. Functionality of the knockdown was verified at mRNA and protein levels by RT-PCR and Western blot analysis, respectively

(Fig. 18A). Gene silencing of p53 by si p53 smart also attenuated glutamate toxicity shown by an increased cell viability in the MTT assay (Fig. 18B) indicating that the observed protection was in fact attributed to p53 silencing.

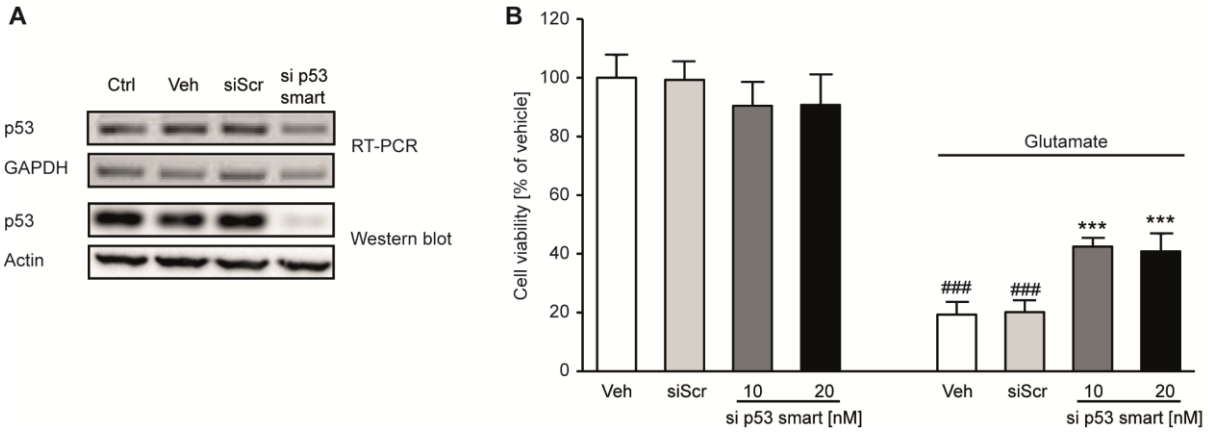

Figure 18: Selective p53 knockdown attenuates glutamate toxicity

A: Knockdown of p53 by siRNA a smart pool specifically targeting p53 (si p53 smart, 10 nM) was verified by RT-PCR and Western blot analysis 48 h after transfection. **B:** MTT assay showed protection of cells transfected with different concentrations of si p53 smart compared to cells transfected with scrambled control siRNA (siScr, 20 nM) 48 h prior to glutamate exposure (8 mM, 12.5 h). Data are given as mean + SD (n=8). $^{###}$p<0.001 compared to untreated siScr; ***p<0.001 compared to glutamate treated siScr (ANOVA, Scheffé's test).

3.2.5 Deficiency of p53 fails to preserve mitochondrial integrity

Next, the question was addressed whether protection mediated by p53 gene silencing was also accompanied by preservation of mitochondrial integrity as observed before for PFTα. Therefore, HT-22 cells were stained with MitoTracker® Deep Red, transfected with si p53 and siScr respectively and challenged with glutamate after growing for 48 h. After 14 h of treatment, cells were fixed and mitochondrial morphology was analysed as previously described[71]. Depending on their degree of mitochondrial fragmentation, cells were divided into three categories (Fig. 19A). Glutamate treatment led to enhanced mitochondrial fission reflected in an increase in cells of category II and III and a decrease in category I. Gene silencing of p53 did not alter mitochondrial appearance, but was not able to prevent fragmentation of mitochondria upon glutamate exposure either (Fig. 19A). Since the mitochondrial morphology does not necessarily correspond with their function, MMP was examined after 7 and 14 h of glutamate exposure. FACS analysis of TMRE fluorescence revealed no changes in MMP after 7 h of treatment with glutamate, neither in cells transfected with siScr nor in cells transfected with si p53. Fourteen hours after the onset of glutamate treatment, p53 gene silencing failed to

prevent glutamate-induced breakdown of the MMP. In both measurements CCCP was used as a positive control for mitochondrial depolarisation (Fig. 19B).

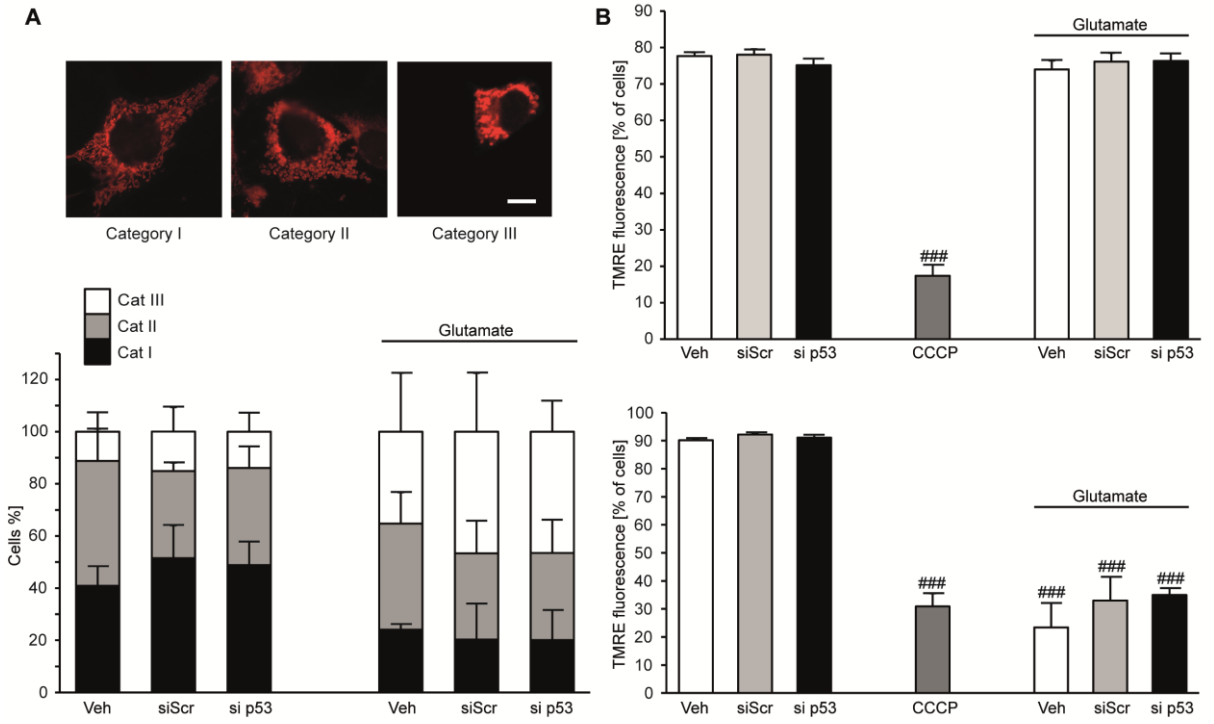

Figure 19: p53 silencing does not preserve mitochondrial morphology and membrane potential

A: Fluorescence photomicrographs showed categories of mitochondrial morphology: Category I (Cat I): elongated, Category II (Cat II): intermediate, Category III (Cat III): fragmented; Scale bar: 10 µm. Cells were stained with MitoTracker® Deep red before transfection with si p53 (20 nM) or siScr (20 nM). After 48 h, cells were challenged with glutamate (3 mM, 14 h) and quantified by counting at least 500 cells per condition blind to treatment. **B:** Cells were transfected with si p53 (20 nM) or siScr (20 nM), 48 h later challenged with glutamate (3 mM) and MMP was determined after 7 h (upper panel) and 14 h (lower panel) of treatment. CCCP was used as positive control for breakdown of MMP. p53 silencing did not alter MMP compared to cells transfected with siScr. Data are given as mean + SD (n=4). $^{###}p<0.001$ compared to untreated siScr (ANOVA, Scheffé's test).

To complete the analysis of mitochondrial function, formation of mitochondrial ROS and ATP levels were determined. Knockdown of p53 again failed to alter enhanced formation of mitochondrial ROS accompanying glutamate toxicity compared to cells transfected with unspecific siScr (Fig. 20A, B). Notably, p53 gene silencing significantly diminished the drop of ATP levels after the glutamate challenge (Fig. 20C). However, the absolute effect was very small and the physiological relevance of this difference remains questionable. Overall, these findings imply that the selective knockdown of p53 was unable to prevent glutamate-induced mitochondrial dysfunction.

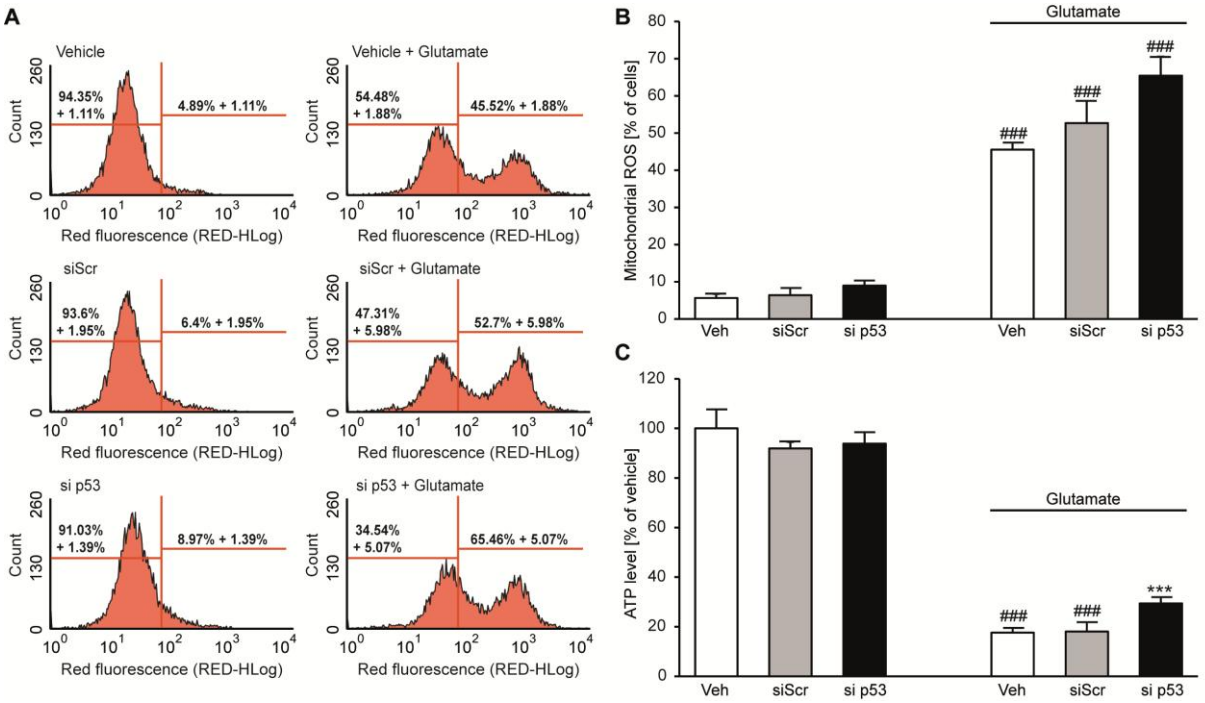

Figure 20: p53 siRNA fails to preserve mitochondrial function

A, B: Cells were transfected with si p53 (20 nM) or siScr (20 nM) and 48 h later exposed to glutamate. MitoSOX measurements depicted enhanced formation of mitochondrial ROS after glutamate treatment (6 mM, 15 h) which was not affected by knockdown of p53; representative plots (A) and quantification (B). Data are shown as mean + SD (n=4). ###p<0.001 compared to untreated siScr (ANOVA, Scheffé's test). **C:** 48 h after transfection with si p53 (20 nM) or siScr (20 nM) cells were treated with glutamate and ATP levels were assessed. Si p53 diminished glutamate-induced (4 mM, 10 h) decrease of ATP levels. Data are shown as mean + SD (n=8). ###p<0.001 compared to untreated siScr; ***p<0.001 compared to glutamate treated siScr (ANOVA, Scheffé's test).

3.2.6 Knockdown of p53 is not able to abolish lipid peroxidation

Since lipid peroxidation is a key mechanism leading to mitochondrial damage and p53 gene silencing failed to prevent mitochondrial morphology and function, it was of interest to investigate the effects of p53 knockdown on lipid peroxidation. To this end, HT-22 cells were transfected with si p53 or siScr, grown for 48 h and challenged with glutamate for 7 h. Afterwards, cells were stained with BODIPY 581/591 C11 and fluorescence was analysed by FACS. Knockdown of p53 did not increase formation of lipid peroxides compared to cells transfected with unspecific control siRNA. Glutamate exposure induced a pronounced shift from red to green fluorescence indicating enhanced lipid peroxidation. This effect was observed for both cells transfected with si p53 and siScr (Fig. 21) meaning that p53 gene silencing was not able to prevent formation of lipid peroxides due to glutamate toxicity.

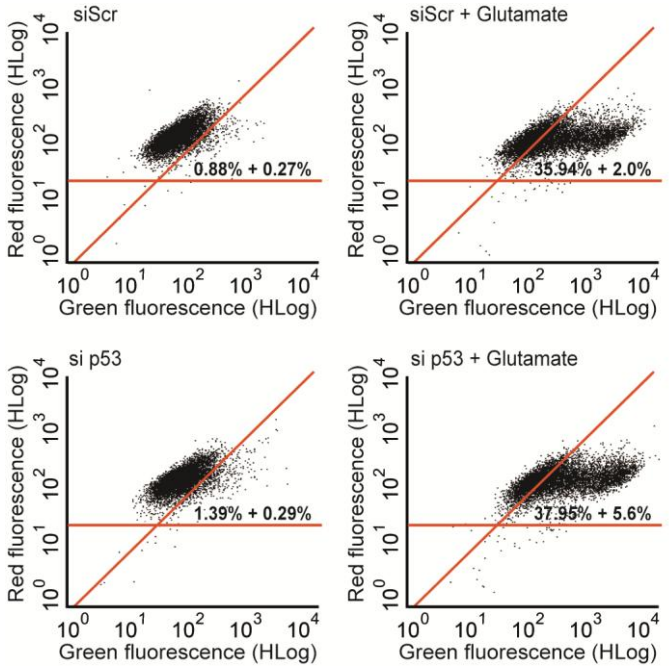

Figure 21: Knockdown of p53 is not able to abolish lipid peroxidation

HT-22 cells were transfected with si p53 (20 nM) or siScr (20 nM), after 48 h treated with glutamate and then stained with BODIPY 581/591 C11 and analysed by FACS. Representative FACS plots showed rightward shift of the cloud upon glutamate treatment (7 mM, 7 h) indicating enhanced lipid peroxidation which was not abolished by gene silencing of p53.

3.2.7 p53 translocation to mitochondria is not involved in oxytosis

Translocation of p53 to the mitochondria has been shown to correlate with neuronal cell death *in vivo* in models of transient global cerebral ischemia[117,118,210] and *in vitro* in models of H_2O_2-induced oxidative stress[101,119]. In order to clarify if this proposed transcriptional independent pro-apoptotic function of p53 also occurs during oxytosis, subcellular localisations of p53 and phospho-p53 were determined by immunocytochemistry. Therefore, mitochondria of HT-22 cells were stained with MitoTracker® Deep Red, and p53 or accordingly, phospho-p53 were visualised by immunostaining using Streptavidin Oregon green. Confocal images showed that under basal conditions both p53 and phospho-p53 were predominantly located in the nucleus. Upon glutamate treatment it seemed that in both cases extranuclear green fluorescence rose implying that p53 (Fig. 22A) as well as phospho-p53 (Fig. 22B) were released from the nucleus. The extent of extranuclear green fluorescence did not vary at 3 and 6 h of glutamate exposure. However, no yellow fluorescence was detectable which would indicate a co-localisation of p53/phospho-p53 with the

mitochondria suggesting that during glutamate-induced oxytosis p53 and also phospho-p53 did not translocate to the mitochondria.

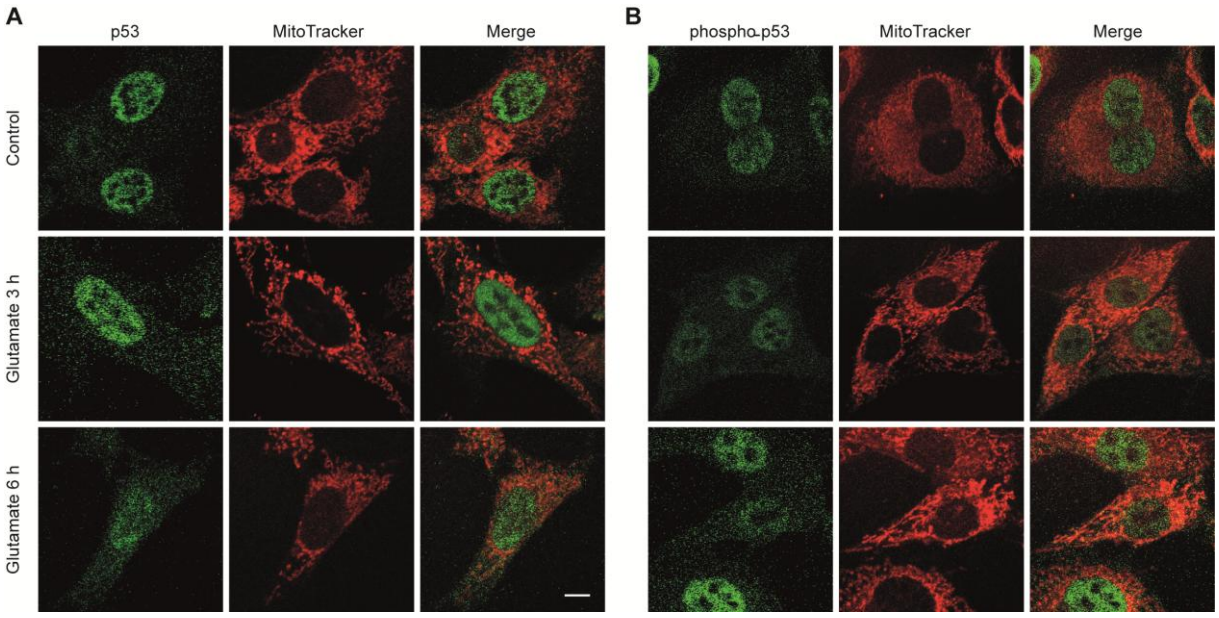

Figure 22: p53 and phospho-p53 do not translocate to mitochondria upon glutamate exposure
A: Confocal pictures (63x objective) showed localisation of p53 after glutamate challenge (3 mM). Mitochondria (red) were stained with MitoTracker® Deep red for 20 minutes immediately before glutamate treatment. After 3 h and 6 h of glutamate exposure, p53 (green) was visualised via immunofluorescence with Streptavidin Oregon green. Scale bar: 10 µm. **B:** Confocal images (63x objective) depicted localisation of phospho-p53 after glutamate challenge (3 mM). Mitochondria (red) were stained with MitoTracker® Deep red immediately before glutamate treatment. After 3 h and 6 h of glutamate exposure, phospho-p53 (green) was visualised via immunofluorescence with Streptavidin Oregon green.

Investigation of co-localisation using fluorescent confocal microscopy alone is not sufficient to rule out p53 translocation to mitochondria upon glutamate-induced cytotoxicity and that the association of p53 with the mitochondria does not trigger death of HT-22 cells. Consequently, PFTµ was tested which inhibits p53 binding to mitochondria[120] for a possible protective effect against glutamate toxicity. MTT assay revealed that PFTµ exhibited a dose dependent toxicity in the present culture system, but was not able to prevent glutamate-induced cell death at any concentration (Fig. 23). Altogether, these observations suggested that p53 translocation to mitochondria was not involved in glutamate mediated oxytosis in HT-22 cells.

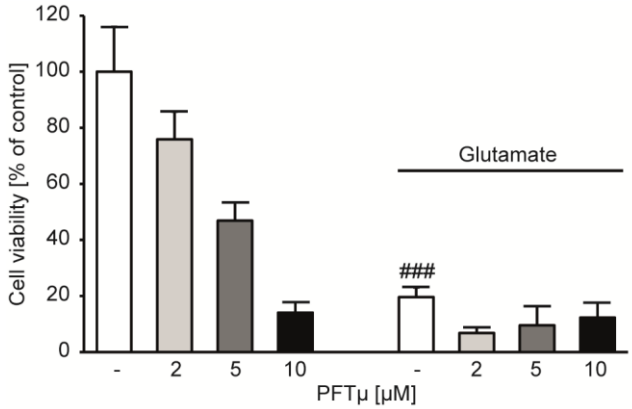

Figure 23: PFTμ does not rescue HT-22 cells

PFTμ showed dose dependent toxicity and was not able to rescue HT-22 cells from glutamate-induced (3 mM, 15 h) cell death as analysed by MTT assay. Data are given as mean + SD (n=8). ###p<0.001 compared to untreated control (ANOVA, Scheffé's test).

3.2.8 Effect of p53 inhibition on p53 transcriptional activity

Besides transcriptional independent induction of apoptosis by direct effects at the level of mitochondria as described above, p53 can also mediate cell death via transcriptional upregulation of several pro-apoptotic or repression of anti-apoptotic target genes[211]. Since a direct effect of p53 at the level of mitochondria seemed only to play a minor role in glutamate-induced oxidative stress, it was postulated that the moderate protective effect of p53 gene silencing on cell viability was mediated via inhibition of the pro-apoptotic transcriptional activity of p53. In order to address this hypothesis a p53 reporter assay was established.

For determination of p53 transcriptional activity, HT-22 cells were first transfected with specific siRNAs and 24 h later with p53-firefly-luciferase reporter plasmid and a renilla-luciferase-plasmid to control for transfection efficiency. After further 24 h, cells were challenged with glutamate and transcriptional activity was recorded via luminescence measurements. Knockdown of p53 significantly reduced p53 transcriptional activity both in the presence and absence of glutamate, while glutamate exposure increased p53 transcriptional activity in control cells (Fig. 24A). Unfortunately, it was not possible to assess the effect of PFTα on p53 transcriptional activity with this assay because it is based on the detection of firefly luciferase-induced luminescence and PFTα has been shown to directly inhibit firefly luciferase activity in concentrations higher than 1 μM[208]. To get a read out for PFTα effects on p53 transcriptional activity, mRNA expression levels of several p53 target genes such as AIF, DRP1, Bid and PUMA known to be associated with mitochondrial function

and regulation of cell death were determined after treatment with glutamate and PFTα. The expression of these genes was compared to the expression in p53 silenced cells in the presence and absence of oxidative stress. RT-PCR again confirmed the knockdown of p53 in cells transfected with si p53, while PFTα did not affect mRNA expression levels of p53. Neither PFTα nor p53 gene silencing induced alterations in the expression levels of the pro-apoptotic factors AIF, DRP1, Bid and PUMA irrespectively of glutamate exposure which itself did not lead to any changes. Knockdown of p53 decreased the mRNA levels of the negative p53 modulator mouse double minute 2 homolog (MDM2) and the cell cycle regulator p21 both with and without glutamate exposure, whereas such regulations were not observed after treatment with PFTα (Fig. 24B). From these data one can assume that the minor protective effect of p53 gene silencing results from the decrease in p53 transcriptional activity.

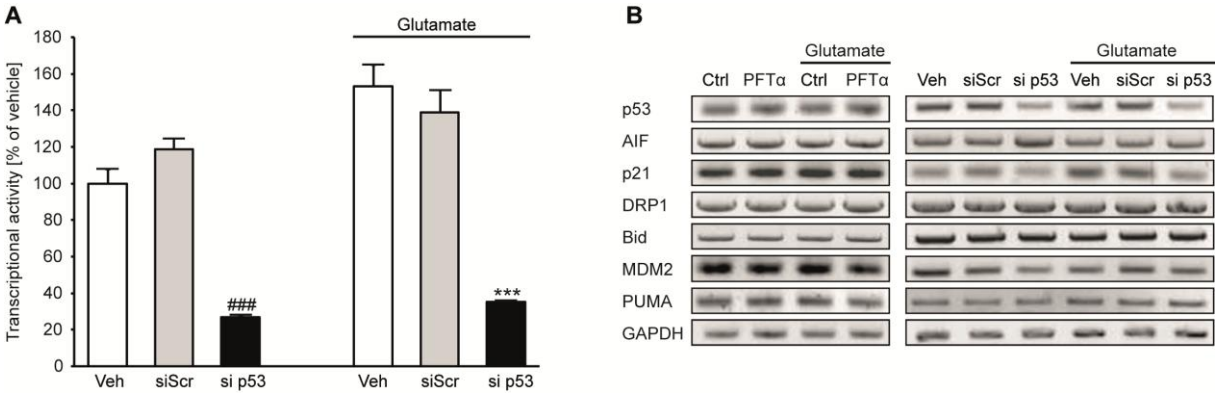

Figure 24: Influence of p53 inhibition on p53 transcriptional activity

A: p53 silencing diminished p53 transcriptional activity. HT-22 cells were transfected with si p53 (20 nM) or siScr (20 nM) and 48 h later, challenged with glutamate. Reporter assay was performed after glutamate challenge (3 mM, 14.5 h). Data are shown as mean + SD (n=4). $^{###}$p<0.001 compared to untreated vehicle; ***p<0.001 compared to glutamate treated vehicle (ANOVA, Scheffé's test). **B:** RT-PCR analysis of p53 target genes after PFTα treatment and glutamate exposure (7 mM, 16 h) or transfection of HT-22 cells with si p53 (20nM) or siScr (20 nM) and following glutamate challenge (7 mM, 15 h) 48 h after transfection.

3.2.9 PFTα acts independently of p53 inhibition

The previous results established protective effects against glutamate toxicity for both PFTα and knockdown of p53, but they varied in their potency, outcome at the level of mitochondria and in transcriptional regulation of p53. Hence, the next step was to examine whether PFTα also exerted functions in addition to p53 inhibition contributing to its protective effect and explaining PFTα mediated restoration of

mitochondrial integrity. For that reason PFTα was applied in p53 silenced cells and cell viability was recorded. Quantification of real-time impedance measurements revealed that PFTα prevented glutamate-induced cell death in p53-depleted HT-22 cells and that the according protective effect was comparable to the effect in control cells receiving siScr. Notably, PFTα administration in p53 silenced cells was more protective than down regulation of p53 alone (Fig. 25A, B).

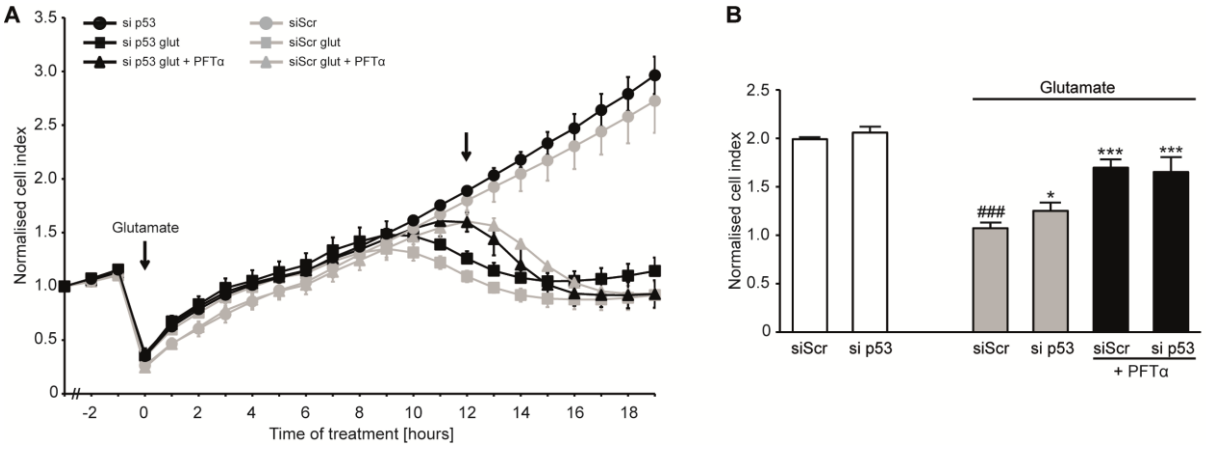

Figure 25: PFTα protects HT-22 cells independently of p53 inhibition

A: xCELLigence real-time measurement revealed protection of PFTα (10 µM) in p53 silenced cells against glutamate (5 mM) toxicity. HT-22 cells were treated with glutamate and PFTα 48 h after transfection with si p53 (20 nM) and siScr (20 nM), respectively. For better visualisation and differentiation of the applied treatments of siRNA and PFTα the data of PFTα treatment alone were not included. **B:** Bar graph evaluation at the 12 h time point from the xCELLigence recordings of A (right black arrow). Data are shown as mean + SD (n=6). $^{###}p<0.001$ compared to untreated siScr; *p<0.05 and ***p<0.001 compared to glutamate treated siScr (ANOVA, Scheffé's test).

These data clearly suggested that PFTα exhibited additional functions in addition to the inhibition of p53 in the model of oxytosis which is supported by previous findings where PFTα has been shown to interact with the aryl hydrocarbon receptor[212] or to suppress the heat shock and glucocorticoid receptor signalling[213]. As these studies were performed in non-neuronal systems, these pathways were not further investigated in the present work. However, previous studies in our laboratory revealed that PFTα prevented decrease of X-chromosomal-linked inhibitor of apoptosis (XIAP) induced by TBI in rats and that PFTα mediated protection of rat embryonic neurons against DNA-damage, glutamate or oxygen glucose deprivation was abolished by inhibition of XIAP[94]. Therefore, expression levels of XIAP were analysed in the present model system. Western blot analysis and corresponding

quantification showed no changes in XIAP protein levels after glutamate treatment and application of PFTα did not affect XIAP expression. However, glutamate exposure induced a strong increase in expression of mitochondrial superoxide dismutase 2 (MnSOD), a key mitochondrial antioxidant enzyme playing also a pivotal role in glutamate toxicity in HT-22 cells[138]. This increase was reduced almost to control levels by simultaneous administration of PFTα (Fig. 26A, B). The enhanced expression of MnSOD upon the glutamate challenge is in line with previous observations by Kim and coworkers[214] and regarded as a compensatory protective mechanism[215]. Consequently, the reduction of MnSOD protein levels by PFTα can probably be considered as a consequence, but not a cause for its protective effect.

The present data demonstrated that PFTα acted upstream or at the level of mitochondria which was either mediated independently of p53 inhibition or reflected additional protective effects which have to be elucidated in future studies.

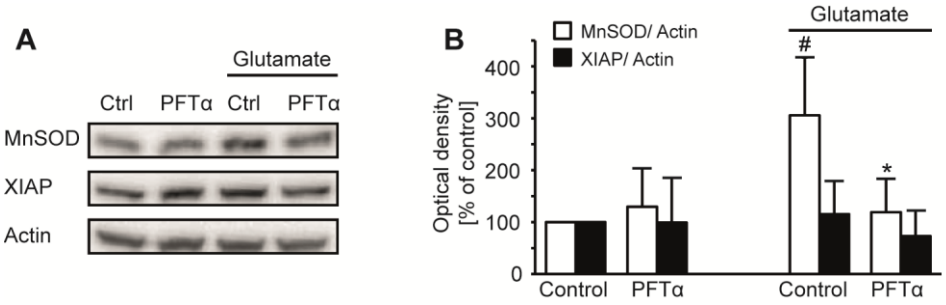

Figure 26: Effect of PFTα on the regulation of MnSOD and XIAP

A: Representative Western blots showed enhanced expression of MnSOD after glutamate challenge (4 mM, 14.5 h) which was prevented by co-treatment with PFTα (10 µM). Both treatments did not alter expression levels of XIAP. **B:** Quantification of 4 independent Western blots revealed significant induction of MnSOD after glutamate exposure. Data are given as mean + SD (n=4). $^{\#}p<0.05$ compared to untreated control; $^{*}p<0.05$ compared to glutamate treated control (ANOVA, Scheffé's test).

3.3 Silencing PHD1 mediates neuroprotection

Pharmacological inhibitors of PHDs and also genetic ablation have successfully been used in the last years in different models of neurodegenerative diseases *in vitro*[154,155,216] and *in vivo*[153,177,186], showing that the family of PHDs plays a substantial role in neuronal demise and represents a promising target for the development of neuroprotective substances and strategies. Although several studies on the effects of gene silencing of different PHD isoforms have been performed, to date it is not clear which of these isoforms exerts the most pronounced impact on neurodegenerative processes. It has been proposed, that the particular functions of the different isoforms depend on experimental conditions, such as the kind of insult and cell type[149]. For cortical neurons exposed to oxidative stress, PHD1 has been reported to be the most important isoform mediating cell death[160]. The particular role of PHD1 for mechanisms of oxidative cell death at the level of mitochondria has not been elucidated so far. Thus the present study focused on the investigation of the impact of PHD isoform 1 on mitochondrial function during oxytosis.

3.3.1 Knockdown of PHD1 attenuates glutamate toxicity

In order to examine the role of PHD1 in the model of oxytosis, HT-22 cells were transfected with two different siRNA sequences selectively targeting PHD1. According knockdown efficiency at the mRNA level was confirmed after 48 h of transfection by RT-PCR. SiPHD1 I effectively reduced expression levels of PHD1 mRNA at the applied concentrations of 20-80 nM, whereas siPHD1 II was most effective at a concentration of 80 nM. Expression of PHD2 and PHD3 mRNA remained unchanged verifying selectivity of the applied siPHD1 I and II (Fig. 27A). However, for investigations of PHD1 function during oxidative stress a reduction of the particular enzyme is required also at protein levels. Western blot analysis revealed a down regulation of PHD1 after 48 h of transfection by both siRNA sequences at the protein level, but the effect was less pronounced than expected from the analyses of mRNA levels and varied a lot as detected by corresponding quantification (Fig. 27B). In order to improve gene silencing-efficiency at the protein level, the transfection time was extended to 72 h and protein levels were evaluated by Western blot analysis. Unfortunately, this elongated incubation with siRNA was not able to further decrease PHD1 protein levels (Fig. 27C) and also a double transfection approach where HT-22 cells were again transfected with the same

siRNA sequence 24 h after the first transfection did not result in a further down regulation of PHD1 protein levels (Fig. 27D). Therefore, functional analyses of partial PHD1 silencing were performed 48 h after siRNA transfection and subsequent glutamate challenge.

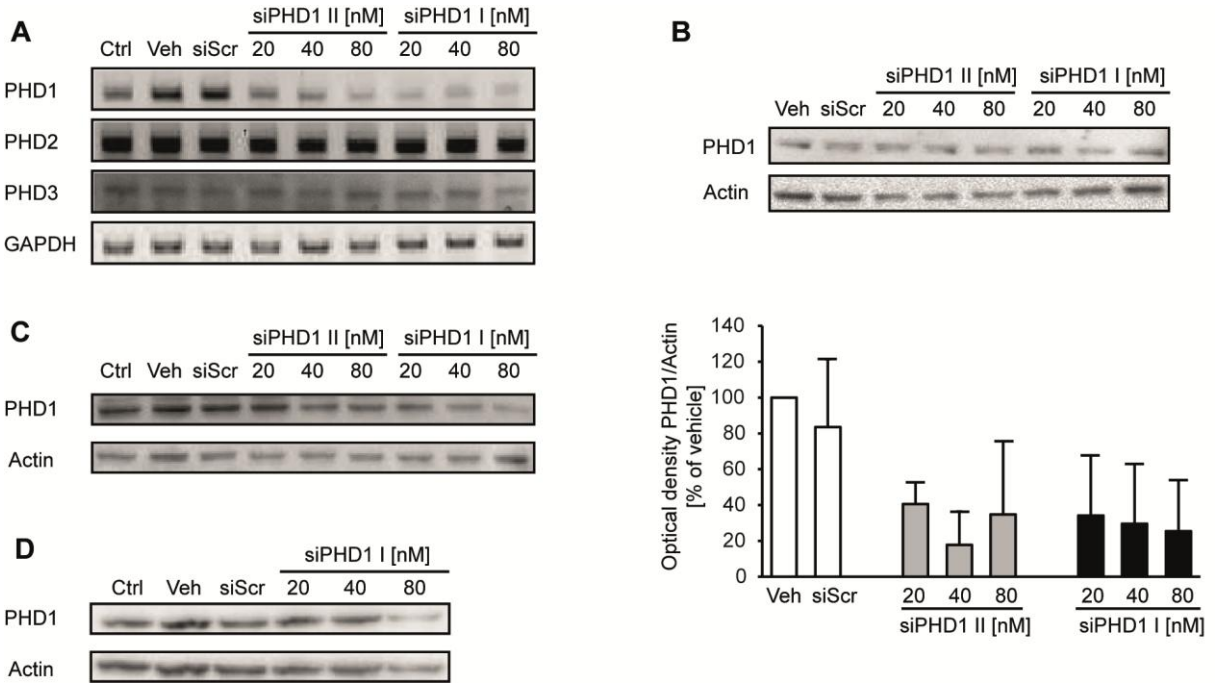

Figure 27: Knockdown of PHD1 by siRNA sequences I and II

A: After 48 h of transfection with siRNAs selectively targeting PHD1 (siPHD1 I and II) or scrambled control siRNA (siScr), RT-PCR analysis revealed specific knockdown of PHD1 by siPHD1 I and II as PHD2 and PHD3 expression levels were unaffected. GAPDH was used as loading control. **B:** Representative Western blot and corresponding quantification of 5 independent Western blots showed small knockdown of PHD1 by both siRNA sequences 48 h after transfection with siPHD1 I and II. **C:** Western blot was performed 72 h after transfection with siPHD1 I and II or siScr. **D:** HT-22 cells were transfected with siPHD1 I or siScr, grown for 24 h and then again transfected with siPHD1 I or siScr. Western blot was performed another 24 h later.

Knockdown of PHD1 by siPHD1 I resulted in increased cell viability compared to cells transfected with unspecific siScr after glutamate treatment shown by MTT assay (Fig. 28A) and real-time impedance measurements revealed a delay of glutamate induced cell death by siPHD1 I of about 3 h (Fig. 28B). Silencing PHD1 with siPHD1 II did not significantly attenuate loss of cell viability due to glutamate challenge, but showed a tendency to protect HT-22 cells against oxytosis (Fig. 28C). This was further supported by shifting the onset of cell death after glutamate exposure for about 2 h compared to cells transfected with unspecific siScr as detected by real-time impedance measurements using the xCELLigence system

(Fig. 28D). The smaller effect of siRNA sequence II compared to sequence I correlated well with the detected minor reduction of PHD1 protein amount by siRNA sequence II (Fig. 27B). In general, down regulation of PHD1 did not affect basal cell viability or proliferation rate (Fig. 28A-D).

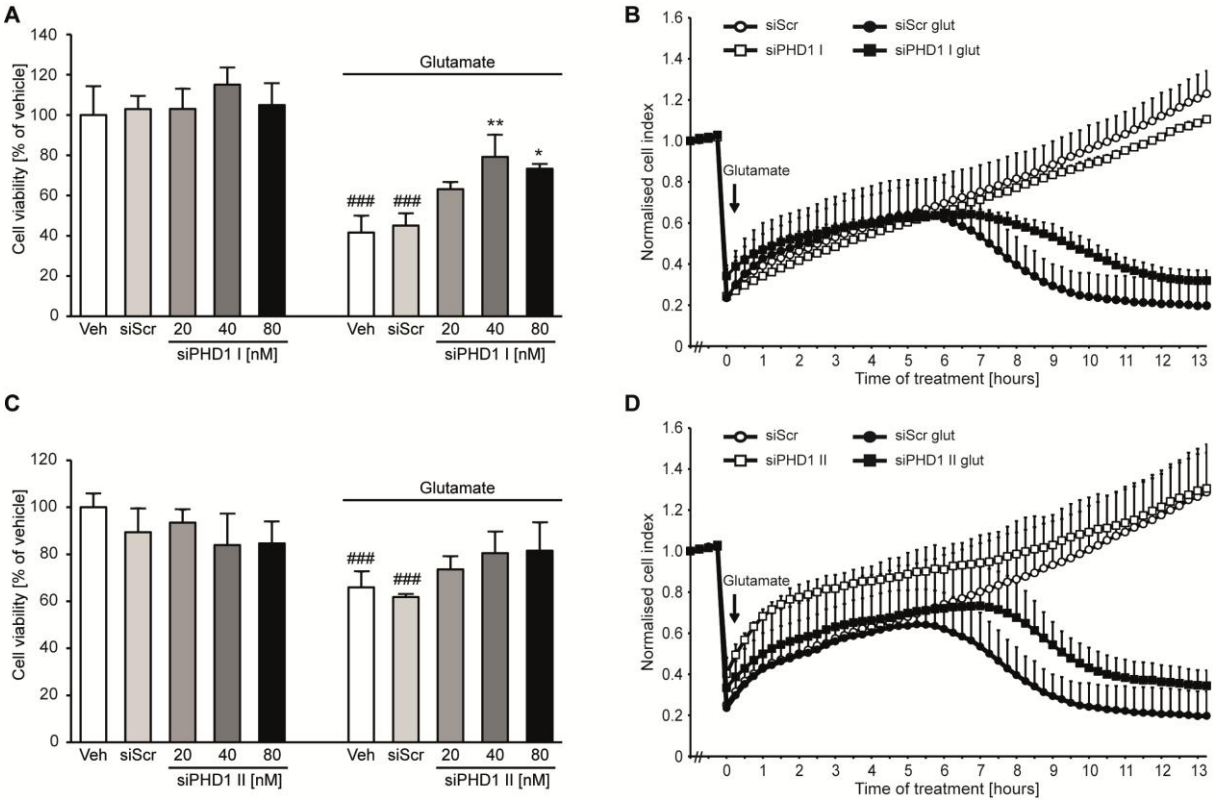

Figure 28: Selective PHD1 silencing attenuates glutamate toxicity

A: HT-22 cells were transfected with siPHD1 I or siScr and 48 h later, treated with glutamate. MTT assay depicted protection of different concentrations of siPHD1 I against glutamate toxicity (5 mM, 14 h) compared to cells transfected with unspecific siScr (80 nM). Data are given as mean + SD (n=4). $^{###}$p<0.001 compared to untreated vehicle; *p<0.05 and **p<0.01 compared to glutamate treated vehicle (ANOVA, Scheffé's test). **B:** xCELLigence real-time measurement: Cells transfected with siPHD1 I (80 nM) for 48 h showed transient protection against treatment with 5 mM glutamate (glut) compared to cells transfected with siScr (80 nM) for 48 h. **C:** MTT assay indicated a tendency to increased cell viability after glutamate challenge (5 mM, 14 h) of cells transfected with siPHD1 II for 48 h prior to glutamate exposure compared to cells transfected with scrambled control siRNA (80 nM). Data are given as mean + SD (n=4). $^{###}$p<0.001 compared to untreated vehicle; (ANOVA, Scheffé's test). **D:** xCELLigence real-time measurement revealed that cells transfected with siPHD1 II (80 nM) for 48 h are transiently protected against treatment with 5 mM glutamate (glut) compared to cells transfected with siScr (80 nM) for 48 h.

3.3.2 PHD1 silencing restores mitochondrial integrity

The above described neuronal protection by PHD1 gene silencing verified previous findings of Siddiq and colleagues in cortical neurons[160]. Nevertheless, so far it is uncertain what happens to mitochondria after knockdown of PHD1 per se and in particular during oxidative stress. For that reason, the next step in the present work was to investigate mitochondrial function after PHD1 down regulation in the presence and absence of glutamate.

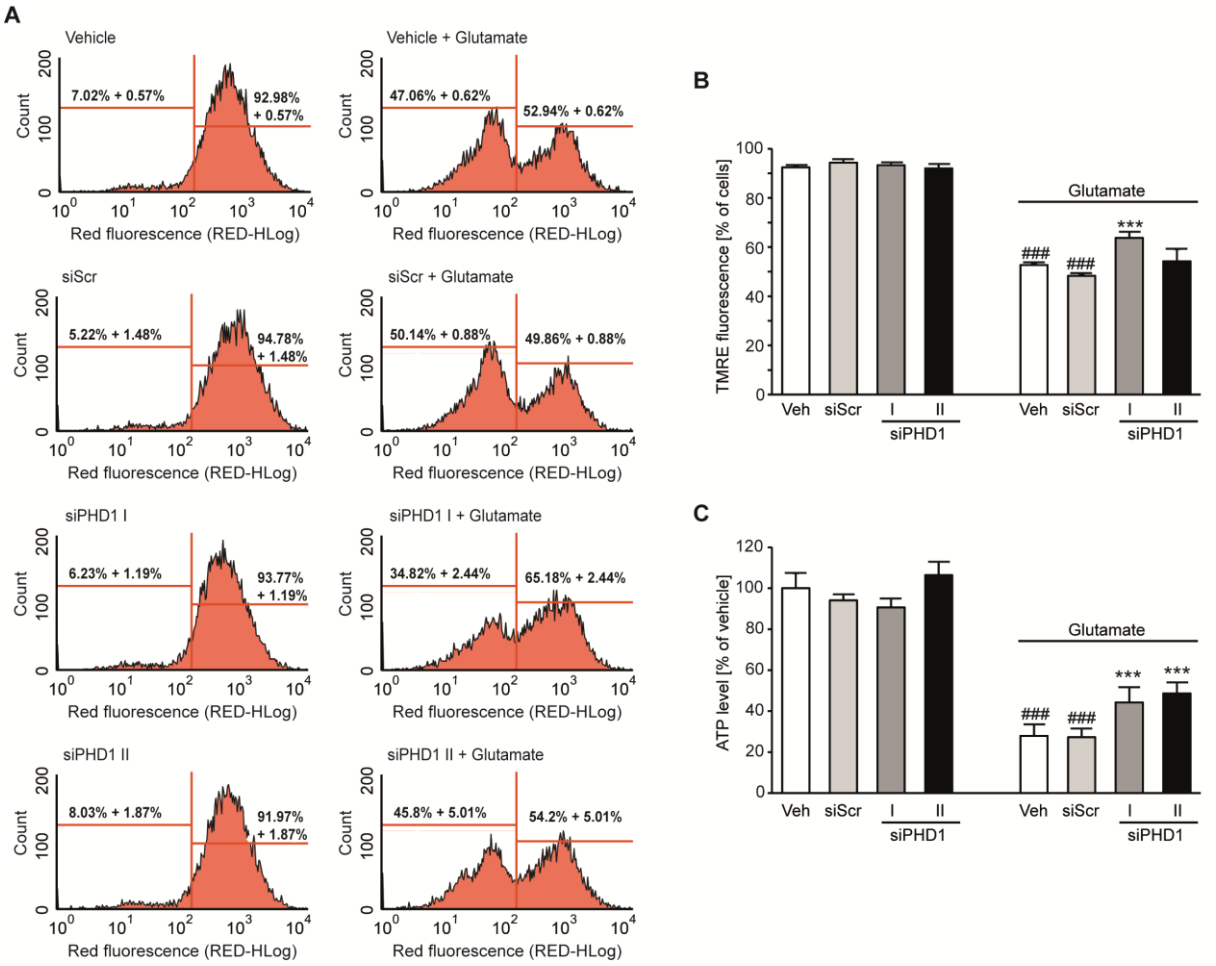

Figure 29: Knockdown of PHD1 restores mitochondrial integrity

A: Representative plots showed restoration of MMP after glutamate exposure (5 mM, 11 h) in cells transfected with siPHD1 I (20 nM) or siPHD1 II (80 nM) 48 h prior to glutamate challenge compared to cells transfected with siScr (80 nM). **B:** Quantification of FACS plots shown in A. Breakdown of MMP indicated by reduced TMRE fluorescence was only partially prevented by siPHD1 II. Data are shown as mean + SD (n=3). $^{###}$p<0.001 compared to untreated siScr; ***p<0.001 compared to glutamate treated siScr (ANOVA, Scheffé's test). **C:** PHD1 silencing reduced glutamate-induced (4 mM, 15 h) loss of ATP levels. HT-22 cells were transfected with siPHD1 I (20 nM), siPHD1 II (80 nM) or siScr (80 nM) and 48 h later, exposed to glutamate. Data are given as mean + SD (n=8). $^{###}$p<0.001 compared to untreated siScr; ***p<0.001 compared to glutamate treated siScr (ANOVA, Scheffé's test).

As shown before, glutamate treatment consistently induced the breakdown of MMP indicated by loss of TMRE fluorescence which was recorded by FACS analysis. SiPHD1 I reduced this leftward shift of the curve showing that knockdown of PHD1 by this particular siRNA sequence was able to attenuate glutamate-induced mitochondrial depolarisation (Fig. 29A). As observed before in measurements of cell viability, siPHD1 II showed minor beneficial effects on MMP that, however, did not reach statistical significance (Fig. 29A, B).

Notably, both siRNA sequences significantly diminished loss of ATP content after glutamate treatment (Fig. 29C) further supporting that down regulation of PHD1 is protective in mitochondria of cells exposed to oxidative stress which is assigned with enhanced formation of ROS.

Therefore, it was not surprising that gene silencing of PHD1 also decreased the amount of mitochondrial ROS after glutamate challenge albeit the effect was again only statistically significant for PHD1 siRNA sequence I and not for sequence II (Fig. 30A, B). It is important to note that down regulation of PHD1 alone did not change any investigated mitochondrial parameters under basal conditions. Overall, these results showed that the siRNA-mediated knockdown of PHD1 was able to restore mitochondrial function in HT-22 cells challenged with glutamate for the induction of oxytosis.

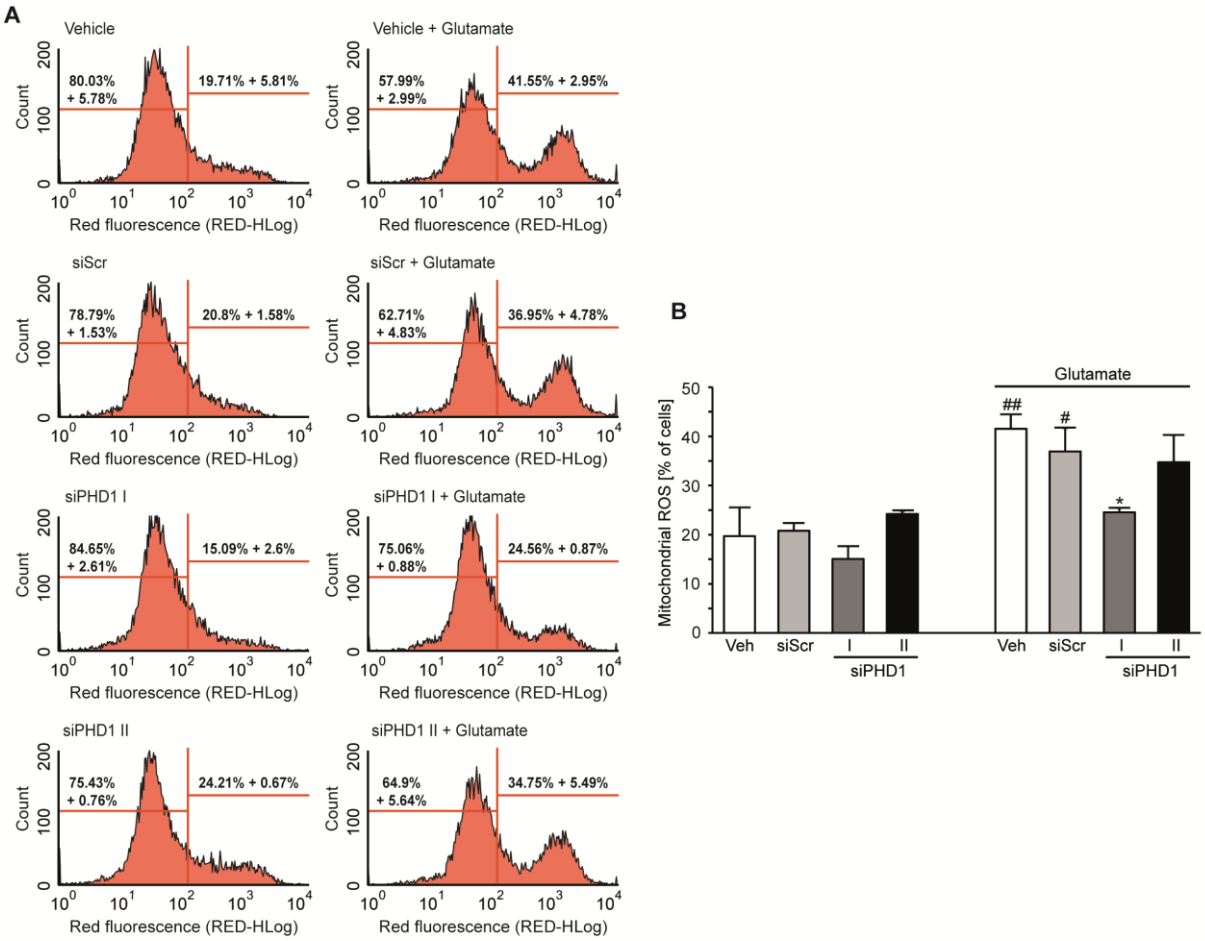

Figure 30: PHD1 silencing prevents mitochondrial ROS formation

A: Representative plots revealed reduced formation of mitochondrial ROS after glutamate challenge (4 mM, 15 h) in PHD1 silenced cells. HT-22 cells were transfected with siPHD1 I (20 nM), siPHD1 II (80 nM) or siScr (80 nM) and 48 h later, treated with glutamate. **B:** Quantification of FACS analysis from A. Glutamate (4 mM, 15 h) induced enhanced production of mitochondrial ROS which was just partially prevented by siPHD1 II. Data are shown as mean + SD (n=3). $^{\#}p<0.05$ and $^{\#\#}p<0.01$ compared to untreated vehicle, *p<0.05 compared to glutamate treated siScr (ANOVA, Scheffé's test).

3.3.3 Deficiency of PHD1 reduces lipid peroxidation

A major reason for mitochondrial demise in glutamate exposed HT-22 cells is the formation of lipid peroxides attributed to glutamate-induced GSH depletion and subsequent activation of LOX[46]. SiRNA-mediated deficiency of PHD1 greatly reduced production of lipid peroxides upon glutamate toxicity. SiRNA sequence I significantly reduced the formation of detrimental ROS by 50% (Fig. 31A, B) while the according ROS reduction by siRNA sequence II was less pronounced and only reached 30% compared to the control siScr (Fig. 31A, B). Both siRNAs did not alter levels of lipid peroxidation under basal conditions. These findings are in line and correlate well with the obtained results on cell viability and mitochondrial function and expose the

selective inhibition of PHD1 as a potential target for inhibition of oxidative neuronal death.

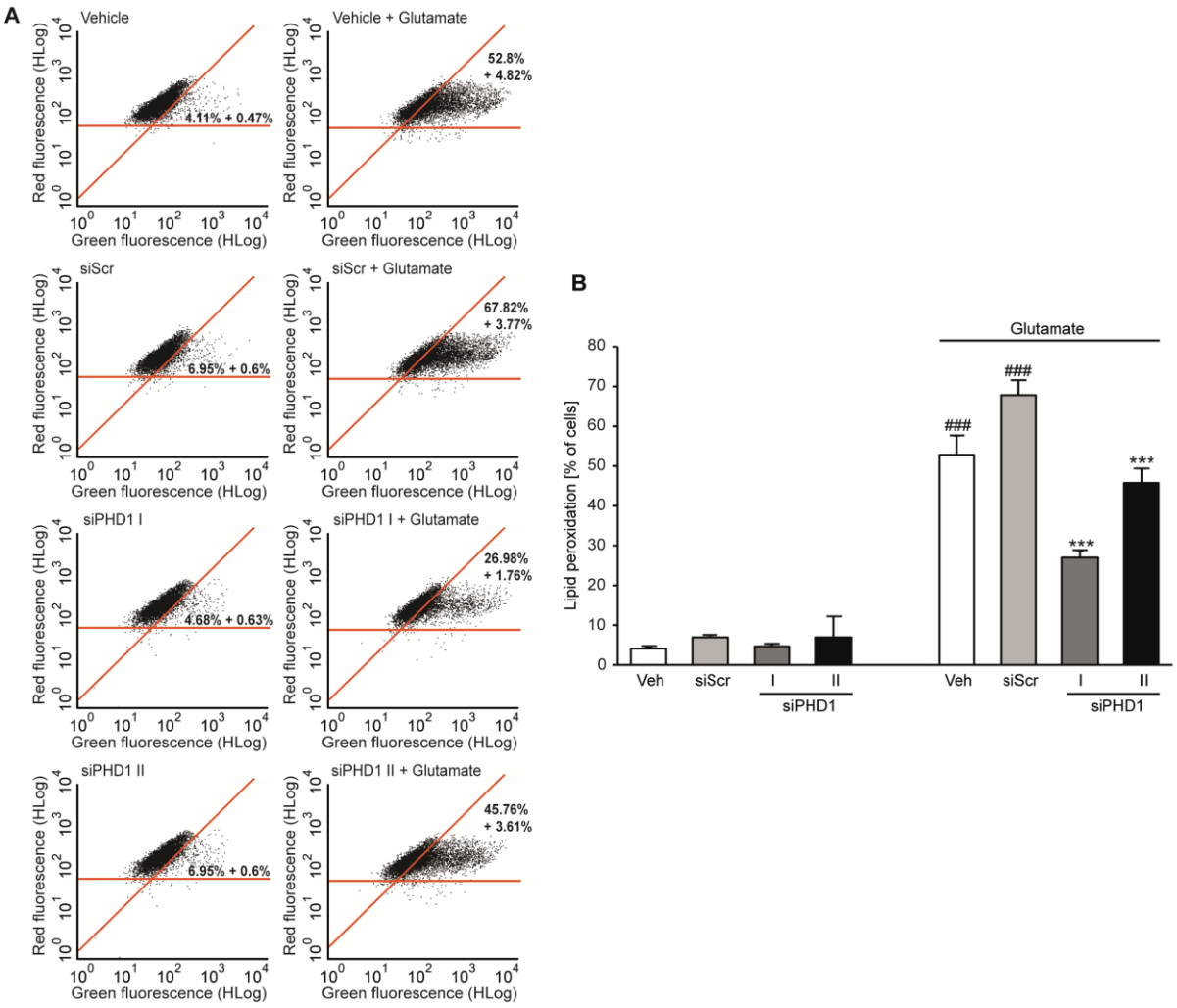

Figure 31: Deficiency of PHD1 reduces lipid peroxidation

A: Representative plots showed reduced lipid peroxidation after glutamate challenge (5 mM, 15 h) in PHD1 silenced cells compared to cells transfected with unspecific siScr. HT-22 cells were transfected with siPHD1 I (20 nM), siPHD1 II (80 nM) or siScr (80 nM) and 48 h later, treated with glutamate. **B:** Quantification of FACS analysis from A. Cells were stained with BODIPY 581/591 and lipid peroxides were measured by FACS analysis after 15 h of glutamate treatment (5 mM). SiPHD1 I and II significantly reduced the formation of lipid peroxides. Data are shown as mean + SD (n=4). $^{###}$p<0.001 compared to untreated siScr; ***p<0.001 compared to glutamate treated siScr (ANOVA, Scheffé's test).

3.4 Pharmacological inhibition of PHDs provides neuroprotection

The data obtained before revealed that the selective siRNA-mediated silencing of PHD1 was capable of attenuating glutamate-induced cell death and attending mitochondrial dysfunction. Albeit the observed effects reached statistical significance, they were rather small. In addition, the selective down regulation of PHD1 did not allow for investigating the relevance of PHD2 and PHD3 for mitochondrial demise and cell death in this model system. In fact, previous studies suggested a contribution of PHD3 to neuronal cell death[193,217]. In order to gain more insight into the effects of global inhibition of PHDs that may result in more pronounced neuroprotection than partial PHD1 silencing, in a next step structurally diverse PHD-inhibitors which do not act isoform specific were tested for their neuroprotective potential and impact on mitochondrial integrity.

3.4.1 Structural diverse PHD-inhibitors prevent glutamate-induced cell death

Since PHDs need iron, 2-oxoglutarate and oxygen as cofactors, withdrawal of these co-substrates is a common strategy to inhibit PHD enzyme activity. Therefore, various iron chelators and analogues of 2-oxoglutarate have been developed and tested for their potential to inhibit PHD activity[142,171]. The deprivation of oxygen is not a suitable tool to diminish PHD enzyme activity in aerobic systems for therapeutic approaches as they require oxygen for normal development, but oxygen represents the physiological mechanism of PHD inhibition in case of hypoxia explaining the oxygen sensing function of the PHD family enzymes[143].

In order to prove both concepts of PHD enzyme inhibition, the present study investigated the effects of the 2-oxoglutarate analogue DHB as well as the iron chelators DFO, CPO and oxyquinoline on cell viability and mitochondrial integrity. Upon glutamate exposure HT-22 cells showed characteristic morphological hallmarks of cell death such as shrivelling and detaching from the bottom of the culture dish. Co-treatment with DFO, DHB, CPO and also oxyquinoline fully prevented these morphological changes, while none of the applied PHD-inhibitors altered the cellular morphology when added to the cells alone (Fig. 32A). Testing different concentrations of oxyquinoline in the MTT assay revealed that oxyquinoline prevented decrease in cell viability due to glutamate exposure in a dose-dependent manner, but also displayed toxic effects of oxyquinoline when applied at higher

concentrations. A concentration of 2 µM emerged as optimal since it was highly protective and not harmful. Further MTT assays showed that DFO and DHB protected HT-22 cells against glutamate-induced cell death from a concentration of 20 µM upwards and did not exhibit any toxicity by themselves. Therefore, a concentration of 20 µM was used for future experiments with both substances. CPO was also able to fully prevent cell death after glutamate exposure, but also decreased cell viability at higher concentrations similar to oxyquinoline. Again, a concentration of 2 µM emerged as the optimal concentration in these studies because it was highly protective and did not damage the cells when applied at control conditions (Fig. 32B).

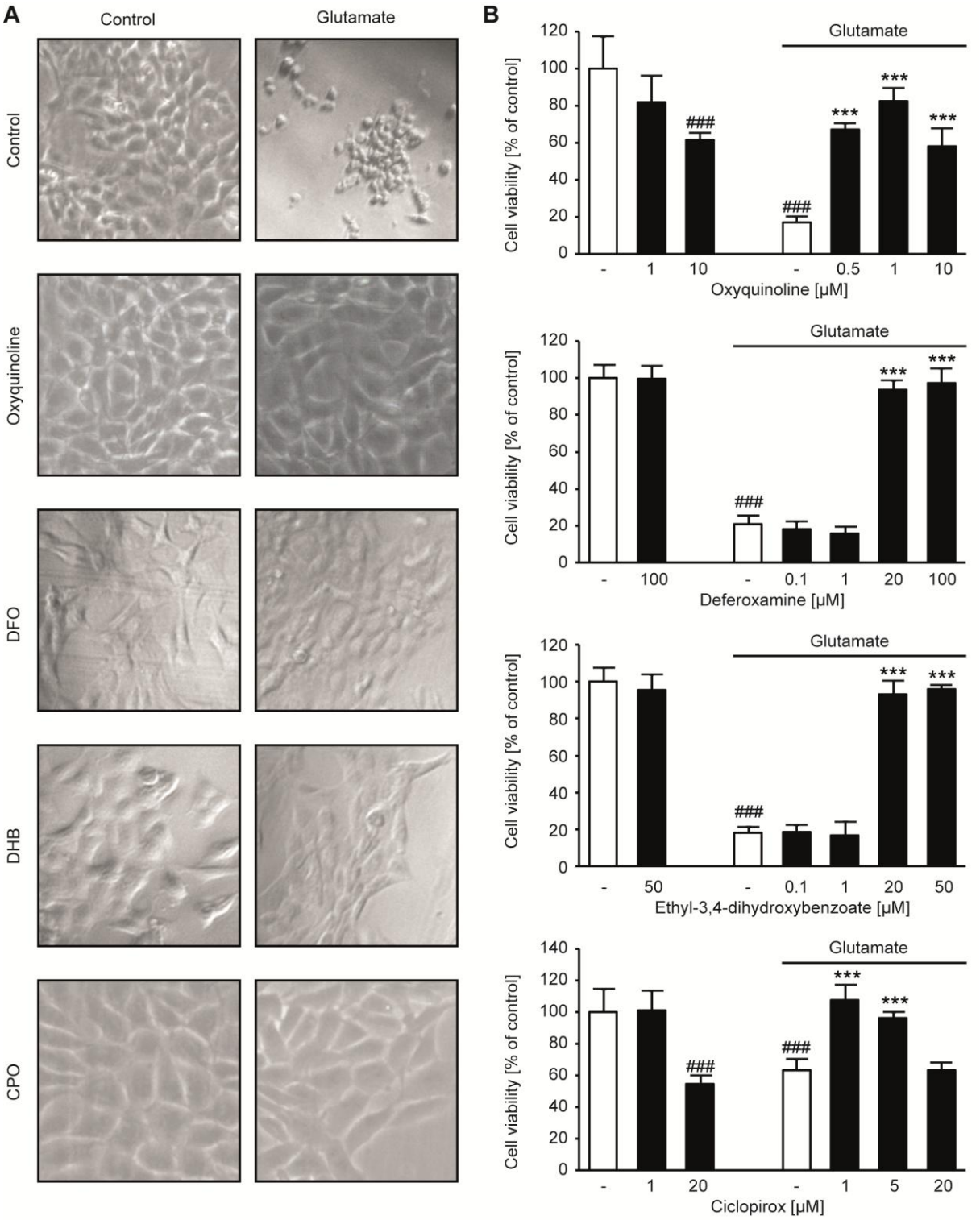

Figure 32: Structural diverse PHD-inhibitors abolish glutamate-induced cytotoxicity

A: Representative pictures (100x magnification) showed morphological changes of HT-22 cells after glutamate challenge. Oxyquinoline (2 µM), DFO (20 µM), DHB (20 µM) and CPO (2 µM) fully preserved cellular appearance of HT-22 cells. **B:** MTT assays revealed protective effect of different concentrations of oxyquinoline, DFO, DHB and CPO against glutamate toxicity (7 mM, 16 h). Data are shown as mean + SD (n=8). $^{###}$p<0.001 compared to untreated control; ***p<0.001 compared to glutamate treated control (ANOVA, Scheffé's test).

Real-time impedance measurements confirmed that the chosen concentrations of PHD-inhibitors did not exhibit intrinsic toxicity and also demonstrated a persistent protective effect which lasted for the whole recording of 23 h (Fig. 33A, B).

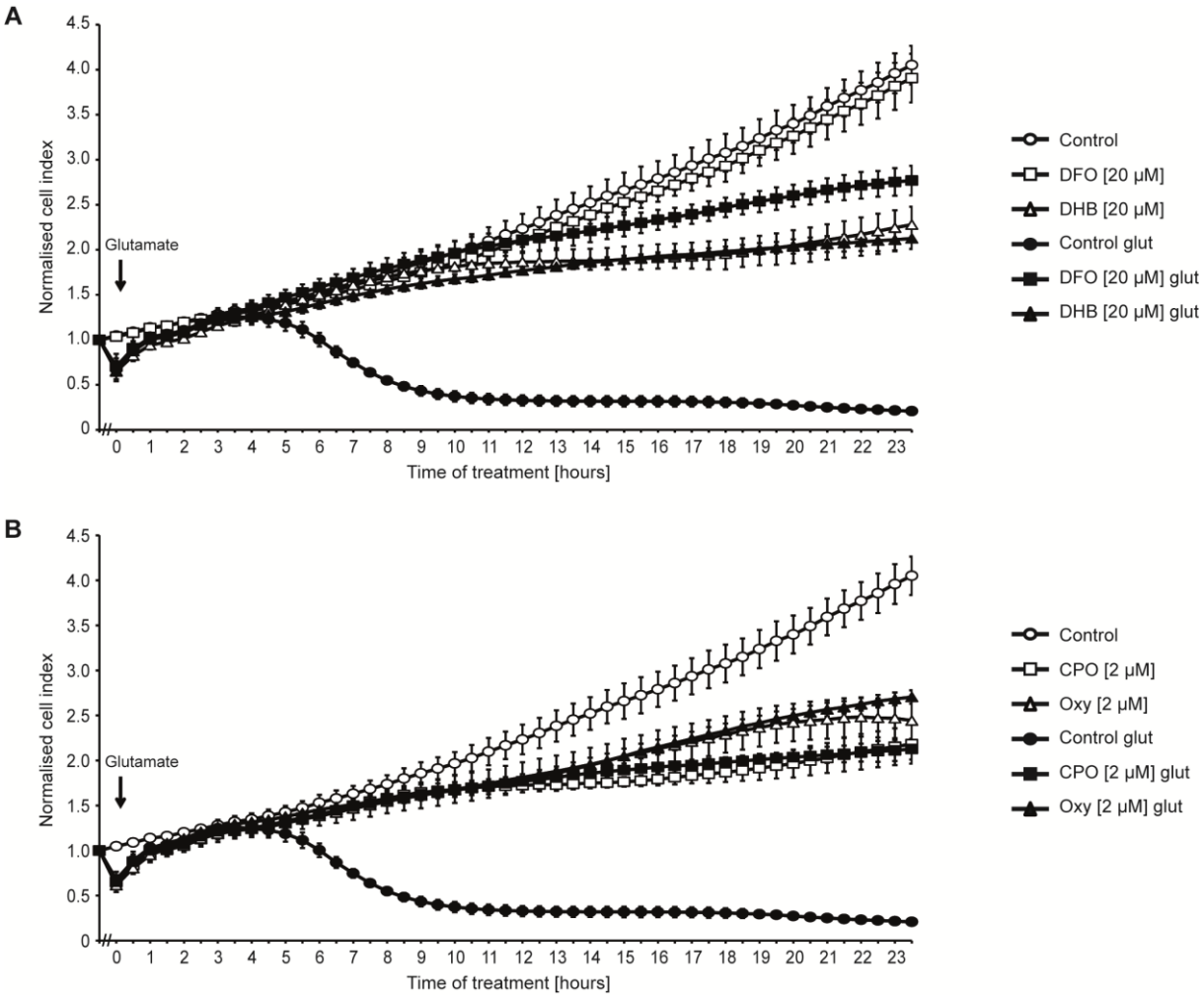

Figure 33: PHD-inhibitors prevent glutamate-induced cell death

A: Real-time impedance measurement revealed persistent protective effect of DFO (20 µM) and DHB (20 µM) against glutamate (5 mM) toxicity lasting for at least 23 h. **B:** CPO (2 µM) and oxyquinoline (2 µM) protected HT-22 cells against glutamate-induced (5 mM) cell death for at least 23 h as shown by real-time impedance measurement. All data were derived from one experiment, but were split in two graphs for clearer visualisation.

These observations imply a very strong neuroprotective potential for all used substances which was further characterised by the administration of oxyquinoline under post-treatment conditions. Therefore, HT-22 cells were challenged with glutamate and oxyquinoline was applied 2, 4, 6, 8 and 10 h later. Cellular impedance was recorded via the xCELLigence system and revealed full protection of cell viability up to 4 h of post-treatment with oxyquinoline (Fig. 34A). Even after 10 h of post-

treatment, oxyquinoline was able to significantly save the remaining viable cells from glutamate-induced cell death (Fig. 34B) underlining the pronounced protective potential of this drug.

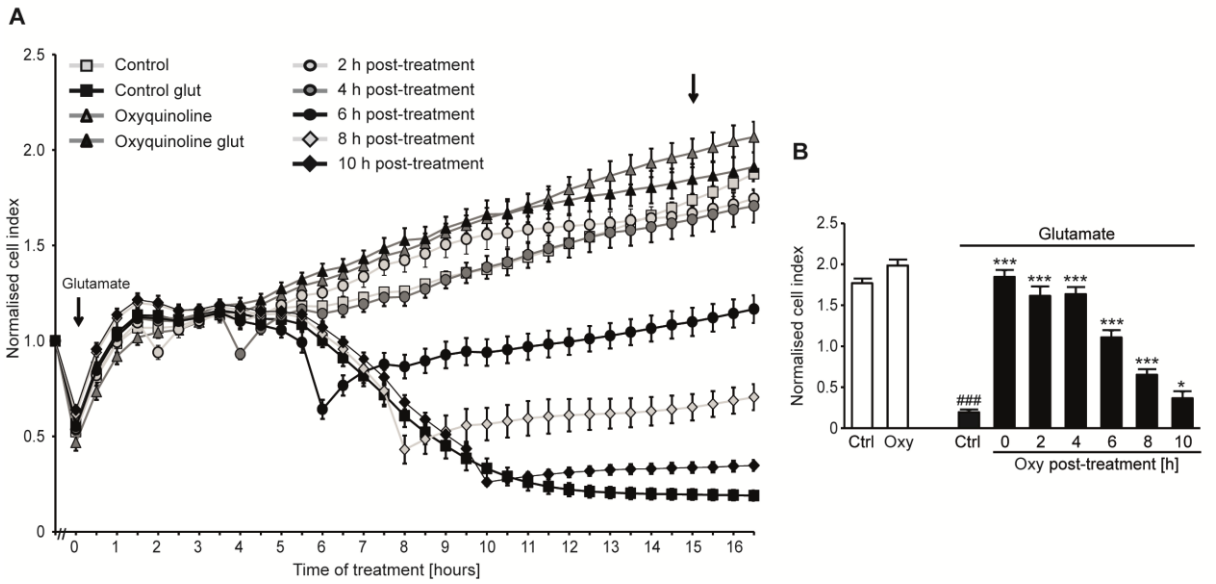

Figure 34: Oxyquinoline attenuates glutamate toxicity under post-treatment conditions

A: Oxyquinoline was applied 2, 4, 6, 8 and 10 h after the onset of glutamate (4 mM) and attenuated glutamate-induced cell death at all time points as shown by xCELLigence measurements. **B:** Bar graph evaluation at the 15 h time point from the xCELLigence recordings of A (right black arrow). Data are given as mean + SD (n=7). ###p<0.001 compared to untreated control; *p<0.05 and ***p<0.001 compared to glutamate treated control (ANOVA, Scheffé's test).

3.4.2 Inhibition of PHDs restores mitochondrial morphology and function

It is well accepted that, once mitochondria are damaged, cells undergo cell death at this 'point of no return'[25]. Hence, the strong effects on cell viability observed before for the PHD-inhibitors imposed the hypothesis that they were also able to preserve mitochondrial integrity and function. To verify this hypothesis mitochondrial morphology and function were investigated. As described and observed before, glutamate challenge induced strong mitochondrial fragmentation. Co-treatment with oxyquinoline was able to conserve the tubular like structure of mitochondria (Fig. 35A) and prevented enhanced mitochondrial fission after glutamate exposure indicated by an increase in cells of category III. Under basal conditions, application of oxyquinoline did not alter mitochondrial appearance (Fig. 35B). In order to check if oxyquinoline could not only restore mitochondrial morphology but also function, ATP

levels and MMP were analysed. HT-22 cells were seeded in white 96-well plates, treated with glutamate and different concentrations of oxyquinoline (1-20 µM) and ATP levels were assessed after 15 h of exposure. Oxyquinoline prevented glutamate-induced drop of ATP levels at all applied concentrations and did not affect ATP contents under basal conditions (Fig. 35C). Restored ATP levels always suggest an intact MMP as this is required for proper ATP synthesis[22].

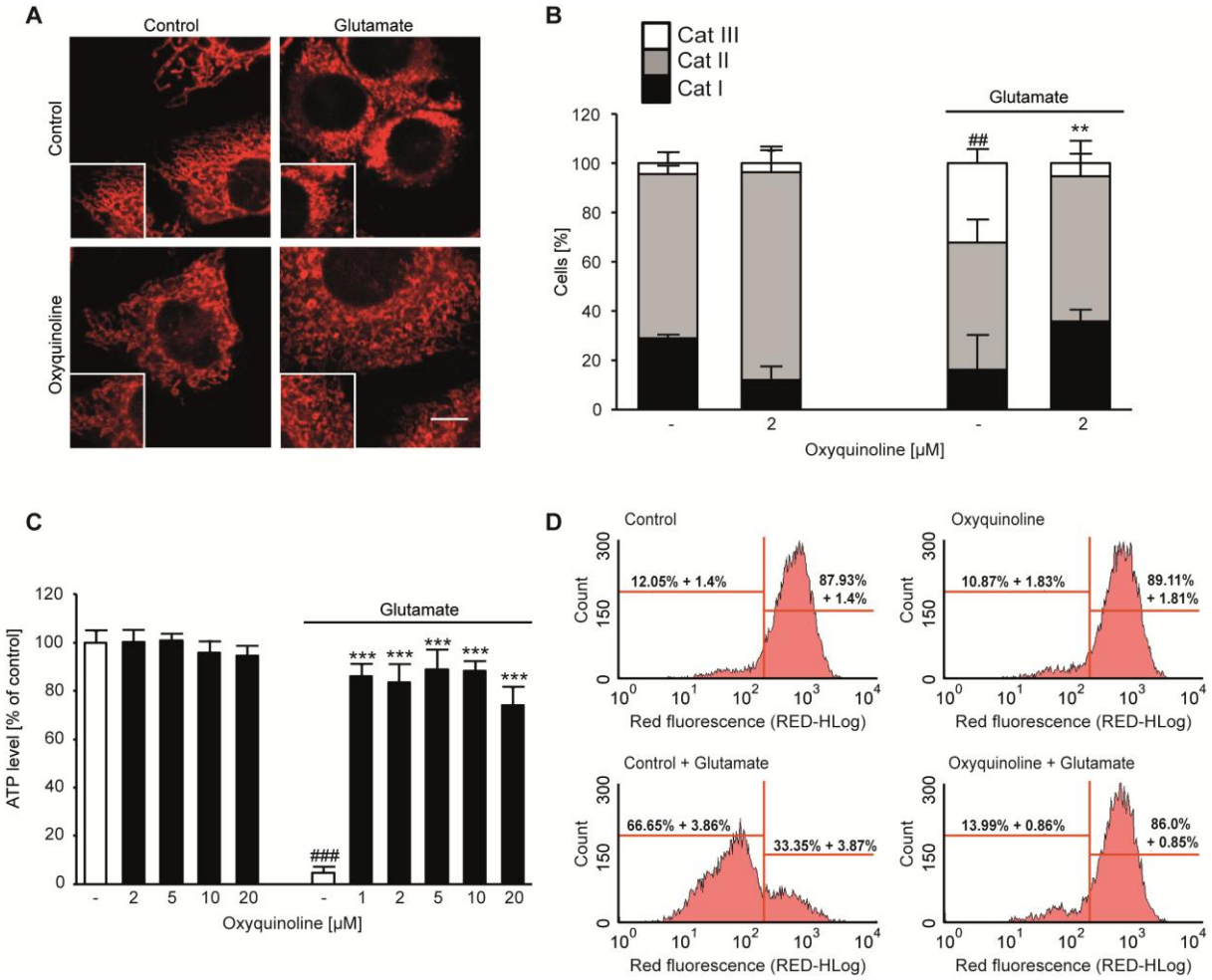

Figure 35: Oxyquinoline preserves mitochondrial morphology and function

A: Representative confocal images (63x objective) showed mitochondrial morphology after treatment with oxyquinoline (2 µM) in the presence and absence of glutamate (3 mM, 14 h). Scale bar: 10 µm. **B:** Quantification of 500 cells counted blind to treatment conditions of 3 independent experiments revealed reduction of glutamate-induced mitochondrial fission by oxyquinoline. Data are given as mean + SD (n=3). $^{\#\#}$p<0.01 compared to Cat III of untreated control; **p<0.01 compared to Cat III of glutamate treated control (ANOVA, Scheffé's test). **C:** Different concentrations of oxyquinoline restored ATP levels after glutamate challenge (7 mM, 15 h). Data are given as mean + SD (n=8). $^{\#\#\#}$p<0.001 compared to untreated control; ***p<0.001 compared to glutamate treated control (ANOVA, Scheffé's test). **D:** Oxyquinoline (2 µM) fully prevented breakdown of MMP after glutamate exposure (7 mM, 15 h).

Nevertheless, MMP was examined by TMRE fluorescence and subsequent FACS analysis to prove this conclusion. Upon glutamate exposure mitochondria were depolarised as indicated by a leftward shift of the curve depicting TMRE fluorescence. Breakdown of MMP was fully abolished by simultaneous administration of oxyquinoline which did not change the basal MMP (Fig. 35D).

Inhibition of PHDs by DFO, DHB and CPO preserved mitochondrial morphology also detected by the reduced percentage of cells containing highly fragmented mitochondria of category III compared to glutamate-damaged cells (Fig. 36A). This effect was only significant for DFO and CPO, but not for DHB because of less pronounced glutamate toxicity in this set of experiments. However, also here quantification showed a significant shift from category III to I in cells co-treated with DHB and glutamate. Neither DFO nor DHB nor CPO changed the mitochondrial structure under basal conditions. Further investigations of ATP levels revealed full restoration by all three inhibitors, which was also significant for DHB in this case. Only at a concentration of 1 µM, DHB was not able to prevent glutamate-induced loss of ATP corresponding well with the data obtained for cell viability, where 1 µM of DHB also failed to prevent cell death after glutamate exposure (Fig. 32B). Under control conditions ATP levels remained unaffected by each of the PHD-inhibitors (Fig. 36B). In order to complete evaluation of mitochondrial function so far, MMP was assessed by TMRE staining and subsequent FACS analysis. Glutamate induced a loss of MMP in 40% of the cells. DFO as well as DHB and CPO completely averted glutamate-induced breakdown of MMP which also did not vary between control cells and cells only treated with a particular PHD-inhibitor (Fig. 36C). These data confirmed the assumption that the PHD-inhibitors investigated in the present work preserved mitochondrial integrity.

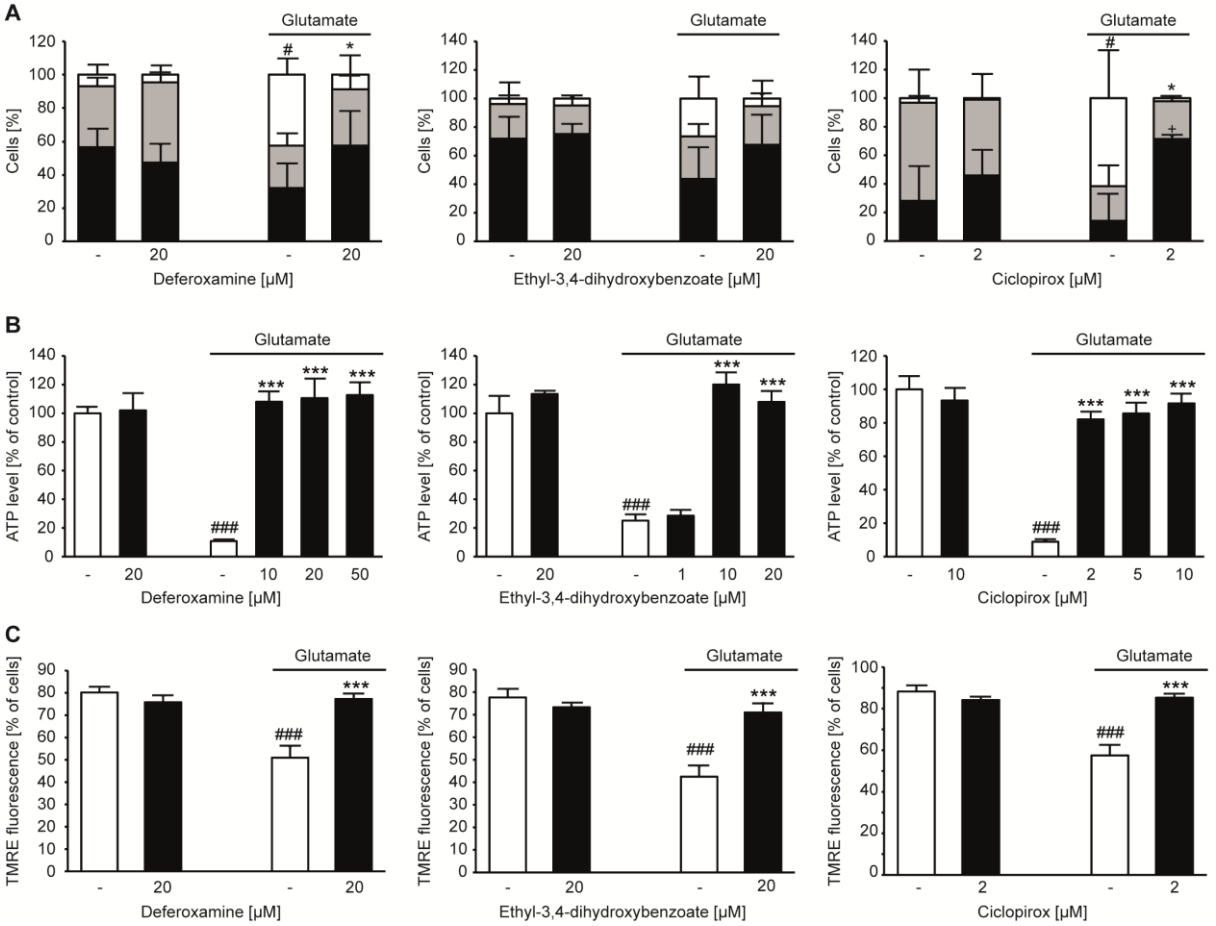

Figure 36: PHD-inhibitors restore mitochondrial morphology and function

A: DFO, DHB and CPO kept mitochondrial morphology and diminished glutamate-induced mitochondrial fission. Data are given as mean + SD (n=4). $^{\#}$p<0.05 compared to Cat III of untreated control; *p<0.05 compared to Cat III of glutamate treated control (ANOVA, Scheffé's test). **B:** Different concentrations of DFO, DHB and CPO abolished loss of ATP in the presence of glutamate (7 mM, 15 h). Data are shown as mean + SD (n=8). $^{\#\#\#}$p<0.001 compared to untreated control; ***p<0.001 compared to glutamate treated control (ANOVA, Scheffé's test). **C:** DFO, DHB and CPO fully prevented breakdown of MMP after glutamate exposure (7 mM, 15 h). Data are given as mean + SD (n=4). $^{\#\#\#}$p<0.001 compared to untreated control; ***p<0.001 compared to glutamate treated control (ANOVA, Scheffé's test).

3.4.3 PHD-inhibitors preserve mitochondrial respiration and abolish mitochondrial ROS formation

Finally, mitochondrial respiration and ROS formation were examined to complement the analysis of mitochondrial function. Therefore, measurements of the OCR were performed with the Seahorse XF96 system. HT-22 cells exposed to glutamate exhibited a decreased basal and maximal respiration and also oxyquinoline somewhat reduced maximal respiration, compared to control cells, but was able to attenuate the drastic perturbation of mitochondrial respiration upon the glutamate

challenge (Fig. 37A). Glutamate-induced mitochondrial demise was again confirmed by the increased formation of mitochondrial ROS at glutamate toxicity shown by enhanced red fluorescence. Simultaneous administration of oxyquinoline fully prevented a rightward shift of the curve and thereby production of mitochondrial ROS which was also not affected by oxyquinoline in control conditions (Fig. 37B).

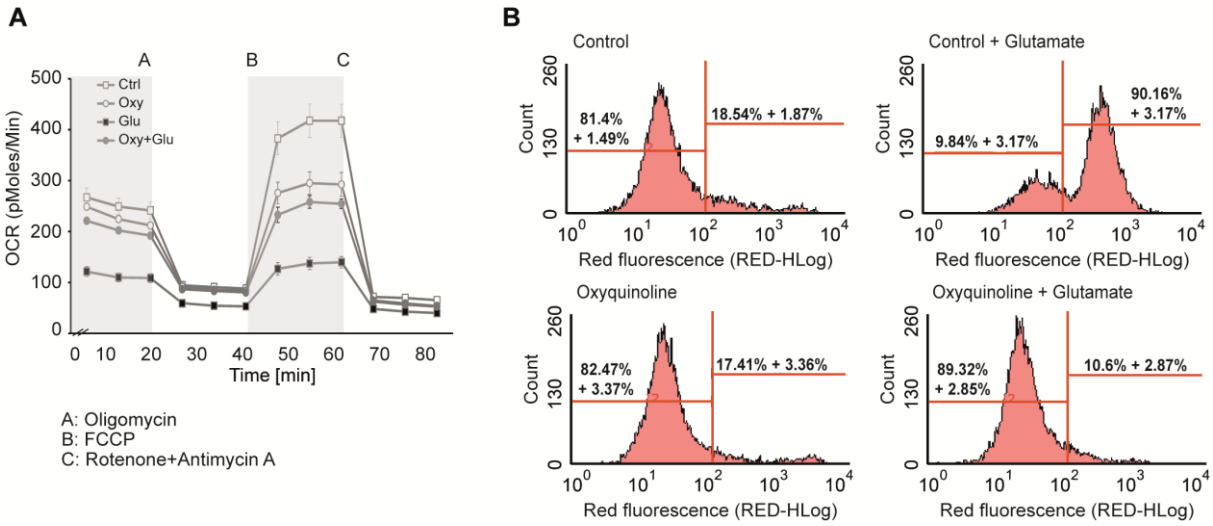

Figure 37: Oxyquinoline preserves mitochondrial respiration and abolishes mitochondrial ROS formation
A: Measurement of the oxygen consumption rate (OCR) revealed restored basal and maximal respiration by oxyquinoline (2 µM) after glutamate treatment (4 mM, 15 h). **B:** Glutamate-induced (7 mM, 14 h) mitochondrial ROS formation was fully abolished by oxyquinoline (2 µM) shown in representative plots from FACS analysis.

It was also not surprising that DFO, DHB as well as CPO had the ability to diminish the reduction of basal and maximal respiration after glutamate challenge. Additionally, these substances decreased maximal respiration per se (Fig. 38A) as observed with oxyquinoline. As a further sign for oxidative stress induced by glutamate, nearly 70% of cells produced an enhanced amount of mitochondrial ROS. Inhibition of PHDs by DFO, DHB or CPO fully preserved mitochondrial ROS formation to control levels. Basal formation of mitochondrial ROS remained unaffected by any of the inhibitors (Fig. 38B). Taking these data together with the observations that the PHD-inhibitors prevented ATP depletion and restored mitochondrial morphology and MMP after glutamate exposure (section 3.4.2), it is concluded that PHD-inhibition via both the 2-oxoglutarate analogue DHB and iron chelation by DFO, CPO or oxyquinoline was sufficient to fully prevent glutamate-induced mitochondrial demise.

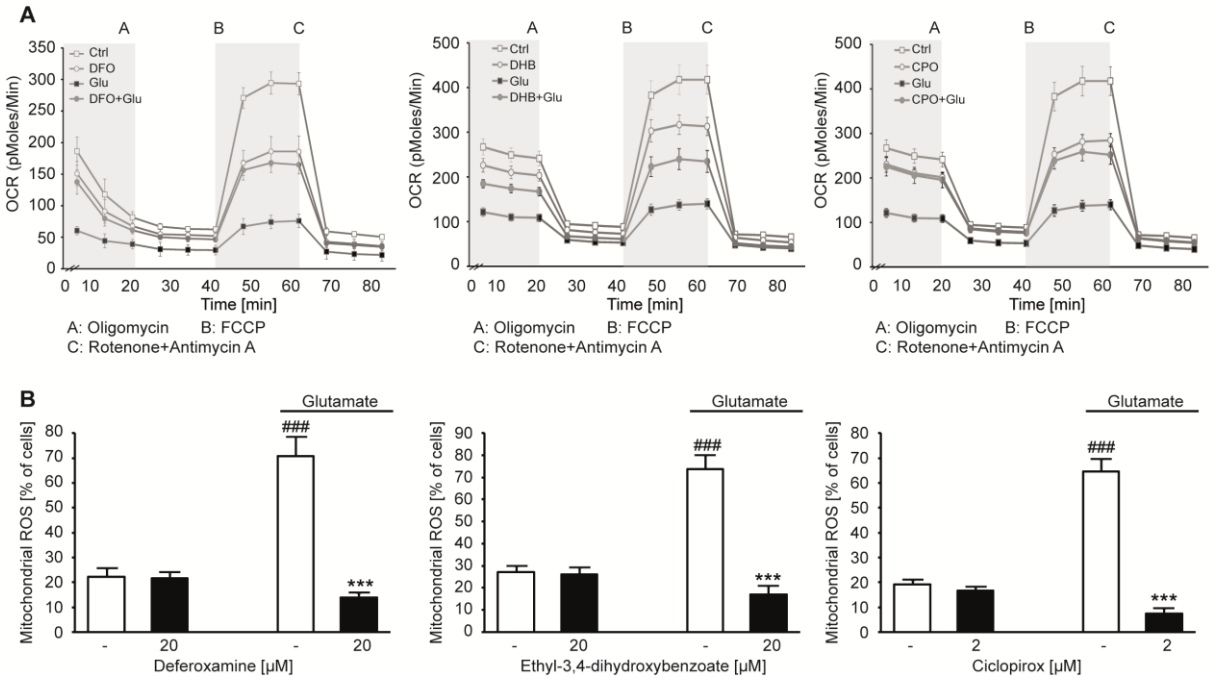

Figure 38: PHD-inhibitors restore mitochondrial respiration and prevent mitochondrial ROS formation
A: DFO (20 µM), DHB (20 µM) and CPO (2 µM) restored basal and maximal respiration after glutamate treatment (4 mM, 15 h) as indicated by measurement of the OCR by the Seahorse system. **B:** Glutamate-induced (3 mM, 14 h) mitochondrial ROS formation was fully prevented by particular PHD-inhibitors detected by MitoSOX staining and subsequent FACS analysis. Data are shown as mean + SD (n=4). $^{###}$p<0.001 compared to untreated control; ***p<0.001 compared to glutamate treated control (ANOVA, Scheffé's test).

3.4.4 Lipid peroxidation is prevented by inhibition of PHDs

As mentioned before, mitochondrial damage is the consequence of glutamate-induced GSH depletion and subsequent lipid peroxidation[46,49]. Since pharmacological inhibition of PHDs provided such a strong protection of mitochondrial integrity and also PHD1 silencing showed reduced lipid peroxidation it was further of interest to detect whether DFO, DHB, CPO and oxyquinoline also interfered with this particular trigger mechanism of oxytosis upstream of mitochondria. Therefore, lipid peroxidation was assessed via staining with BODIPY 581/591 C11 and subsequent FACS analysis. Quantification of representative FACS plots demonstrated increased formation of lipid peroxides which was fully abolished by simultaneous administration of oxyquinoline (Fig. 39A) and also DFO, DHB and CPO entirely prevented lipid peroxidation as shown in the bar graphs (Fig. 39B-D). Basal amount of lipid peroxides was not affected by single treatment with any of the inhibitors (Fig. 39A-D). These findings suggested that the PHD-inhibitors used in this work act upstream of mitochondria and potentially inhibit LOX activity.

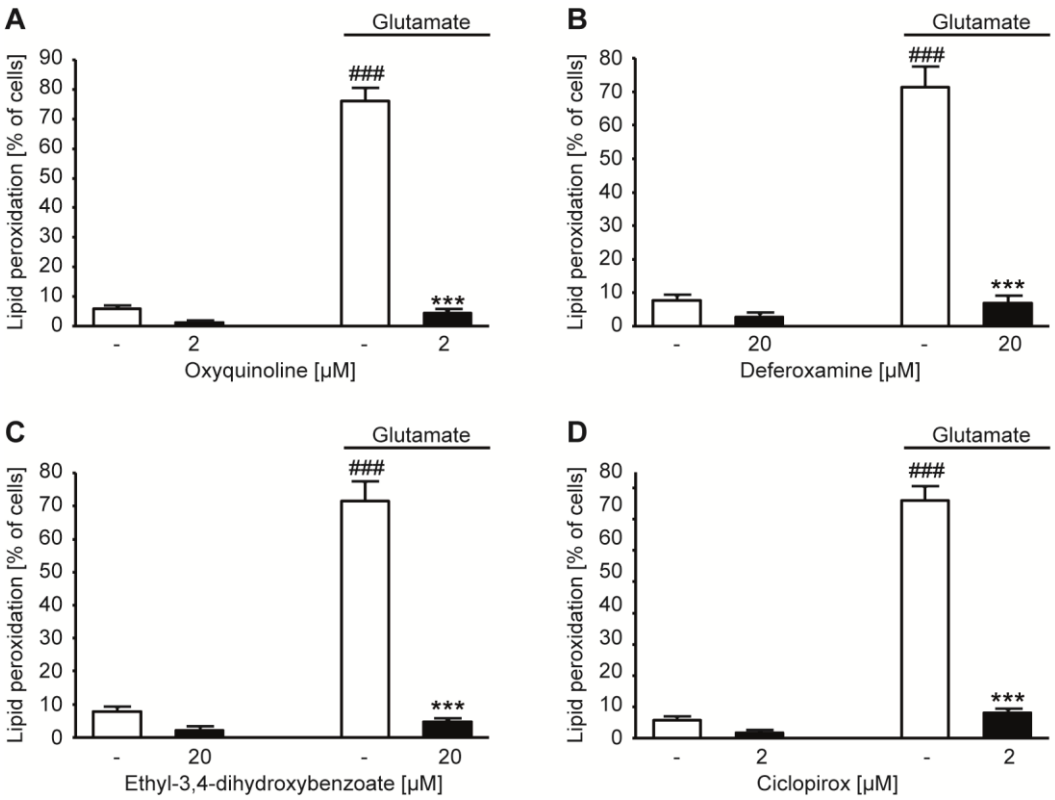

Figure 39: Lipid peroxidation is prevented by PHD-inhibition

BODIPY 581/591 C11 staining detected formation of lipid peroxides after glutamate challenge (5 mM, 13.5 h) which was fully abolished by co-treatment with oxyquinoline **(A)**, DFO **(B)**, DHB **(C)** and CPO **(D)**. Data are shown as mean + SD (n=4). ###p<0.001 compared to untreated control; ***p<0.001 compared to glutamate treated control (ANOVA, Scheffé's test).

3.4.5 Glutamate-induced glutathione depletion is not restored by oxyquinoline

In order to further elucidate the mechanisms underlying protection against glutamate-induced cell death mediated by inhibition of PHDs, GSH levels were next determined because a drop in GSH is regarded as the starting point of oxytosis inducing lipid peroxidation through activation of LOX[42]. At this point, only oxyquinoline was applied for the further study, since this substance has been shown to be a rather specific inhibitor of PHDs with less pronounced iron chelating properties[152], even though specific targeting of PHDs has also been described for DFO[155]. Similar to previous reports[42,46], glutamate induced a rapid and sustained decrease of GSH levels within 2 h and up to 10 h of exposure. Remarkably, it was not possible to detect any GSH in HT-22 cells at 10 h post glutamate exposure because the amount of GSH dropped below detection limits. Surprisingly, although oxyquinoline fully prevented cell death,

lipid peroxidation and the according morphological changes after glutamate exposure it was not able to rescue the observed drop in GSH levels (Fig. 40) indicating that PHD inhibition by oxyquinoline provided neuroprotective effects downstream of GSH depletion.

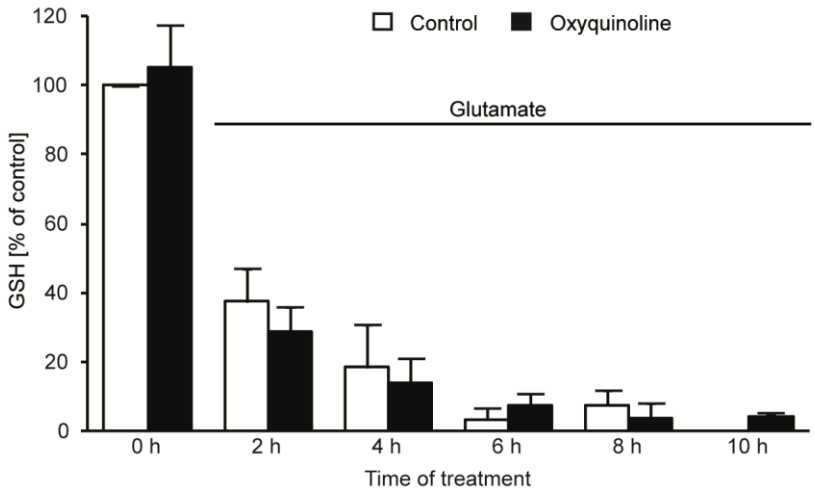

Figure 40: Glutathione depletion is not diminished by oxyquinoline

Measurement of GSH revealed rapid decrease of GSH after glutamate exposure (5 mM). Oxyquinoline was not able to restore GSH levels. Data are given as mean + SD (n=4).

3.4.6 Oxyquinoline exhibits antioxidative properties

The results described before showed that oxyquinoline fully abolished lipid peroxidation and formation of mitochondrial ROS, but was not able to prevent glutamate-induced GSH depletion which is considered to be a key trigger for the development of oxidative stress. In order to elucidate the underlying mechanism of oxyquinoline effects on ROS metabolism in HT-22 cells and the neuroprotective effect despite GSH depletion, formation of soluble ROS was investigated in an early phase of oxytosis. Therefore, HT-22 cells were challenged with glutamate for 6 h, followed by staining with DCF and subsequent FACS analysis. Exclusive treatment with oxyquinoline did not change basal levels of soluble ROS, while glutamate enhanced green fluorescence of DCF reflecting formation of soluble ROS (Fig. 41A) and corresponding well with the results of the previous GSH measurements. This increase in soluble ROS was reduced by 50% upon co-treatment with oxyquinoline (Fig. 41B), suggesting some antioxidative properties of oxyquinoline. To further confirm this conclusion, HT-22 cells were treated with different concentrations of H_2O_2 and oxyquinoline, and cell viability was detected using the MTT assay.

Oxyquinoline prevented the loss of cell viability induced by concentrations of 600 µM and 700 µM H_2O_2 in a dose-dependent manner, but failed to protect against H_2O_2 at a concentration of 800 µM (Fig. 41C) confirming antioxidative properties of oxyquinoline.

Since these findings could not exclusively explain the observations at the level of mitochondria in glutamate-induced cell death, another question was whether oxyquinoline was able to regulate the antioxidative defence of mitochondria by changing their protein expression pattern. To this end mRNA and protein expression levels of MnSOD were examined. RT-PCR analysis revealed no changes in the mRNA amount of MnSOD either in the presence of glutamate or oxyquinoline or a combination of both. As previously described in section 3.2.9 protein levels of MnSOD increased after 14 h of glutamate exposure detected by Western blot. Co-treatment with oxyquinoline inhibited this increase (Fig. 41D). As assumed for PFTα before, the reduction of MnSOD protein levels by oxyquinoline is regarded as a consequence of the protective effect and not as a cause for protection since the upregulation of MnSOD in response to glutamate toxicity seems to be a compensatory mechanism to cope with enhanced oxidative stress[215]. Further, oxyquinoline treatment alone did not change MnSOD expression levels.

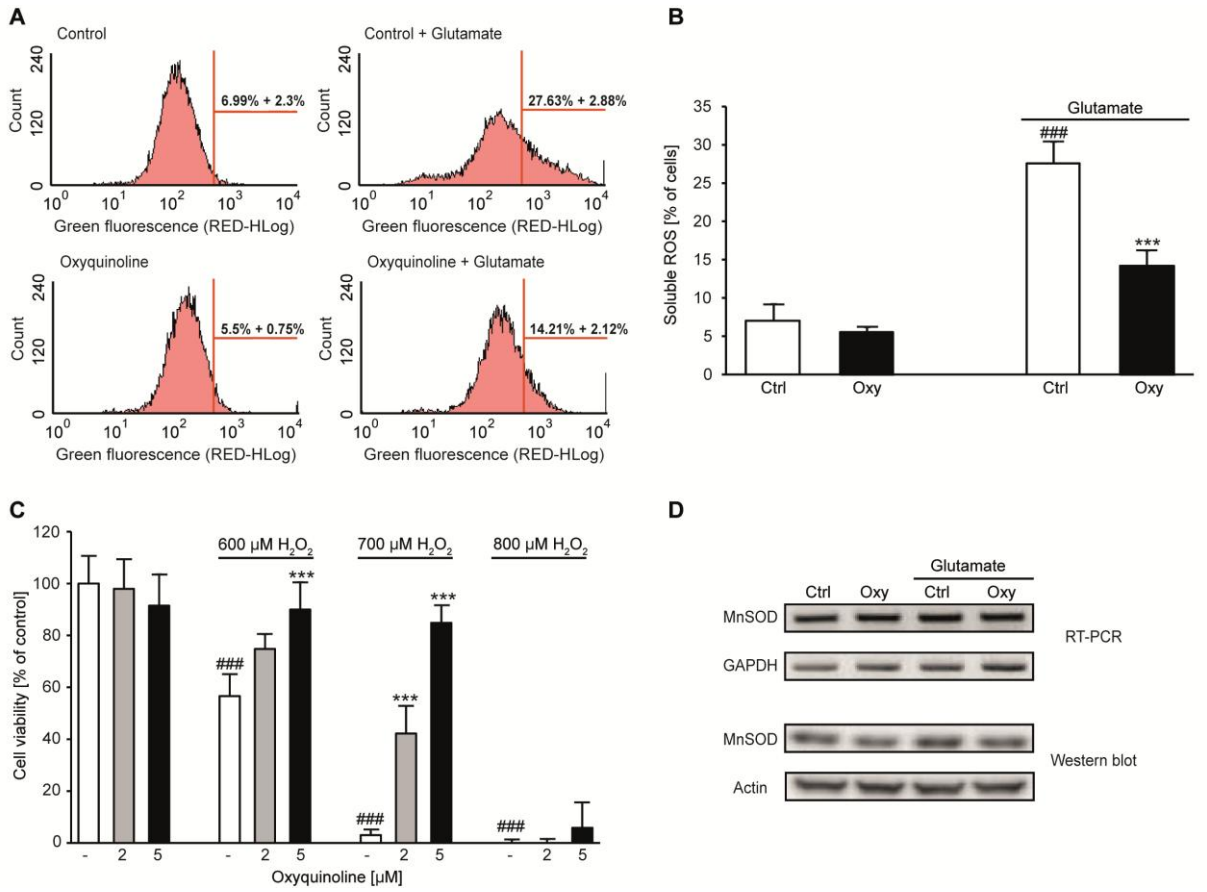

Figure 41: Oxyquinoline exhibits antioxidative properties

A: Representative plots from DCF staining and subsequent FACS analysis displayed formation of soluble ROS after 6 h of glutamate challenge (4 mM). Oxyquinoline (2 µM) halved this increase in ROS. **B:** Quantification of plots from A showed partial reduction of soluble ROS by oxyquinoline. Data are shown as mean + SD (n=4). ###p<0.001 compared to untreated control; ***p<0.001 compared to glutamate treated control (ANOVA, Scheffé's test). **C:** MTT assay revealed dose dependent protection of oxyquinoline against oxidative stress induced by H_2O_2 (14 h). Data are shown as mean + SD (n=8). ###p<0.001 compared to untreated control; ***p<0.001 compared to respective H_2O_2-treated control (ANOVA, Scheffé's test). **D:** RT-PCR detected no changes in mRNA expression levels of MnSOD by particular treatment. Western blot analysis showed enhanced expression of MnSOD protein after glutamate challenge (4 mM, 14 h) which was reduced back to control levels by co-treatment with oxyquinoline (2 µM). Oxyquinoline alone did not affect MnSOD expression levels.

3.4.7 The eIF2α/ATF4 pathway is regulated by oxyquinoline

ATF4 has been shown to correlate with oxidative stress[169,218] and also to regulate and interact with PHDs[165,166]. Hence, the impact of oxyquinoline on ATF4 expression was investigated also because the previous reports suggested upregulation and activation of this transcription factor as an underlying mechanism of oxyquinoline mediated neuronal protection. Western blot analysis showed increased expression of ATF4 after 4 h of glutamate exposure. Co-treatment with oxyquinoline seemed to further enhance ATF4 protein levels, but oxyquinoline alone showed only marginal

effects on ATF4 expression in HT-22 cells after 4 h of incubation (Fig 42A). At 14 h after the onset of the glutamate challenge ATF4 levels declined, while simultaneous administration of oxyquinoline prevented this down regulation of ATF4 protein (Fig. 42C). Messenger RNA expression levels of ATF4 remained unchanged for any treatment condition at both 4 h and 14 h as detected by RT-PCR (Fig. 42B, D).

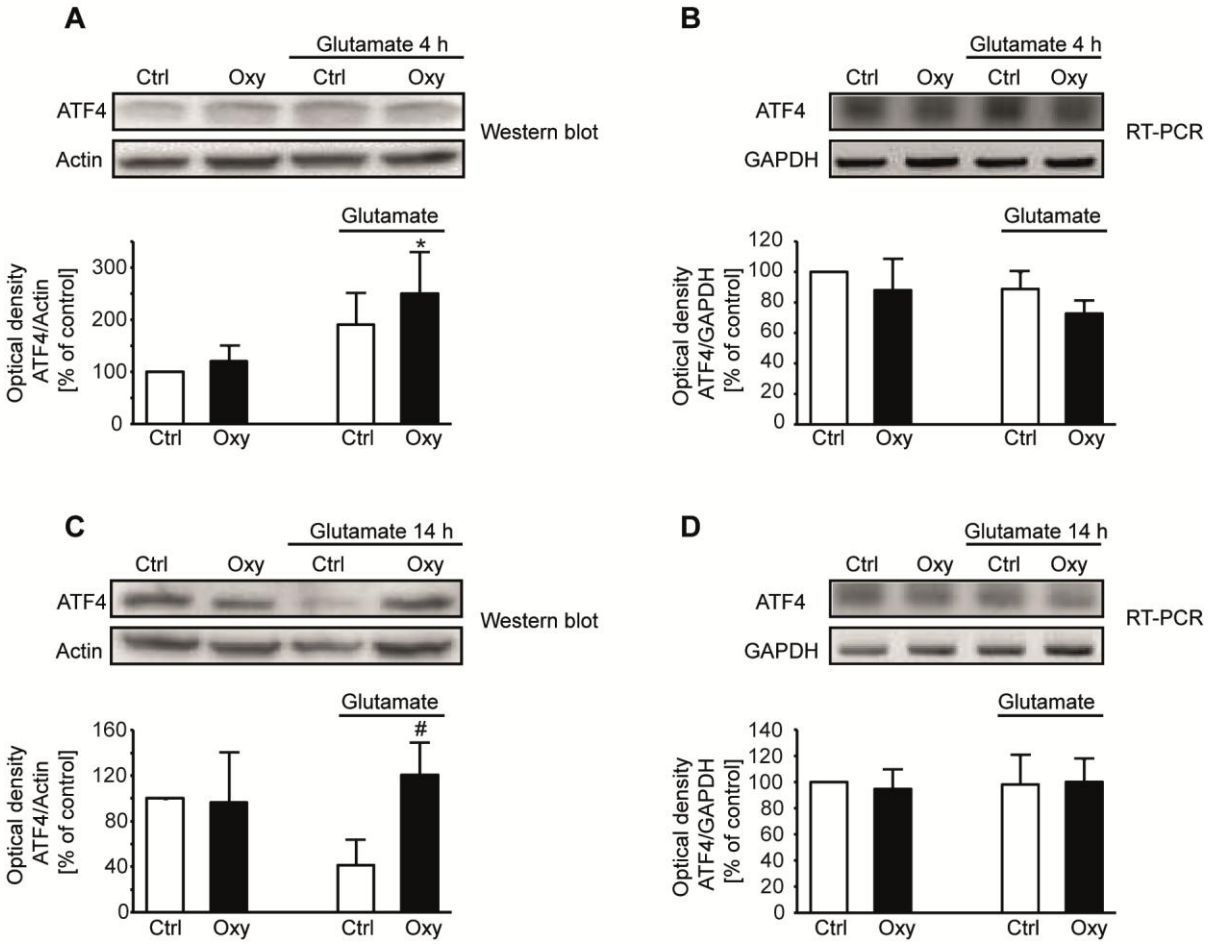

Figure 42: Oxyquinoline regulates ATF4 expression levels

A: Representative Western blots and corresponding quantification of 4 independent Western blots showed upregulation of ATF4 after glutamate challenge (4 mM, 4 h) in the presence and absence of oxyquinoline (2 µM). Data are shown as mean + SD (n=4). *p<0.05 compared to untreated control (ANOVA, Scheffé's test). **B:** RT-PCR and corresponding quantification (n=3) detected no changes in mRNA expression levels of ATF4 after oxyquinoline (2 µM) treatment in the presence and absence of glutamate (4 mM, 4 h). **C:** Representative Western blots and appendant quantification of 4 independent Western blots depicted down regulation of ATF4 after glutamate treatment (4 mM, 14 h) which was prevented by co-treatment with oxyquinoline (2 µM). Data are shown as mean + SD (n=4). $^{\#}$p<0.05 compared to glutamate treated control (ANOVA, Scheffé's test). **D:** RT-PCR and corresponding quantification (n=4) detected no changes in mRNA expression levels of ATF4 after oxyquinoline (2 µM) treatment in the presence and absence of glutamate (4 mM, 14 h).

This is in line with findings by Yukawa and colleagues reporting that changes in ATF4 protein levels were attributed to enhanced translation of ATF4 mRNA and not enhanced transcription[219].

Furthermore, the xCT is a known target of ATF4[220] and concomitantly plays a central role in glutamate-induced oxytosis since its inhibition by glutamate gears the oxidative stress machinery[42]. After 4 h of treatment, oxyquinoline alone and also glutamate significantly increased xCT levels while the combination had just a small effect (Fig. 43A). Similar to the expression pattern of ATF4, levels of xCT were decreased after 14 h of glutamate exposure. This decrease was prevented by co-treatment with oxyquinoline (Fig. 43A).

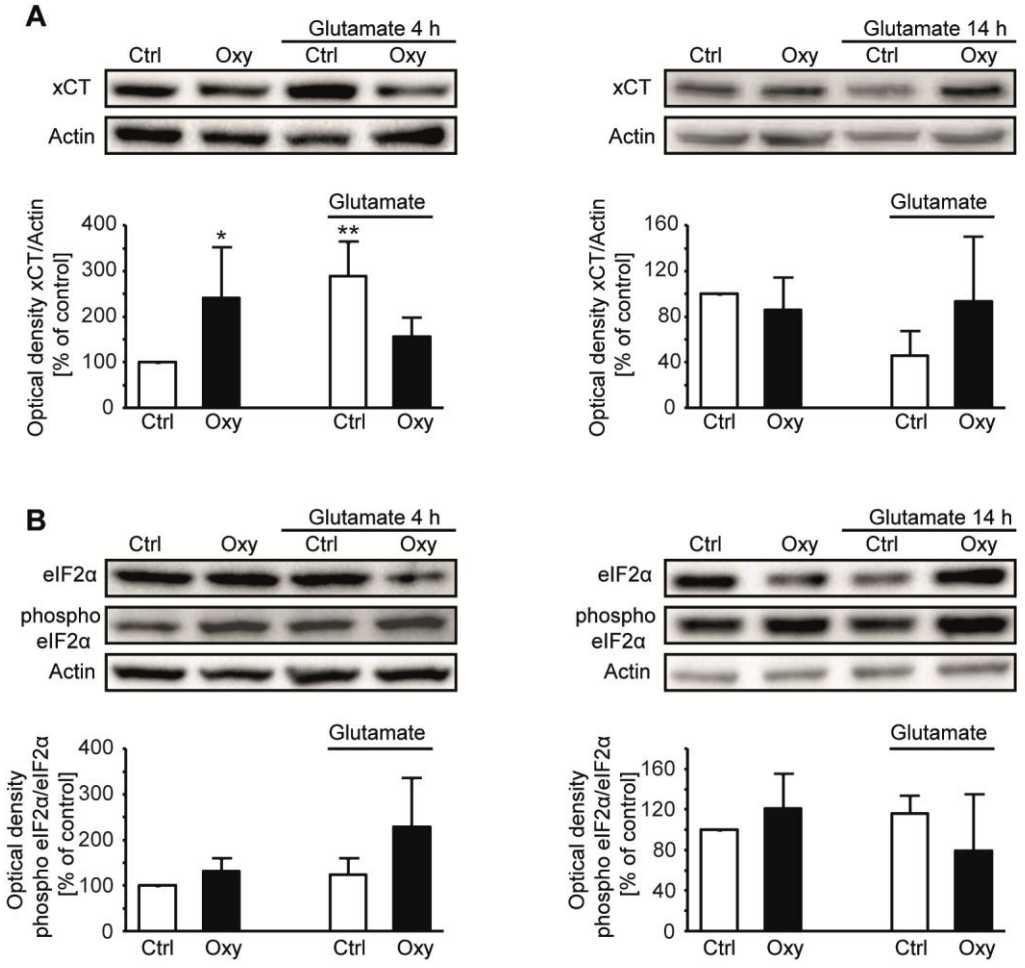

Figure 43: Oxyquinoline regulates expression levels of xCT and phosphorylation of eIF2α

A: Representative Western blots and corresponding quantification of 5 independent Western blots showed regulation of xCT after treatment with oxyquinoline (2 µM) in the presence and absence of glutamate (4 mM) at 4 h and 14 h of exposure. Data are shown as mean + SD (n=5). *p<0.05 and **p<0.01 compared to untreated control (ANOVA, Scheffé's test). **B:** Representative Western blots and corresponding quantification of 4 independent Western blots depicted regulation and phosphorylation of eIF2α after treatment with oxyquinoline (2 µM) in the presence and absence of glutamate (4 mM) at 4 h and 14 h of exposure.

In order to determine whether the regulation of both proteins was controlled by the eIF2α/ATF4 pathway, the phosphorylation state of eIF2α at both 4 h and 14 h after glutamate treatment was investigated next. The phosphorylation of eIF2α seemed to be transiently enhanced at 4 h in the presence of glutamate and oxyquinoline, but remained unchanged after 14 h of treatment (Fig. 43B).

3.4.8 Oxyquinoline protects against oxytosis independent of ATF4

The data presented before clearly showed a regulation of ATF4 by oxyquinoline. In order to address the question whether this modulation was required for oxyquinoline mediated protection, HT-22 cells were transfected with a siRNA selectively targeting ATF4, 48 h later challenged with glutamate and simultaneously treated with oxyquinoline. AV/PI staining and subsequent FACS analysis demonstrated that oxyquinoline protected both cells transfected with unspecific siScr and siATF4 against glutamate toxicity to a similar extent. Notably, ATF4 silencing alone increased the amount of AV and PI positive cells indicating cell death already under conditions of ATF4 depletion. The toxicity exerted by ATF4 gene silencing was prevented by oxyquinoline (Fig. 44A). Further, real-time impedance measurements revealed that ATF4 silenced cells die faster than cells transfected with siScr upon glutamate exposure proposing that ATF4 down regulation rendered HT-22 cells more susceptible to oxidative stress. This is in line with the observations of AV/PI staining where the amount of dead cells in ATF4 silenced cells exceeded the amount in cells transfected with control siScr after glutamate exposure. Real-time recordings also showed that knockdown of ATF4 slowed down the proliferation rate of HT-22 cells. Importantly, these measurements uncovered that oxyquinoline mediated protection in cells transfected with siATF4 seemed not to be as persistent as previously observed for the effects of oxyquinoline against glutamate toxicity (Fig. 44B). The protective effects of oxyquinoline after knockdown of ATF4 were also confirmed by MTT assay (Fig. 44C), although these data suggested that ATF4 silencing diminished the beneficial effects of oxyquinoline because the protection was not as pronounced as observed in the AV/PI staining. This discrepancy is explained by the different methods applied. For the FACS analysis, a defined number of cells, in this case 10 000, was analysed while in the MTT assay the amount of MTT reagent reduced by the remaining viable cells in one well is detected and correlates with cell viability and cell proliferation. The resulting absorption is not only dependent on cell viability, but

also cell number and since ATF4 slowed down the proliferation of the HT-22 cells compared to cells transfected with siScr, here the signal was lower because of a minor cell number per well. This effect is graded during FACS analysis, since in this method single cells are counted thereby, the apparent smaller effect of oxyquinoline in the MTT assay compared to AV/PI staining can be explained.

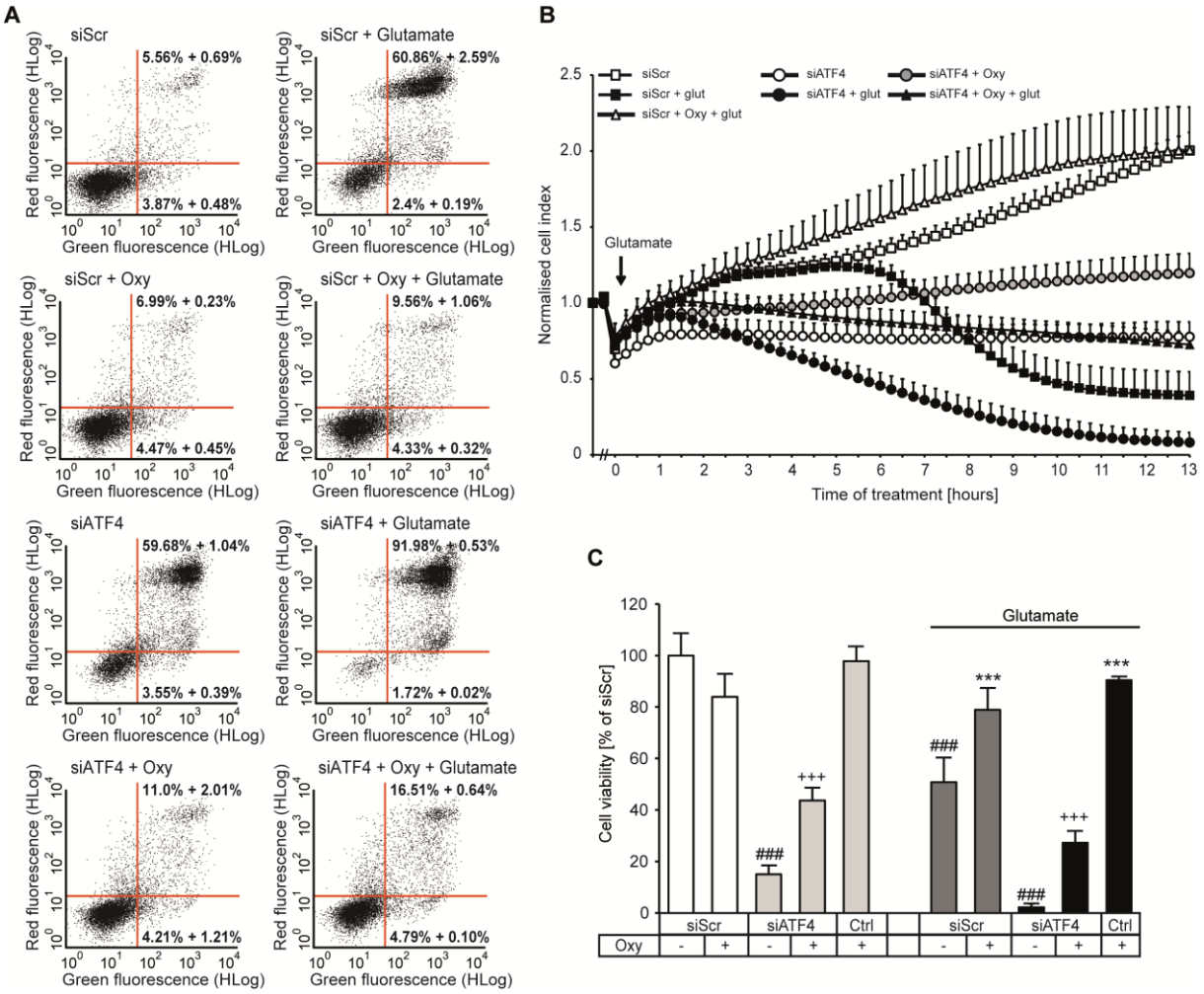

Figure 44: ATF4 silencing does not abolish oxyquinoline mediated protection

A: HT-22 cells were transfected with a siRNA selectively targeting ATF4 (siATF4, 40 nM) or a control siRNA (siScr, 40 nM) and after 48 h exposed to glutamate and oxyquinoline (2 µM). Representative dot plots of AV/PI staining and subsequent FACS analysis showed cell death after glutamate challenge (6 mM, 25 h) and toxicity of siATF4 (40 nM). Oxyquinoline abolished both toxicity of glutamate treatment and ATF4 silencing. **B:** xCELLigence measurement revealed restored protective effect against glutamate toxicity (6 mM) of oxyquinoline (2 µM) in ATF4 silenced cells which was performed by transfection with siATF4 (40 nM) 48 h before onset of treatment. Transfection with siScr (40 nM) was accordingly performed. **C:** MTT assay confirmed toxicity of ATF4 knockdown. HT-22 cells were transfected with siATF4 (40 nM) or siScr (40 nM) and after 48 h exposed to glutamate (5 mM, 17 h) and oxyquinoline (2 µM). Data are shown as mean + SD (n=8). $^{###}$p<0.001 compared to untreated siScr; ***p<0.001 compared to glutamate treated siScr, $^{+++}$p<0.001 compared to respective siATF4 (ANOVA, Scheffé's test).

Toxic effects by ATF4-gene silencing were likely attributed to the enhanced formation of soluble ROS which occurred in a time-dependent manner after incubation with ATF4 siRNA (Fig. 45A). Co-treatment with oxyquinoline during transfection prevented this ROS formation due to down regulation of ATF4 (Fig. 45B). Overall, these data suggested that the observed oxyquinoline mediated upregulation of ATF4 may contribute to the protective effect of the PHD-inhibitor, but was dispensable.

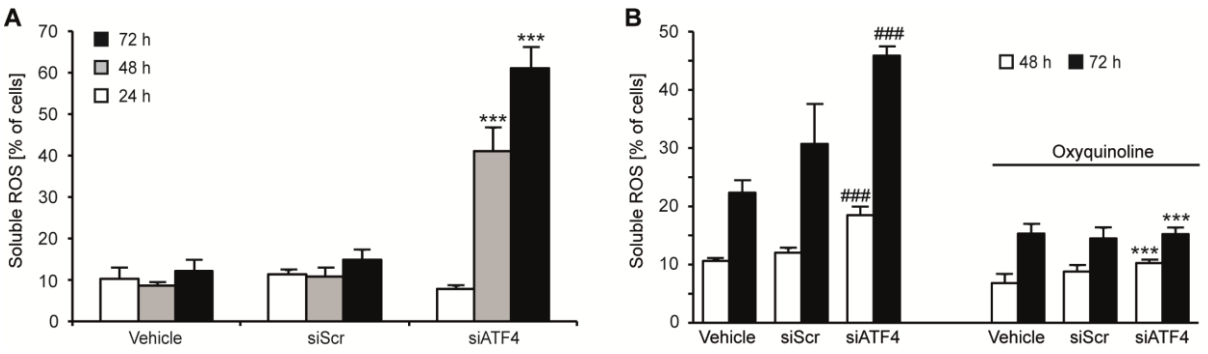

Figure 45: ATF4 silencing induces formation of soluble ROS

A: DCF staining and subsequent FACS analysis revealed time-dependent enhanced formation of soluble ROS in cells transfected with siATF4 (40 nM) compared to cells transfected with siScr (40 nM). Data are shown as mean + SD (n=4). ***p<0.001 compared to respective vehicle (ANOVA, Scheffé's test). **B:** Co-treatment with oxyquinoline (2 µM) from the point of transfection prevented formation of soluble ROS induced by knockdown of ATF4 detected by DCF staining and following FACS analysis. Data are given as mean + SD (n=4). ###p<0.001 compared to respective untreated vehicle, ***p<0.001 compared to respective oxyquinoline-treated vehicle (ANOVA, Scheffé's test).

3.5 Inhibition of PHDs prevents ferroptosis

3.5.1 Erastin sensitivity of HT-22 cells

In 2012, Dixon and colleagues first described ferroptosis, a new cell death paradigm in cancer cells which was also induced by the inhibition of the X_c^--transporter. This form of cell death was characterised as 'morphologically, biochemically, and genetically distinct from apoptosis, necrosis, and autophagy' and was induced by the small molecule erastin[74].

In the present work, erastin was applied to HT-22 cells to examine whether this way of X_c^--inhibition also leads to cellular impairment in this particular neuronal cell line. After 16 h of treatment, erastin induced cell death in a concentration-dependent manner at concentrations of 0.5-3 µM reflected by a loss of cell viability in the MTT assay (Fig. 46). As for functional analysis an adequate damage is required, erastin

concentrations of 2 µM were used for further experiments, since erastin reduced cell viability to almost 20% of control at this concentration.

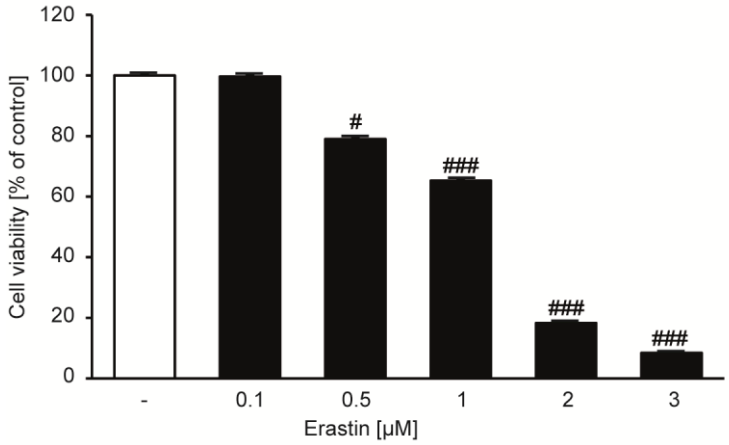

Figure 46: Erastin sensitivity of HT-22 cells

MTT assay revealed dose-dependent loss of cell viability after erastin exposure (16 h). Data are shown as mean + SD (n=8). $^{\#}p<0.05$ and $^{\#\#\#}p<0.001$ compared to untreated control (ANOVA, Scheffé's test).

3.5.2 Targeting PHDs inhibits erastin-induced cell death

Erastin exposure induces death of HT-22 cells apparently via similar mechanisms as glutamate[221]. Since ferroptosis is considered to be iron dependent and, additionally is prevented by iron chelators, whose on-target effectors are PHDs[142], the question arose whether inhibition of PHDs is able to prevent erastin-induced cell death[75]. To this end, HT-22 cells were simultaneously treated with erastin and the PHD-inhibitors DFO, CPO and oxyquinoline which act via iron chelation. MTT assay revealed strong toxicity by erastin indicated by a reduction in cell viability to about 10%. Inhibition of PHDs by any of the aforementioned substances fully prevented erastin-induced cell death. In order to confirm that the observed protection was attributable to inhibition of PHD family proteins and not the result of an overall iron chelation, further the 2-oxoglutarate analogue DHB was tested. Application of DHB also completely abolished loss of cell viability after erastin exposure (Fig. 47).

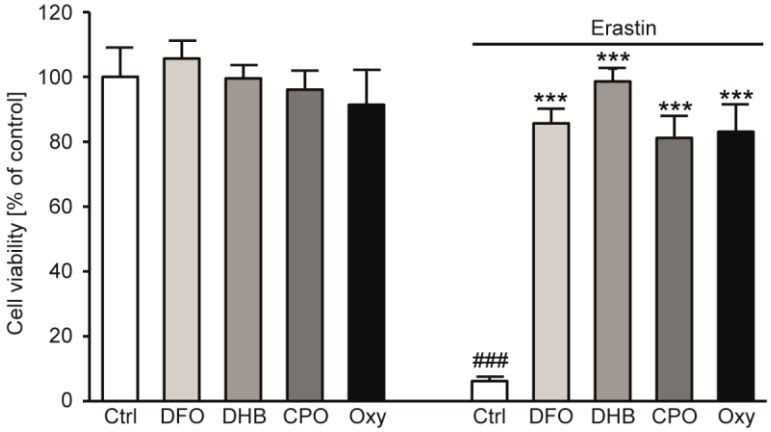

Figure 47: PHD-inhibitors prevent erastin-induced ferroptosis

DFO (20 µM), DHB (20 µM), CPO (2 µM) and oxyquinoline (2 µM) protected HT-22 cells against erastin-induced cell death (1 µM, 15 h) detected by MTT assay. Data are shown as mean + SD (n=8). $^{###}$p<0.001 compared to untreated control, ***p<0.001 compared to erastin-treated control (ANOVA, Scheffé's test).

Furthermore, real-time impedance measurements demonstrated that the knockdown of PHD1 by siPHD1 I attenuated erastin-induced cell death as well, although this effect was only transient (Fig. 48). Altogether, these data suggested that PHDs may contribute to erastin-induced cell death and represent a suitable target to prevent ferroptosis.

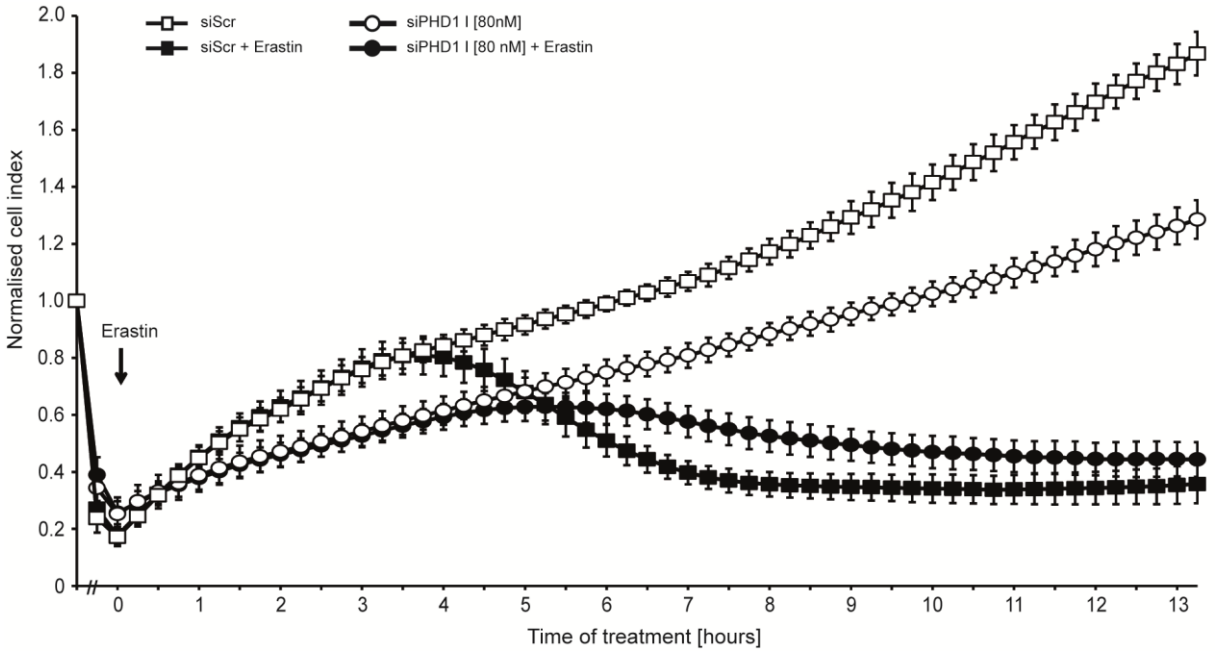

Figure 48: PHD1 silencing delays erastin toxicity

HT-22 cells were transfected with siPHD1 I (80 nM) or siScr (80 nM) and 48 h later treated with erastin. Knockdown of PHD1 delayed erastin-induced cell death (2 µM) recorded by real-time impedance measurement.

4 Discussion

The aim of the present study was to elucidate the role of p53 and PHDs in neuronal oxytosis, a form of regulated cell death induced by oxidative stress, with particular focus on mitochondrial integrity and function. Pharmacological inhibition of p53 and PHDs and siRNA-mediated down regulation of p53 and PHD1 attenuated mitochondrial damage and glutamate-induced oxidative death in neuronal HT-22 cells. Thereby, these proteins emerged as promising targets for neuroprotective strategies.

The first part of this thesis clearly showed that both pharmacological and genetic approaches inhibiting p53 function are capable of attenuating glutamate-induced cytotoxicity in HT-22 cells. However, the p53-inhibitor PFTα was more potent than p53 silencing regarding cell viability and furthermore, analyses of mitochondrial morphology, membrane potential and ROS formation revealed a protection of mitochondrial integrity only for PFTα, but not for p53 knockdown by RNA interference, suggesting that PFTα in contrast to p53 down regulation acts upstream or at the level of mitochondria. Moreover, these data propose additional effects of PFTα beyond inhibiting p53 function, and even a mechanism independent of p53 is conceivable. This conclusion is supported by the finding that PFTα was able to prevent cell death attributed to oxytosis in HT-22 cells depleted of p53. Further, in contrast to effects observed after p53 silencing, PFTα did not alter mRNA expression levels of p53 target genes.

The second part of the study revealed that different pharmacological strategies to inhibit members of the PHD family as well as selective gene silencing of PHD1 using siRNA approaches protected HT-22 cells against glutamate-induced cell death and preserved mitochondrial integrity, thus, identifying PHDs as contributors to oxytosis upstream of mitochondria. However, the effect of PHD1 siRNA regarding cell viability was rather small and transient compared to the pharmacological inhibitors. This phenomenon was also consistent throughout all analysed mitochondrial parameters and attributable to insufficient down regulation of PHD1 protein amount.

Moreover, the PHD-inhibitor oxyquinoline was shown to regulate the eIF2α/ATF4 pathway, but ATF4 silencing did not affect oxyquinoline-mediated protection of HT-22 cells suggesting that the observed regulation of ATF4 by oxyquinoline was dispensable for its neuroprotective effect.

Finally, the present work established the concept of ferroptosis in HT-22 cells. Both pharmacological inhibition of PHDs and selective knockdown of PHD1 prevented erastin-induced ferroptosis demonstrating that members of the PHD family were not only involved in mediating oxytosis, but also in ferroptosis.

4.1 Impact of mitochondrial demise in oxytosis

Mitochondrial dysfunction and demise appear early in all major neurodegenerative diseases[130] and are hallmarks of oxytosis caused by increased oxidative stress[49,69,71]. In HT-22 cells, glutamate induces an initial small wave of ROS which is followed by a second pronounced burst of ROS originating from the impaired mitochondria[46]. Accordingly, in the present study a strong increase in mitochondrial ROS production was observed after the glutamate challenge (Fig. 15B) and associated with cell death. Using the mitochondrial uncoupler FCCP and the complex III-inhibitor antimycin A in glutamate treated HT-22 cells, the mitochondrial ETC was identified as the primary source of mitochondrial ROS[46]. Further investigations in isolated mitochondria from rat brain showed that complex I accounted for the enhanced ROS production in response to glutamate[222]. However, inhibition of complex I with rotenone failed to prevent glutamate-induced ROS formation and subsequent cell death of HT-22 cells, but the inhibition of mitochondrial complex III with antimycin A and the mitochondrial uncoupler FCCP protected HT-22 cells against glutamate toxicity and following ROS production[46].

Under physiological conditions, the intact function of mitochondrial complexes is required for proper mitochondrial respiration to comply with cellular energy demand[123,124]. In the current work, measurements of the OCR to determine mitochondrial respiration revealed decreases of both basal and maximal respiration in cells exposed to glutamate (Fig. 37A) indicating a disturbed function of the mitochondrial complexes. Considering the aforementioned beneficial effects of different inhibitors of mitochondrial complexes in the paradigm of oxytosis[46] and the increased production of mitochondrial ROS of HT-22 cells exposed to glutamate, one would rather have expected an enhanced instead of a decreased activity of the ETC in HT-22 cells challenged with glutamate. Thus, the impaired mitochondrial respiration may reflect an adaptive mechanism of the dying cells against the substantial oxidative stress. This notion is supported by findings in HT-22 cells resistant to glutamate which also exhibited reduced mitochondrial respiration[223].

Notably, the cells analysed in the present study were assessed after long term glutamate treatment, i.e. after 15 h when most of the cells and their mitochondria were irreversibly damaged and, therefore, did not respire anymore. This conclusion is further supported by the observation that after long term glutamate treatment for about 14 h nearly 70% of the cells challenged with glutamate were dead (Fig. 13D).

Another hallmark of oxytosis indicating mitochondrial demise is the breakdown of the MMP (Fig. 12A) and the subsequent loss of ATP (Fig. 12B) because of increased oxidative stress[43,69,72] which was shown to result in the end in the release of Cyt c from the mitochondria[44] and the translocation of AIF to the nucleus[43,56]. Both, Cyt c release and AIF translocation are indicating the permeabilisation of the mitochondrial membrane which marks the point at which a cell is irreversibly damaged[25]. Investigations from our laboratory using fluorescently-labelled AIF in HT-22 cells demonstrated that once AIF was discharged from the mitochondria in response to glutamate toxicity, it rapidly translocated to the nucleus, where it mediated nuclear pyknosis and, accordingly, cell death[43]. These results were also confirmed *in vivo* in mice. Already twenty-four hours after ischemia induced by MCAO, AIF immunofluorescence was found in the nucleus and associated with DNA fragmentation[56]. These results confirmed that under conditions of cellular stress the mitochondrial fate decides on life and death of neurons.

In the past years, several mechanisms and proteins have been described to act upstream of mitochondrial demise, but the picture is yet not completed[25]. One prominent protein that acts upstream of mitochondrial damage in paradigms of oxidative stress induced cell death is Bid[26,43,56]. In the model of oxytosis it was shown by confocal fluorescence microscopy that Bid translocated to the mitochondria upon glutamate challenge and that interference with such translocation by specific inhibitors of Bid was capable of preventing cell death[43,63]. Furthermore, siRNA-mediated down regulation of Bid was able to restore the MMP after glutamate treatment[43]. All these observations emphasise the crucial role of Bid regulation for mitochondrial function and cellular maintenance. However, in the present study the expression of Bid mRNA was not enhanced in response to glutamate exposure, suggesting that post-translational modifications of Bid were responsible for the observed Bid-dependent mitochondrial damage and cell death. A prominent post-translational modification of Bid associated with cell death is the proteolytic cleavage of full-length Bid to tBid by caspases or calpains[224]. Via enhanced activation of

caspases[93,96] p53 may contribute to Bid-mediated mitochondrial demise independently of transcriptional regulation.

Another protein that was shown to play a major role for mitochondrial demise during oxytosis is DRP1[51,225]. DRP1 is a GTPase which regulates mitochondrial fission processes, a characteristic of mitochondrial impairment. In HT-22 cells glutamate-induced mitochondrial demise was marked by enhanced mitochondrial fragmentation (Fig. 11). It was previously shown in our laboratory using fluorescence microscopy that after glutamate exposure DRP1 translocated to the mitochondria[51]. MdiviA, a specific inhibitor of DRP1 and also siRNA-mediated knockdown of DRP1 prevented glutamate-induced cell death in the model system of oxytosis. Moreover, mdiviA was able to attenuate tBid-induced mitochondrial fragmentation and subsequent death of HT-22 cells[51] linking Bid and DRP1 and highlighting the pivotal role of both proteins for mitochondrial integrity.

Both Bid and DRP1 are under the transcriptional control of p53[226] and therefore, their expression levels were analysed in the present study to evaluate potential effects of p53 inhibition on these key regulators of mitochondrial integrity. The transcriptional regulation of Bid and DRP1 in response to glutamate and p53 knockdown respectively is further discussed in chapter 4.2.

Moreover, there are likely still many mechanisms and pathways yet to be identified which may contribute to mitochondrial impairment in oxytosis. For example, using specific PHD-inhibitors in this thesis revealed a new target to promote mitochondrial protection in the setting of oxytosis. To date, these inhibitors were only shown to attenuate cell death in different models of neurodegenerative diseases[153–155,160]. Furthermore, inhibition of PHDs protected against direct mitochondrial toxins such as 3-nitropropionic acid[158]. Here, it was demonstrated for the first time that inhibition of PHDs was also able to restore mitochondrial function in a model of lethal oxidative stress in neurons.

The current work showed that protection of HT-22 cells against glutamate-induced cell death by inhibition of p53 with PFTα and both pharmacological PHD-inhibitors and siRNA-mediated PHD1 gene silencing was accompanied by preserved mitochondrial morphology and function although these interventions were not able to prevent all metabolic alterations mediated by glutamate which occur upstream of mitochondria. For example, PFTα failed to prevent the first burst of ROS attributed to lipid peroxidation (Fig. 16) and oxyquinoline was not capable of preventing the drop

of GSH levels in response to glutamate exposure (Fig. 40) and subsequent formation of soluble ROS (Fig. 41A).

Overall, the findings of the present study highlight the crucial role of mitochondria in oxytosis. Furthermore, the current data demonstrated the importance of mitochondrial integrity for neuroprotection and confirmed mitochondrial damage as the ‘point of no return’[25] in cell death signalling.

4.2 The role of p53 in glutamate-induced oxytosis

The tumor suppressor protein p53 mainly mediates cell death via the transcriptional induction of pro-apoptotic genes[93,107,226]. The control of p53 transcriptional activity is crucial for determining whether a pro- or an anti-apoptotic cascade is activated in response to toxic stimuli[85]. Using a luciferase-based reporter assay, the present study clearly revealed that glutamate induced an increase in p53 transcriptional activity in HT-22 cells. Silencing p53 reduced p53 transcriptional activity both in the presence and absence of glutamate (Fig. 24A).

Previously, enhanced p53 transcriptional activity in neurons was also indirectly shown by the upregulation of p53 itself[94] and its target genes such as Bax, PUMA or NOXA[110,121] in response to several insults such as DNA damage[93,102], TBI[94] or hypoxic-ischemic brain damage[110,121]. Notably, the increased transcriptional activity of p53 in HT-22 cells after the glutamate challenge was not accompanied by an enhanced expression of p53 mRNA after glutamate treatment (Fig. 24B) which initially questioned the relevance of p53 in mediating oxytosis.

Under physiological conditions p53 levels are tightly controlled in a negative feedback loop by the E3 ligase MDM2 which represents a transcriptional target of p53[211]. Upon induction of p53, MDM2 levels rise and in turn MDM2 targets p53 for ubiquitination and its subsequent proteasomal degradation[227]. Under conditions of stress, inhibition of MDM2 allows for enhanced p53 expression[211,227]. In the present study, p53 silenced cells exhibited a reduced expression of MDM2 in the presence and absence of glutamate (Fig. 24B) indicating that the negative feedback loop was intact, even under conditions of oxidative stress.

PUMA is one of the most prominent target genes of p53 acting direct at the level of mitochondria where it can interact with Bax[110] to induce Cyt c release[109,228] and ultimately, cell death. In a model of epilepsy, the induction of status epilepticus by intra-amygdala administration of kainic acid in mice resulted in elevated PUMA levels and subsequent cell death[229]. Application of PFTα blocked enhanced expression of PUMA and attenuated kainic acid-mediated cell death. Accordingly, $PUMA^{-/-}$ mice were protected against neuronal damage induced by status epilepticus[229] demonstrating the pro-death function of PUMA. Additionally, in the CA1 region of rat brains, PUMA levels were shown to be increased in the mitochondria in response to transient global cerebral ischemia and preceded Cyt c release[110] underlining the crucial role of PUMA for mitochondrial impairment. In contrast, in the present model

of oxytosis PUMA levels were not altered upon the glutamate challenge, although mitochondrial demise is an established hallmark of oxytosis[49,69,71]. Furthermore, neither PFTα nor siRNA-mediated knockdown of p53 affected the expression levels of PUMA mRNA (Fig. 24B) proposing that oxytosis does not depend on PUMA regulation and activity.

As highlighted in chapter 4.1 mitochondria represent the central organelle which determines life and death of a cell. AIF, Bid and DRP1 are known p53 target genes[226] highly associated with the damage of mitochondria. In the HCT116 colon cancer cell line, mRNA levels of AIF were shown to be regulated by basal p53, but did not significantly alter upon induction of genotoxic stress with cisplatin despite increased p53 levels[230]. Accordingly, in HT-22 cells expression levels of AIF mRNA remained unchanged after the glutamate challenge. However, p53 levels were not increased after glutamate treatment. Furthermore, HCT116 cells lacking p53 displayed reduced AIF levels compared to wild-type cells[230]. In contrast, knockdown of p53 in HT-22 cells which was accompanied by a reduced p53 transcriptional activity did not alter AIF levels, suggesting that p53 transcriptional activity did not regulate AIF mRNA expression levels.

Whether p53 directly regulates transcription of DRP1 in neurons is not clear so far[226]. In HT-22 cells, the glutamate challenge did not alter expression levels of DRP1, although DRP1 is a known mediator of mitochondrial demise in this cell death paradigm and its down regulation was previously shown to prevent oxytosis[51]. Irrespective of enhanced expression levels of DRP1, a recent study demonstrated that a direct interaction between p53 and DRP1 was required to perturb mitochondrial function in striatal neurons overexpressing mutant huntingtin[231]. Therefore, it is conceivable that knockdown of p53 disrupted the described interaction between p53 and DRP1 and thereby contributed to the protective effect of p53 siRNA. However, it is so far unknown whether p53 and DRP1 directly interact with each other in the model system of glutamate-induced cell death and whether this interaction then mediates oxytosis.

The mouse Bid genome locus contains a functional p53-binding element[232]. Accordingly, Bid mRNA levels were upregulated in a p53-dependent manner in different cells lines[232]. Furthermore, Bid plays a key role during mitochondrial demise in oxytosis[43,49,71]. Nevertheless, in the present work Bid mRNA expression levels were not affected by glutamate challenge or silencing of p53 (Fig. 24B) further

suggesting that p53 transcriptional activity plays a minor role for the induction of oxytosis.

When analysing p53 target genes, the most striking observation was the decrease of p21 after p53 knockdown both in the presence and absence of glutamate. p21 is a key modulator of p53-induced senescence and plays also a crucial role for cellular survival[85,92,211]. Yu *et al.* reported that $p21^{-/-}$ cancer cells were more susceptible towards p53-induced apoptosis[233,234]. This is probably attributable to p21 mediating p53-dependent cell cycle arrest. High levels of cell cycle inhibitors such as p21 can prevent the induction of apoptosis via transcriptional upregulation of pro-apoptotic genes, since the ability of the cell cycle inhibitors to lead to cell cycle arrest exceeds the pro-apoptotic signalling[234]. Furthermore, previous findings in different cell death models showed that PFTα-mediated protection was accompanied by reduced expression levels of p21[235–238]. In contrast, in the present study PFTα did not alter p21 mRNA expression levels, but still prevented glutamate-induced death of HT-22 cells. Considering these findings and the differential outcome on cell viability after p53 down regulation opposed to PFTα application one can assume that lowered p21 levels rendered HT-22 cells more vulnerable to oxidative stress induced by glutamate. This may further explain the missing mitochondrial protection and the less pronounced neuroprotective effect of p53 siRNA on cellular resistance against oxytosis despite efficient p53 down regulation.

Overall the conclusion that p53 transcriptional activity played a minor role in glutamate-induced oxytosis in HT-22 cells was supported by three key findings of this study. First, glutamate treatment did not induce p53 expression levels. Second, the overall effect of p53 silencing on cell viability was only moderate and transient and third, knockdown of p53 failed to protect mitochondria. One reason for the minor importance of p53 in oxytosis could be the nature of HT-22 cells which were derived from mouse hippocampal neurons and immortalised using a temperature-sensitive SV-40 T antigen[195]. This antigen is able to bind and thereby repress p53 function[239] diminishing its influence on cellular homeostasis and life cycle.

4.2.1 PFTα mediates mitochondrial protection

The small molecule pifithrin-α (PFTα)[96,207,240] and its derivatives[120,241,242] are specific inhibitors of p53 whose neuroprotective potential was demonstrated in several studies[94,96,121,229,235,242,243]. For example, pre-treatment with PFTα significantly reduced neuronal infarction in mice subjected to MCAO[96]. Furthermore, PFTα protected primary neurons against Aβ toxicity[96] and attenuated neuronal cell death in response to genotoxic agents[96,98,122]. In order to characterise the role of p53 in glutamate-induced oxytosis PFTα was used in the present study.

Analyses of cell viability using different methods such as the MTT assay, real-time impedance measurements and AV/PI staining and subsequent FACS analysis (Fig. 13, 14) revealed a strong protective potential of PFTα in the present model of oxytosis in neuronal HT-22 cells. Furthermore, this compound was able to prevent cell death when applied up to 4 h after the onset of the glutamate challenge (Fig. 14) confirming previous findings *in vivo* where administration of PFTα up to 1 h after MCAO[235] and up to 6 h after TBI[94] mediated beneficial effects.

In the current model system, the protective effect was not restricted to the level of cell viability, but also observed at the level of mitochondria as indicated by full preservation of mitochondrial integrity, i.e. restored MMP and inhibition of mitochondrial ROS formation after glutamate exposure (Fig. 15). This is in line with previous findings from our laboratory showing that co-treatment with PFTα prevented enhanced mitochondrial fragmentation in response to oxidative stress[68] and that pre-treatment with PFTα attenuated depolarisation of the mitochondrial membrane potential after exposure to glutamate or Aβ in cultured hippocampal neurons[96]. In contrast, Sohn and colleagues claimed that PFTα provided protective effects downstream of mitochondrial damage. However, these results were obtained in a model of irradiation-induced DNA damage which in contrast to the current model system of oxidative stress involved caspase activation[238]. Overall, the full protection of mitochondria by PFTα in the present study suggested that in paradigms of oxytosis PFTα mediated its protective effects upstream or at the level of mitochondria.

In order to further characterise the mechanism and time window of PFTα-mediated protection lipid peroxidation was examined as an upstream event of mitochondrial demise. Enhanced formation of ROS is a hallmark of oxytosis and occurs in two steps[46]. Initially, activation of LOX leads to lipid peroxidation 6-8 hours after the onset of glutamate which in turn triggers mitochondrial ROS production[46,49]. Although PFTα

fully blocked the formation of mitochondrial ROS it only partially reduced lipid peroxidation. Furthermore, the amount of lipid peroxides after 7 h and 15 h of glutamate exposure did not differ (Fig. 16) indicating that PFTα acted downstream of the first burst of ROS, but prevented the second increase in ROS formation that mainly derived from impaired mitochondria. This hypothesis was further supported by the established time frame of about 4 hours for PFTα post-treatment to rescue HT-22 cells from glutamate-induced cell death (Fig. 14) and correlated with the 'point of no return' marking the event of fatal mitochondrial damage[25,49]. However, in a model of hypoxic-ischemic brain damage in rats PFTα failed to prevent lipid peroxidation, but still reduced infarct size[121]. Indeed, this model of oxidative stress was quite distinct from glutamate-induced oxytosis since hypoxic-ischemic brain damage was shown to involve caspase activation in contrast to oxytosis[121]. Furthermore, Nijboer and colleagues observed an induction of p53 and PUMA levels upon hypoxic-ischemic brain damage[121] which was not detected in the paradigm of oxytosis in the present study (Fig. 24B).

PFTα has been developed as an inhibitor of p53 transcriptional activity[207] and shown in several different model systems to suppress the expression of a number of pro-apoptotic p53 target genes such as Bax[94,96,242], PUMA[121,229] or NOXA[121] in response to various toxic stimuli. In the present study, however, PFTα did not exert any differences in mRNA expression levels of AIF, Bid, DRP1 or PUMA (Fig. 24B) in the presence or absence of glutamate suggesting that PFTα protected HT-22 cells independently of p53-related transcriptional modifications. Glutamate treatment alone also did not change mRNA expression levels of AIF, Bid, DRP1 or PUMA proposing that oxytosis was not primarily based on transcriptional upregulation of these genes. Nevertheless, it is possible that p53-regulated genes not investigated here were altered in response to glutamate exposure and that this effect was reversed by PFTα at the level of transcription. Furthermore, unchanged mRNA levels do not allow the assumption that the protein expression levels were not modified as well, since changes at the protein level can be attributed to enhanced translation or post-translational modifications. Earlier investigations in synaptosomes revealed that PFTα preserved MMP[122,209] in these subcellular preparations suggesting that PFTα-mediated protection did not only depend on inhibition of p53 transcriptional activity, but was rather promoted by the inhibition of p53 translocation to the mitochondria. The inhibition of mitochondrial localisation of p53 by PFTα was demonstrated for

example in rats in a model of ischemia/reperfusion injury of the kidney[236] and also after transient global cerebral ischemia[118]. In contrast, PFTα failed to prevent mitochondrial translocation of p53 after hypoxic-ischemic brain injury in mice[121]. However, investigations in the present study revealed that p53 translocation to the mitochondria was not involved in oxytosis (Fig. 22) proposing a p53-independent mode of action of PFTα.

Remarkably, PFTα attenuated cell death in response to glutamate also in cells depleted of p53 (Fig. 25) confirming the conclusion that PFTα exerted additional effects that were independent of p53. This assumption was further supported by the minor effects of p53 siRNA regarding cell viability, and the observations that PFTμ failed to prevent death of HT-22 cells upon glutamate treatment (Fig. 23). The p53-inhibitor PFTμ inhibits translocation of p53 to the mitochondria[120], thus normally mediating its protective effect[121]. Although both PFTα and PFTμ share the property to prevent translocation of p53 to the mitochondria, just PFTα prevented glutamate-induced death of HT-22 cells in the present study. Taken together, the findings that PFTα was protective in p53 silenced cells and PFTμ failed to prevent oxytosis strongly suggest that PFTα acted independently of p53.

According to the hypothesis that PFTα mediated its protection independently of p53, PFTα has also been shown to protect p53-deficient HCT116 colon cancer and H1299 lung carcinoma cells against DNA damage[238]. The authors hypothesised that this p53-independent way of protection might involve the cell cycle regulator cyclin D1[238]. Whether cyclin D1 plays a role in glutamate-induced oxytosis needs to be determined, since the aforementioned mechanism of cyclin D1 regulation was identified in a caspase-dependent cell death paradigm[238]. Furthermore, PFTα inhibited production of nitric oxide (NO) after treatment with lipopolysaccharide (LPS) in the presence and absence of p53 in a murine macrophage-like cell line[244]. The authors suggested that PFTα mediated the reduced NO production independent of p53 via down regulation of interferon-β, but they did not prove this hypothesis in p53 silenced cells[244]. Interferon-β could represent a target by which PFTα provided neuroprotection in HT-22 cells.

Previous studies in hepatocytes further identified the activation of the aryl hydrocarbon receptor[212] and in colon cancer cells the suppression of heat shock and glucocorticoid receptor signalling[213] as possible p53-independent targets of PFTα. In contrast, Murphy *et al.* did not observe any effect of PFTα on the glucocorticoid

receptor signalling or the chaperone machinery in fibroblasts or HEK cells[237]. These diverse findings suggest that the effects of PFTα depend on the cell type and the experimental settings.

Furthermore, PFTα was shown to maintain NF-κB survival signalling in cultured neurons exposed to camptothecin or oxygen glucose deprivation[98]. These results were also confirmed in mice after TBI, where PFTα even enhanced NF-κB activity under basal conditions and in response to the insult. The enhanced NF-κB activity was further indicated by an increased expression of NF-κB target proteins such as XIAP[94]. In contrast, in HeLa cells PFTα did not affect NF-κB activity[213]. Earlier investigations in our laboratory using a NF-κB reporter assay revealed that in HT-22 cells exposed to glutamate the NF-κB signalling pathway played a minor role[209]. Moreover, PFTα did not affect NF-κB transcriptional activity or its nuclear localisation in oxytosis[209]. These observations lead to the conclusion that in the present study PFTα did not mediate its protective effect via the NF-κB pathway.

In order to further elucidate potential underlying mechanisms of PFTα-mediated protection, the protein levels of XIAP and MnSOD were examined (Fig. 26). XIAP is a member of the inhibitors of apoptosis protein family who function as negative regulators of caspases[37]. In HT-22 cells, XIAP levels remained unchanged upon glutamate challenge and also PFTα did not alter XIAP protein amount neither in the presence nor absence of glutamate. These data suggest that the XIAP regulation was not involved in PFTα-induced protection in the paradigm of oxytosis in HT-22 cells. Notably, Plesnila and colleagues observed in rats exposed to TBI a degradation of XIAP in the damaged brain tissue which was prevented by simultaneous administration of PFTα[94]. However, in contrast to oxytosis in HT-22 cells TBI was accompanied by an increased expression of p53[94] and may also involve caspase activation.

MnSOD is a part of the antioxidant defence of mitochondria. Its main function is the dismutation of O_2^- to H_2O_2. Overexpression of MnSOD rendered HT-22 cells resistant to glutamate toxicity and restored ATP levels in the presence of glutamate[138]. Furthermore, knockdown of MnSOD resulted in an increased glutamate sensitivity and augmented formation of mitochondrial ROS in response to glutamate exposure[138]. A detrimental effect of reduced MnSOD expression was also observed *in vivo*, where $MnSOD^{+/-}$ mice exhibited exacerbated neurological outcome and increased infarct volume after focal cerebral ischemia compared to wild-type

littermates[245]. MnSOD$^{-/-}$ mice die shortly after birth underlining the crucial role of MnSOD for development and cellular maintenance[246]. In the present study, glutamate treatment strongly increased MnSOD protein levels while administration of PFTα did not alter MnSOD expression both in the presence and absence of glutamate (Fig. 26). Such enhanced expression of MnSOD in response to the glutamate challenge was previously also observed in a comprehensive proteomic study in HT-22 cells[214]. This glutamate-induced upregulation of MnSOD can be regarded as a compensatory mechanism of the cell to cope with the oxidative stress induced by glutamate[215]. Therefore, the reduction of MnSOD protein in response to PFTα treatment was probably rather the consequence than the cause of PFTα-mediated protection.

Overall, the present study showed a strong neuroprotective effect of PFTα in glutamate-induced oxytosis upstream or at the level of mitochondria either independent of p53 inhibition or accompanied by additional effects which remain to be clarified.

4.2.2 p53 silencing does not prevent mitochondrial demise

In order to further elucidate the role of p53 in glutamate-induced oxytosis, p53 was silenced using RNA interference. Down regulation of p53 delayed cell death in response to glutamate exposure for about 2 hours (Fig. 17). This is in line with previous reports from other model systems of neuronal cell death in the literature. For example, Crumrine and colleagues observed reduced infarct size after MCAO in both homo- and heterozygous p53 knockout mice[100] and p53$^{-/-}$ mice were also protected against global cerebral ischemia compared to p53$^{+/+}$ mice[205]. Further, genetic deletion of p53 reduced cell death in response to kainic acid in isolated neurons[99] as well as whole animals[247], and also prevented cytotoxicity in a model of HD[97].

Although in the present study p53 silencing attenuated glutamate-induced cell death, it failed to preserve mitochondrial integrity indicated by enhanced mitochondrial fission, ROS formation and breakdown of the MMP (Fig. 19, 20). This contrasts findings of Bae and co-workers who reported reduced mitochondrial depolarisation in p53$^{-/-}$ primary cortical neurons after transfection with mutant huntingtin compared to p53 wild-type cells[97]. Further, synaptosomes of p53$^{-/-}$ mice were protected against loss of MMP after oxidative stress induced by glutamate or Fe^{2+} exposure[122].

In HT-22 cells, formation of lipid peroxides occurs upstream of mitochondrial demise[49]. In the present study, p53 silencing failed to prevent lipid peroxidation (Fig. 21) and consequently, mitochondrial function was impaired.

Unexpectedly, knockdown of p53 significantly attenuated the glutamate-induced drop of ATP levels (Fig. 20) despite perturbed mitochondrial function. The absolute effect on ATP levels by p53 gene silencing in glutamate challenged cells, however, was fairly small. Thus, the physiological relevance of this restoration of ATP levels may also be minor. Potentially, this effect even only reflected the small protective effect mediated by down regulation of p53 regarding cell viability. Nevertheless, HCT116 colon cancer cells lacking p53 have been shown to generate the majority of their ATP via glycolysis instead of aerobic respiration[88] serving as a possible explanation how p53 silenced HT-22 cells could exert higher ATP levels in case of glutamate treatment than cells transfected with scrambled control siRNA. To confirm this notion further experiments are required such as analysis of mitochondrial respiration or production of lactate to determine whether p53 silenced HT-22 cells exhibit an increased rate of glycolysis which could account for the restored ATP levels.

For further characterisation of the relationship between mitochondria and p53 in oxytosis, subcellular localisation of p53 and phospho-p53 was examined by immunocytochemistry and following confocal microscopy (Fig. 22). Contrary to previous reports demonstrating translocation of p53 to the mitochondria in response to oxidative stress[101,117–119,210] neither p53 nor phospho-p53 showed mitochondrial co-localisation upon glutamate challenge. Although further methods such as subcellular fractionation and subsequent Western blot analysis are needed to fully rule out that p53 and accordingly phospho-p53 translocate to the mitochondria during oxytosis, the obtained data suggest that mitochondrial localisation of p53 did not play a major role in glutamate-induced cell death and that p53-mediated toxicity probably rather relied on transcriptional effects beyond the current analysis. This conclusion is further supported in the model of oxytosis by the missing protection of PFTμ (Fig. 23) which inhibits mitochondrial association of p53[120].

Altogether these results suggest that rather the inhibition of pro-apoptotic transcriptional effects than the inhibition of direct mitochondrial interactions of p53 mediated the observed delay of cell death by p53 siRNA.

4.2.3 Differential effects of p53 gene silencing and pharmacological p53 inhibition

As described before, both genetic deletion and pharmacological inhibition of p53 improved the outcome in many models of neuronal damage[98,100,205,242]. Therefore, the remarkable difference regarding neuronal protection between PFTα treatment and p53 gene silencing in the present study was rather unexpected. However, one has to keep in mind that using siRNA approaches as performed in the present thesis is not sufficient to achieve a sustained full knockout of p53 levels and according transcriptional repression. In contrast, a concentration of 10 µM PFTα is rather high and presumably able to fully block p53 function resulting in pronounced and sustained neuroprotective effects including mitochondrial protection. Notably, there are also reports demonstrating that heterozygous, i.e. partial knockout of p53 reduced deleterious effects of ischemia to a greater extent than homozygous p53 gene deletion[100,101] emphasising the importance of controlled p53 activity and underlining the divergent functions of p53 from pro-survival to pro-death activities[91]. Vaseva *et al.* suggested that the greater protective effect of a heterozygous p53 knockout is attributed to a disruption of the p53-CypD complex which is involved in the PTP pore and a maintained weak p53-dependent apoptotic program[101].

Furthermore, the present work showed that PFTα mediated protection against glutamate toxicity also in p53 silenced HT-22 cells (Fig. 25) suggesting that additional, p53-independent effects of PFTα were responsible for the observed protective effects on cell viability and, in particular on mitochondrial morphology and function.

Differences between the pharmacological inhibition of p53 and its genetic deletion have also been reported by the group of Rosanna Parlato[204,206] supporting the hypothesis of p53-independent effects of PFTα. They found that PFTα reduced the amount of apoptotic cells in a model of Pol I-specific transcription initiation factor IA (TIF-IA) depleted dopaminergic neurons[204], while p53 knockout in TIF-IA depleted medium spiny neurons induced apoptosis[206]. In addition, in a murine macrophage like cell line it was shown that PFTα diminished LPS-induced expression of inducible nitric oxide synthase (iNOS), while iNOS levels remained unchanged after siRNA-mediated p53 silencing[244].

Considering the effects at the level of mitochondria, the missing mitochondrial protection of p53 down regulation using siRNA approaches serves as another

possible explanation for the minor neuroprotective effect of p53 siRNA compared to PFTα. The discrepancy regarding mitochondrial protection highlights the crucial role of a proper mitochondrial function for neuroprotection and supports a p53-independent effect of PFTα at the level of mitochondria.

Besides this direct effect at the level of mitochondria, also the differential regulations of the p53 target genes p21 and PUMA after siRNA-mediated p53 knockdown compared to PFTα administration could explain their diverse impacts on mitochondria. In the current study, silencing p53 reduced p21 expression levels, while they were unaffected after PFTα application and both treatments did not alter PUMA expression patterns. In cancer cells a decline in p21 and restored PUMA levels in response to UV-light induced DNA damage was associated with mitochondrial demise and following cell death[248] which is in line with the findings presented in this work that p53 knockdown failed to preserve mitochondrial integrity and function. Moreover, disruption of both p21 and PUMA protected HCT116 cells against cell death induced by either p53-overexpression, DNA damage or hypoxia[233].

Overall these results confirmed the neuroprotective potential of PFTα in the model of oxytosis in neuronal cells and provided evidence for additional effects of this compound beyond p53 inhibition which account for PFTα mediated mitochondrial protection.

4.3 The role of PHDs in oxytosis

Global inhibition of PHDs has been shown to protect neurons in different models of neurodegenerative diseases such as stroke[153–155], PD[156,157] and AD[158,159]. Using RNA interference, a recent study identified PHD1 as the most relevant isoform of the PHD family in oxidative stress induced cell death in neurons[160]. It was demonstrated that only the knockdown of PHD1 was able to prevent cell death of cortical neurons in response to the glutamate analogue homocysteate, whereas, in contrast, siRNAs targeting PHD2 and PHD3 failed to provide such protective effects[160]. Thus, the authors concluded that PHD1 is the PHD isoform with the most impact on neuronal oxidative cell death.

The exact mechanism how PHD1 promotes cell death is not elucidated so far. The post-translational modification of HIF-1 towards increased degradation is a major function of PHDs, and increased HIF activity upon PHD-inhibition, e.g. under conditions of low oxygen, may exert cytoprotective effects. However, pharmacological PHD-inhibitors prevented homocysteate-induced death of HT-22 cells despite siRNA-mediated HIF-1 or HIF-2 gene silencing indicating that increased HIF activity was dispensable for the observed neuroprotective effects by PHD-inhibition. Notably, HIF-1 silencing alone partially prevented cell death confirming that in oxytosis, HIF rather contributed to cell death, but not to protective effects of PHD-inhibition[160]. This observation and the missing protection of PHD2 knockdown against homocysteate toxicity are in line with previous reports showing that HIF-1 is mainly regulated via PHD2[150].

Other targets of PHD1 that may be linked to death signalling also in glutamate-induced oxytosis include the large subunit of RNA polymerase II (Rpb1)[163] and ATF4[165]. PHD1 could modify RNA polymerase II activity via interaction with Rpb1, thereby inducing transcription of pro-death genes such as PUMA, CHOP, TRB3 or LOX[171]. At least for the LOX a pivotal role in oxytosis has been previously demonstrated[49]. The hypothesis that the LOX could be a downstream target of PHD1 is supported by the finding that knockdown of PHD1 attenuated glutamate-induced lipid peroxidation (Fig. 31). Furthermore, PHD1 has been shown to regulate and interact with ATF4[165], a transcription factor displaying both anti-apoptotic[167,168] and pro-apoptotic properties[169,170] depending on the cellular system and the experimental settings. Unpublished data from *in vivo* experiments in mice exposed to intracerebral haemorrhage (ICH) showed that PHD inhibition prevented neuronal cell death by

suppressing ATF4-dependent pro-death gene expression. In contrast to these findings *in vivo*, the current work demonstrated toxic effects of ATF4 down regulation (Fig. 44) which were attenuated by PHD-inhibition. It is therefore unlikely that ATF4 displayed the predominant target by which PHD1 contributed to glutamate-induced oxytosis. The relationship between PHD-inhibition and ATF4 is discussed in detail in chapter 4.3.3.

Overall, the present study verified the neuroprotective potential of PHD1 in the model system of oxytosis and focused on the impact of PHD1 on mitochondrial function since mitochondria are the crucial organelles deciding on life and death[25].

4.3.1 Different concepts of PHD inhibition provide neuroprotection

In the present study, selective targeting of PHD1 with siRNA sequences I and II confirmed the neuroprotective effect of PHD1 knockdown previously described by Siddiq and colleagues[160]. Both siRNAs transiently protected HT-22 cells from glutamate-induced cell death (Fig. 28). Furthermore, analyses of mitochondrial function showed that MMP, ATP levels and mitochondrial ROS formation were preserved by PHD1 siRNAs (Fig. 29, 30) suggesting an effect of PHD1 inhibition upstream or at the level of mitochondria. Since PHD1 gene silencing reduced formation of lipid peroxides (Fig. 31) an effect upstream of mitochondria is more likely. The effect of siRNA sequence II compared to sequence I was consistently smaller throughout all experiments which correlated well with the detected minor reduction of PHD1 protein amount by siRNA sequence II (Fig. 27).

Notably, the overall effects were fairly small, initially challenging the hypothesis on the proposed key role for PHD1 in oxytosis. However, Western blot analyses after 48 hours of siRNA transfection revealed that the reduction of PHD1 protein levels using either siRNA sequence I or II was minor compared to the corresponding pronounced effect of the siRNA approach at the mRNA level (Fig. 27). This discrepancy between gene silencing effects on mRNA and protein could explain the minimal effect of PHD1 siRNA regarding cell viability and protection of mitochondrial integrity since the remaining enzyme activity was likely sufficient to promote cell death, probably via transcriptional induction of pro-death genes[171].

In order to improve gene silencing-efficiency, the siRNA transfection time was extended to 72 hours. Unfortunately, this procedure did not further reduce PHD1 protein levels and also a double transfection approach which was previously

described to sufficiently silence PHD1[249] did not increase gene silencing efficiency (Fig. 27). The siRNA sequences were obtained from Sigma Aldrich (for details s. chapter 2.1.6) and designed with the Rosetta siRNA Design Algorithm which usually achieves a knockdown efficiency at mRNA levels of more than 75%.

Besides insufficient siRNA sequences, a rather high protein stability of PHD1 could be another reason for these difficulties to knockdown PHD1. This hypothesis is supported by findings in primary murine proximal tubular cells where PHD1 protein first started to degrade after 24 h of treatment with cycloheximide[249]. In the human osteosarcoma cell line U2OS, however, levels of endogenous PHD1 already declined after 90 minutes of cycloheximide exposure[174]. Since for HT-22 cells no data on PHD1 protein stability and transcriptional turnover are available, the question remains whether a particular high stability of the PHD1 protein aggravates its down regulation.

To achieve a better inhibition of PHD function and to further prove the neuroprotective and in particular “mitoprotective” concept of PHD inhibition in paradigms of oxytosis, the pharmacological PHD-inhibitors DFO, CPO and oxyquinoline acting via iron chelation and the 2-oxoglutarate analogue DHB were used. According to the results using siRNA approaches to silence PHD1 all applied pharmacological inhibitors completely prevented glutamate-induced mitochondrial demise indicated by restored MMP, preserved ATP levels and mitochondrial respiration (Fig. 35-38). Consequently, and in line with previous findings in similar models of neuronal oxidative stress[145,155,160], glutamate-induced cell death was fully inhibited (Fig. 32) by all applied inhibitors. These results also propose a protective effect for the pharmacological PHD-inhibitors upstream or at the level of mitochondria. Accordingly, formation of mitochondrial and lipid peroxides was fully abolished as well (Fig. 37-39). However, the effects obtained by pharmacological inhibition were much more pronounced and sustained in comparison with the attempts of PHD1 gene silencing.

These inconsistencies regarding efficiency to prevent cell death between siRNA approaches and the small molecule inhibitors could be attributed to several reasons. First, knockdown of PHD1 was not very effective, resulting in remaining enzyme activity which was still able to promote cell death, while the pharmacological inhibitors likely fully blocked PHD function. Second, the inhibitors may not act on one particular isoform of the PHD family suggesting that maybe also inhibition of PHD isoform 2 and 3 contributed to the protection against glutamate-induced cell death. However, in

primary cortical neurons knockdown of both isoforms 2 and 3 in contrast to PHD1 did not prevent cell death in response to oxidative stress[160]. Furthermore, PHD3 knockout mice were not protected against neuronal demise in a model of MCAO, while $PHD2^{+/-}$ mice exhibited improved neuronal function compared to wild-type controls[177]. Additionally, previous studies reporting enhanced cell death after overexpression of PHD3 or SM-20 in PC12 cells and sympathetic neurons[192,193] indicated a rather pro-apoptotic function of PHD3 which could be prevented by the use of pharmacological inhibitors in the present model of oxytosis. To clarify whether inhibition of PHD3 contributed to cellular protection in HT-22 cells, one would have to investigate the influence of this PHD isoform in this particular cell line.

Since *in vivo* models suggested a beneficial effect for reduced PHD2 expression in models of neurodegeneration[177,186], it would also be of great interest to further elucidate the role of PHD2 in paradigms of oxytosis by either overexpression or down regulation, although knockdown of PHD2 failed to prevent homocysteate-induced cell death in primary neurons[160].

Furthermore, off target effects of the pharmacological PHD-inhibitors could account for their greater neuroprotective potential. Especially, the use of iron chelators implies this assumption since several enzymes involved in neuronal cell death depend on iron in their catalytic domain[75]. One prominent representative of iron dependent enzymes with pro-apoptotic functions is the protein family of lipoxygenases[72,75]. All iron chelators used in the present study fully prevented glutamate-induced lipid peroxidation, but this was also the case for the 2-oxoglutarate analogue DHB and for PHD1 gene silencing (Fig. 31, 39) suggesting that this effect was not caused by an off-target iron chelation, but rather a consequence of PHD inhibition. Moreover, it was demonstrated that the broad iron chelator DFO specifically targets PHDs[155].

Since the 2-oxoglutarate analogue DHB showed the same effects as the iron chelating PHD-inhibitors regarding cellular and mitochondrial protection and also PHD1 gene silencing exhibited the same albeit smaller effects, the data presented in this study suggest that the observed effects were caused by inhibition of the PHD enzyme family. Furthermore, this inhibition provided protection of HT-22 cells against glutamate-induced cell death upstream of mitochondria.

4.3.2 PHD-inhibition mediates neuroprotection upstream of mitochondria

The present study clearly demonstrated that both pharmacological inhibition of PHDs and PHD1 gene silencing mediated protection against glutamate-induced cell death accompanied by mitochondrial protection suggesting an action upstream or at the level of mitochondria.

Previous studies in HIF-1α silenced cells showed protective effects of PHD-inhibitors against glutamate and 3-nitropropionic acid[158,160,161] suggesting that HIF-1α independent effects also contributed to the protection of mitochondria observed in the present study. Moreover, in skeletal muscle fibres depletion of PHD1 induced resistance to oxidative stress and preserved mitochondrial function after ischemia independently of HIF-induced adaptations[176].

One prominent HIF-independent target of PHDs is Rpb1, the large subunit of RNA polymerase II. In human clear renal carcinoma cells, both PHD1 and PHD2, but not PHD3 have been shown to interact with and to hydroxylate Rpb1 in response to H_2O_2-induced oxidative stress[163]. Via this mechanism PHDs are able to modify RNA polymerase II activity and influence transcription independent of HIF. Prominent pro-death genes regulated by RNA polymerase II are 12-LOX and PUMA. It is conceivable that the interaction between PHD1 and Rpb1 leads to enhanced transcription of PUMA and 12-LOX. Consequently, Karuppagounder and colleagues suggested a model where PHD-inhibitors mediate neuroprotection via suppression of pro-death genes such as PUMA or 12-LOX via the modification of RNA polymerase II activity[171].

Since inhibition or deletion of LOX are well established to mediated neuroprotection associated with preserved mitochondrial integrity[49], suppression of 12-LOX activity by PHD-inhibitors may explain the observed beneficial effects of the compounds at the level of mitochondria. In addition, PHD1 gene silencing reduced lipid peroxidation, and this could not be attributed to an off-target iron chelation leading to LOX-inhibition as proposed for pharmacological PHD-inhibitors as an additional mode of action. Notably, all of the applied PHD-inhibitors as well as PHD1 siRNA sequence I reduced lipid peroxidation already under control conditions (Fig. 31, 39). Although these effects were not significant, they further support the model of Karuppagounder[171]. In order to verify whether changes in LOX expression significantly contributed to mitochondrial protection mediated by PHD-inhibition one

would have to examine LOX expression levels. Preliminary studies addressing this question, however, showed that oxyquinoline treatment did not affect protein expression levels of 12-LOX rebutting the hypothesis that the protective effect of PHD inhibition is mediated via modified LOX expression.

To further specify the mechanism how PHD-inhibition interfered with the glutamate-induced death cascade in HT-22 cells, GSH levels were determined in the presence and absence of oxyquinoline (Fig. 40) since the drop in GSH levels represents the starting point of oxytosis[42]. Although oxyquinoline fully inhibited glutamate-induced cell death and subsequent mitochondrial demise, it failed to prevent GSH depletion in response to glutamate-induced X_c^--inhibition. It has also previously been observed for curcumin[59] or actinomycin D[46] that protection against oxidative stress induced cell death in HT-22 cells can be achieved although GSH levels are depleted. The data regarding the GSH levels and lipid peroxidation indicated that oxyquinoline mediated its protection downstream of GSH depletion, but upstream of LOX activity. However, it is important to note that a direct inhibitory effect of oxyquinoline on LOX was ruled out by determination of IC_{50} values for oxyquinoline by our collaborators from New York (Prof. Rajiv Ratan, Burke-Cornell Medical Research Institute, White Plains, New York, USA). The IC_{50} for both 12- and 15-LOX was with >45 µM and >30 µM (unpublished data) much higher than the required concentration of 2 µM to achieve protection of HT-22 cells against glutamate toxicity. Additionally, structural analyses showed that oxyquinoline did not fit into the active centre of 12-LOX[152].

In summary, this study provides evidence that inhibition of PHDs leads to mitochondrial protection and accordingly, neuroprotection. The exact mechanism of action remains to be established, but likely includes HIF-independent multimodal regulation of enzymes involved in oxidative stress. Unpublished data from mice and rats exposed to ICH suggest that at least oxyquinoline acted via a reduction of ATF4 transcriptional activity and thereby, prevented enhanced expression of pro-death genes. Therefore, the regulation of the eIF2α/ATF4 pathway by oxyquinoline in glutamate-induced oxytosis was a further subject of the present study.

4.3.3 PHD inhibition and the eIF2α/ATF4 pathway

The transcription factor ATF4 represents another HIF-independent target of PHDs since it has been shown to directly interact with both PHD1 and PHD3[165,166].

In the present study, analyses of ATF4 expression levels revealed that according to Yukawa and colleagues ATF4 mRNA levels remained unchanged upon any treatment, e.g. glutamate or oxyquinoline because ATF4 protein amount is mainly regulated by preferential translation instead of increased transcription[219]. In contrast, oxyquinoline increased ATF4 protein expression levels after 4 h. After 14 hours of glutamate exposure ATF4 protein levels declined which was prevented by co-treatment with oxyquinoline (Fig. 42). This is in line with previous findings where PHD inhibition by DMOG and siRNA-mediated knockdown of PHD3 stabilised ATF4 protein in HeLa cells[166]. This effect was explained by an oxygen-dependent ubiquitination associated with PHD3 activity[250], although an *in vitro* prolyl hydroxylation assay did not identify ATF4 as a substrate of PHD3[165].

The down regulation of ATF4 in response to glutamate and its prevention by co-treatment with oxyquinoline suggested an anti-apoptotic function of ATF4 in the present model system of oxytosis. This hypothesis was further supported by the basal toxicity induced by siRNA-mediated down regulation of ATF4 (Fig. 44) that was associated with enhanced ROS formation (Fig. 45). Furthermore, previous studies demonstrated that overexpression of ATF4 attenuated glutamate-induced death of HT-22 cells[220] and that HT-22 cells initially resistant to glutamate became more susceptible to this compound after knockdown of ATF4[218]. The crucial function of ATF4 for cellular homeostasis and maintenance is also supported by the fact that $ATF4^{-/-}$ MEFs need supplementation of non-essential amino acids and reducing agents for proper cell growth[168]. Moreover, ATF4 knockout mice are blind, subfertile and anaemic[167]. Nevertheless, Lange and co-workers reported that these ATF4 knockout mice exhibited significantly smaller infarct sizes after MCAO compared to wild-type control animals implying a pro-apoptotic function of ATF4[169]. Since these mice display such an impaired phenotype, the physiological relevance of this finding remains unclear. However, a pro-apoptotic effect of ATF4 was further suggested in HEK293 cells where an overexpression of ATF4 induced enhanced formation of ROS[170] contrasting the findings of the present study.

Considering the different studies performed in the last years the role of ATF4 appears quite complex and its impact on cellular survival seems to be dependent on the

model system and the toxic stimulus. Overall, in HT-22 cells the anti-apoptotic functions of ATF4 seem to be more relevant as indicated by the toxic effect of the ATF4 siRNA. Additionally, the down regulation of ATF4 protein amount in response to glutamate exposure could reduce ATF4 pro-survival signalling and therefore be a prerequisite for the induction of cell death.

In HT-22 cells, ATF4 has been shown to be regulated by eIF2α. Enhanced phosphorylation of eIF2α increased ATF4 levels and subsequently xCT expression, thereby mediating cellular survival because of restored GSH levels[220,251]. In the present work, an enhanced phosphorylation of eIF2α was observed after 4 h of oxyquinoline treatment in the presence and absence of glutamate correlating with the protein expression levels of ATF4 at this time point. However, after 14 h of glutamate exposure eIF2α phosphorylation status remained unchanged in contrast to decreased ATF4 protein amount. Single administration of oxyquinoline slightly enhanced eIF2α phosphorylation, while the results in the presence of glutamate were less clear due to high variability. Overall, the regulation of ATF4 protein levels after 4 h of treatment and after 14 h at least under basal conditions correlates with the phosphorylation of eIF2α.

The regulation of the ATF4 downstream target xCT did not fit that well to the proposed eIF2α/ATF4/xCT pathway. After 4 h of treatment, oxyquinoline dramatically increased xCT levels under basal conditions (Fig. 43) while ATF4 was only slightly enhanced. However, in the presence of glutamate, oxyquinoline raised ATF4 protein levels much more than xCT protein. These results suggest that the regulation of xCT via the eIF2α/ATF4 pathway was not involved in oxyquinoline-mediated neuronal protection. Notably, in earlier studies in HT-22 cells exposed to glutamate a protection initiated via this pathway was accompanied by restored GSH levels[218,220,251]. Accordingly, oxyquinoline failed to prevent the glutamate-induced decline of GSH levels in the present study, although co-treatment with oxyquinoline restored the levels of the xCT after 14 h of glutamate toxicity. Together with the aforementioned studies[218,220,251] these data confirm that the eIF2α/ATF4/xCT pathway was likely not involved in oxyquinoline-mediated protection of HT-22 cells in the model of oxytosis.

Besides xCT, ATF4 exhibits several other target genes involved in cell death[252] whose regulation could account for the beneficial effects of oxyquinoline. In order to clarify whether the observed changes in ATF4 expression were responsible for the

oxyquinoline-mediated protection against glutamate-induced oxytosis, cell viability of HT-22 cells depleted of ATF4 was assessed (Fig. 44). Silencing ATF4 did not abolish the neuroprotective effect of oxyquinoline indicating that ATF4 was dispensable for this effect at least in the paradigm of oxytosis. The findings on ATF4 of the present study, however, stand in contrast to recent unpublished observations from Saravanan Karuppagounder who showed that in primary cortical neurons ATF4 levels were increased in response to homocysteate-induced oxidative stress. Notably, oxyquinoline failed to inhibit this increase, although it prevented cell death. Furthermore, this study demonstrated that oxyquinoline significantly improved neuronal outcome in rodent models of ICH. This beneficial effect of oxyquinoline was HIF-independent and attributed to a reduced ATF4 transcriptional activity induced by less hydroxylation of ATF4 due to PHD inhibition. The reduction of ATF4 transcriptional activity was associated with a significant lower expression of ATF4-dependent pro-death genes such as tribbles homolog 3. Therefore, it is conceivable that an alteration of ATF4 transcriptional activity by oxyquinoline could also account for its protective effect in HT-22 cells, although the knockdown of ATF4 siRNA suggested that ATF4 expression is dispensable for oxyquinoline-mediated protection. Overall, the present investigations suggest so far that oxyquinoline does not act via the eIF2α/ATF4/xCT pathway and that restoration of ATF4 protein levels is not required for protection of HT-22 cells. However, it would be of great interest to determine ATF4 transcriptional activity in cells treated with glutamate and oxyquinoline simultaneously to check whether oxyquinoline induces changes in ATF4 transcriptional activity which could account for the protection of HT-22 cells as observed *in vivo*.

4.4 PHD inhibition protects against ferroptosis

Ferroptosis has been characterised as a non-apoptotic iron-dependent form of cell death in cancer cells which depends on the generation of soluble and lipid ROS through the Fenton reaction and iron-dependent enzymatic reactions amongst others catalysed by LOX, xanthin oxidases or catalases[74]. For example, lipid peroxides produced by LOX can react with free Fe^{2+} via the Fenton reaction (Fig. 49) to generate radicals which can further trigger lipid peroxidation in a radical chain reaction or damage proteins and DNA[75,253]. Therefore, enhanced oxidative stress due to the Fenton reaction is associated with diverse neurodegenerative diseases[253]. Indirect evidence for the involvement of the Fenton reaction in neurodegeneration comes from the observation that iron chelators are protective in different models of neuronal cell death[155,156,158,159].

$$R\text{-}OOH + Fe^{2+} \longrightarrow R\text{-}O^{\bullet} + HO^{-} + Fe^{3+}$$

Figure 49: Fenton reaction

Generation of soluble and lipid ROS mediating ferroptosis was induced by the small molecule erastin which inhibits the X_C^--transporter[74,77] similar to glutamate in the paradigm of oxytosis[46]. Hence, the concept of ferroptosis has recently been linked to death signalling pathways in neurons[142]. Furthermore, it has been demonstrated that the ferroptosis-inhibitor ferrostatin-1 prevented glutamate-induced cell death in rat organotypic hippocampal slice cultures[74]. These findings strongly suggest a high similarity between oxytosis and ferroptosis. However, ferroptosis in cancer cells did not involve mitochondrial demise[74] which in turn represents a hallmark of oxytosis[49,66,71]. The present study showed that erastin was able to induce cell death in HT-22 cells (Fig. 46) suggesting that ferroptotic pathways can be activated in these neuronal cells. Further investigations in our laboratory demonstrated that erastin-induced death of HT-22 cells was accompanied by mitochondrial demise indicated by enhanced mitochondrial fission, a loss of ATP levels and a breakdown of the mitochondrial membrane potential[254] providing evidence that oxytosis and ferroptosis share common features of intrinsic cell death pathways.

The current thesis further demonstrated that both knockdown of PHD1 and pharmacological PHD inhibition were protective against erastin toxicity (Fig. 48, 49).

These data support the recently imposed hypothesis suggesting PHDs as an interesting target in ferroptosis[75] since PHDs are regarded as iron sensors[149]. However, in 2013, Speer and colleagues postulated that the protective effects of iron chelators in the model of erastin-induced ferroptosis[74] should be attributed to the inhibition of PHDs instead of a direct inhibition of the Fenton reaction[142]. This conclusion was confirmed in the present thesis by showing that not only the iron chelators DFO, CPO and oxyquinoline protected HT-22 cells against erastin toxicity, but also the knockdown of PHD1 delayed erastin-induced cell death (Fig. 48), and the 2-oxoglutarate analogue DHB prevented loss of cell viability in response to erastin (Fig. 49). Overall, these findings demonstrated that the protective effect of PHD inhibition occurred independently of blocking the Fenton reaction through iron chelation. Furthermore, these results imply a crucial role for PHDs in erastin-induced ferroptosis.

Besides iron chelators, antioxidants are known to inhibit formation of ROS from the Fenton reaction[75]. Since oxyquinoline displayed antioxidative properties indicated by a concentration-dependent protection against H_2O_2-induced cell death (Fig. 41) and reduced ROS formation in cells depleted of ATF4 (Fig. 45), one could argue that the protection against erastin-induced cell death by oxyquinoline was rather mediated by its antioxidative capacity than by PHD inhibition. However, the beneficial effect of PHD1 siRNA sequence I in the same setting proved a direct inhibition of PHDs rather than an antioxidative effect of oxyquinoline as the underlying mechanism of protection, since the siRNA does not exhibit an antioxidative function. It is more likely that the assumed inhibitory effect of both pharmacological and genetic inhibition of PHDs on the transcription of pro-death genes such as LOX[171] contributed to the protective effect against erastin toxicity since LOX is one of the key enzymes providing lipid peroxides required for the Fenton reaction[75]. In order to prove this hypothesis, the effect of PHD-inhibition on lipid peroxidation has to be investigated in the case of erastin treatment.

Recent data from our laboratory clearly showed that the Bid-inhibitor BI-6c9 prevented erastin-induced lipid peroxidation, mitochondrial demise and subsequent death of HT-22 cells and vice versa, the ferroptosis-inhibitor ferrostatin-1 prevented glutamate-induced lipid peroxidation, mitochondrial demise and subsequent death of HT-22 cells in the paradigm of oxytosis suggesting that in HT-22 cells, ferroptosis and oxytosis are highly similar and exhibit common cell death mechanisms.

Therefore, it is very likely that PHD inhibition in terms of erastin-induced oxytosis would result in reduced levels of lipid peroxides as already shown in the model system of oxytosis (Fig. 31, 39).

In summary, the present study provided first evidence for a beneficial effect of PHD inhibition in terms of erastin-induced ferroptosis in neuronal cells.

5 Summary

Mitochondrial dysfunction and demise are hallmarks of many neurological disorders and neurodegenerative diseases. Since mitochondria are the key organelles providing energy, they are regarded as the power house of the cell. Mitochondria are further involved in Ca^{2+}-homeostasis, ROS formation and cellular metabolism underlining their pivotal role for cellular homeostasis beyond ATP production. Under conditions of stress, mitochondria regulate the 'point of no return' in intrinsic cell death pathways, which marks the decision point between life and death. Once the mitochondria are irretrievably damaged, they drive the cell into death.

Especially neurons rely on a proper mitochondrial function, since neuronal cells exhibit a pronounced energy demand and are rarely renewed. Consequently, mitochondrial protection displays a promising strategy to protect neurons from death.

Previously, the two proteins p53 and PHD1 have been associated with neurodegeneration. Hence, the aim of this study was to investigate the role of those two proteins in neuronal cell death and to evaluate the neuroprotective potential of their particular inhibitors PFTα and DFO, DHB, CPO and oxyquinoline, respectively. Additionally, underlying mechanisms should be elucidated by which these inhibitors mediate their neuroprotective effects.

In this study, immortalised mouse hippocampal HT-22 cells were used since they represent an established model of caspase-independent cell death induced by glutamate, termed oxytosis. Moreover, erastin was applied in the same cell line to induce a mode of cell death called ferroptosis.

The first part of this study revealed that siRNA-mediated knockdown of p53 delayed glutamate-induced cell death in HT-22 cells for about 2 h, but failed to prevent lipid peroxidation or mitochondrial damage depicted as enhanced mitochondrial fragmentation, depolarisation of the mitochondrial membrane, increased mitochondrial ROS formation and a loss of ATP levels. Both p53 and phospho-p53 did not translocate to the mitochondria upon glutamate challenge indicating that oxytosis was not attributed to a direct action of p53 at the level of mitochondria. The inhibition of p53 transcriptional activity by knockdown of p53, which was determined by a reporter assay established in this work, could serve as a possible explanation for the observed delay of cell death.

In contrast, the pharmacological p53-inhibitor PFTα prevented glutamate-induced cell death of HT-22 cells more efficiently and was still able to rescue these cells when

applied up to 4 h after the onset of glutamate treatment. Furthermore, PFTα abolished lipid peroxidation and subsequently preserved mitochondrial integrity which was indicated by reduced mitochondrial fission, attenuated formation of mitochondrial ROS and restored mitochondrial membrane potential and ATP levels. Notably, PFTα rescued HT-22 cells depleted of p53 from glutamate-induced cell death.

These results exposed a pronounced neuroprotective potential of PFTα which occurred at the level of mitochondria and independently of p53.

The second part of this thesis demonstrated the neuroprotective potential of PHD inhibition by the use of structural diverse PHD-inhibitors and siRNAs selectively targeting PHD1. Both concepts of PHD inhibition reduced generation of lipid peroxides and preserved mitochondrial morphology and function indicated by restored mitochondrial respiration and membrane potential and abolished mitochondrial ROS formation, revealing that PHD inhibition acts upstream of mitochondrial demise. Remarkably, the effects by siRNA-mediated PHD1 silencing were less pronounced than those achieved by pharmacological inhibitors. These differences in efficacy were likely attributed to the insufficient knockdown by the siRNA approach. Nevertheless, these findings exposed the selective inhibition of PHD1 and the broad pharmacological inhibition of the PHD enzyme family as promising strategies to achieve mitochondrial rescue and subsequent neuroprotection.

Previously, PHDs have been shown to interact with the transcription factor ATF4. The present study revealed that oxyquinoline was able to prevent the glutamate-induced down regulation of ATF4. However, oxyquinoline was still able to prevent oxytosis in cells depleted of ATF4. Therefore, the observed regulation of ATF4 protein levels after oxyquinoline application emerged as dispensable for oxyquinoline mediated protection in oxytosis, although previous studies *in vivo* suggested a modification of ATF4 transcriptional activity as mode of action for oxyquinoline. Overall, the exact mechanism by which PHD inhibition and, in particular oxyquinoline induced neuroprotection in the paradigm of oxytosis remains elusive so far.

Finally, PHD inhibition was also shown to protect HT-22 cells against erastin-induced ferroptosis further supporting the pivotal role of PHDs in neuronal demise and the potential of PHD inhibition as a promising therapeutic strategy in the treatment of neurodegenerative diseases, where oxidative stress contributes to progressive mitochondrial dysfunction and neuronal death.

6 Zusammenfassung

Eine der wichtigsten Aufgaben von Mitochondrien ist die Bereitstellung von Energie in Form von ATP. Daher werden sie oft auch als Kraftwerke der Zelle bezeichnet. Darüber hinaus erfüllen Mitochondrien zentrale Funktionen im Zellstoffwechsel: Sie regulieren die zelluläre Ca^{2+}-Homöostase und tragen durch die Bildung von reaktiven Sauerstoffspezies (ROS) wesentlich zu physiologischen Alterungsprozessen bei.

Da neuronale Zellen einen sehr hohen Energiebedarf aufweisen, sind sie in besonderem Maße auf die physiologischen Funktionen der Mitochondrien angewiesen. Sobald die Mitochondrien irreversibel geschädigt sind, können sie über intrinsische Signalkaskaden den programmierten Zelltod einleiten. Daher spielen Mitochondrien eine Schlüsselrolle in der neuronalen Apoptose. Es konnte beispielsweise gezeigt werden, dass viele neurologische Störungen und neurodegenerative Erkrankungen mit Fehlfunktionen in den Mitochondrien einhergehen. Deshalb wird der Schutz von Mitochondrien zunehmend als eine Strategie zur wirkungsvollen Bekämpfung und Behandlung dieser Erkrankungen verfolgt.

Zwei Proteine, die möglicherweise in der Entstehung und Progression neurodegenerativer Erkrankungen eine Rolle spielen, sind p53 und die Isoform 1 der HIF-prolyl-4-hydroxylasen (PHD). Das Ziel der vorliegenden Arbeit war daher, die Funktion dieser beiden Proteine im neuronalen Zelltod näher zu untersuchen und ihr Potenzial als neue Zielstrukturen in der Neuroprotektion zu erforschen. Zu diesem Zweck wurde die murine, hippocampale Zelllinie HT-22 verwendet, die ein etabliertes Modellsystem zur Erforschung des Caspase-unabhängigen intrinsischen Zelltods darstellt, der in diesem Modell durch die extrazelluläre Zugabe von Glutamat hervorgerufen wird. Diese Art des Zelltods wird auch als Oxytose bezeichnet. Des Weiteren wurde die Substanz Erastin eingesetzt, um den Tod der HT-22 Zellen nach dem Muster der Ferroptose herbeizuführen.

Im ersten Teil der Arbeit wurden die Effekte einer verminderten Expression von p53, die durch den Einsatz einer p53 siRNA erreicht wurde, auf den neuronalen Zelltod untersucht. Eine Reduktion der p53-Spiegel konnte den durch Glutamat provozierten Tod der HT-22 Zellen um circa zwei Stunden verzögern. Dagegen war die Reduktion der p53 Proteinmenge nicht in der Lage, die Oxidation von Lipiden und die sich anschließende Schädigung der Mitochondrien zu verhindern. Diese zeigte sich in einem erhöhten Fragmentierungsgrad der Mitochondrien, einer vermehrten

Produktion von ROS in den Mitochondrien sowie einer Depolarisation der mitochondrialen Membran. Diese Depolarisation zog einen Abfall der ATP-Spiegel nach sich. Die Beeinträchtigung der Mitochondrienfunktion wurde jedoch nicht durch einen direkten Einfluss von p53 auf die Mitochondrien ausgelöst, da weder für p53 noch für phosphoryliertes p53 eine Translokation zu den Mitochondrien nach Glutamatbehandlung gezeigt werden konnte. Die Durchführung eines Reporter-Assays offenbarte weiterhin eine Reduktion der transkriptionellen Aktivität von p53 in Zellen, die zuvor mit p53 siRNA behandelt worden waren.

Im Gegensatz dazu zeigte der p53-Inhibitor PFTα eine ausgeprägte Protektion der HT-22 Zellen gegenüber Glutamat und war auch in der Lage, die Struktur und Funktion der Mitochondrien zu erhalten, was sich in einem tubulären Erscheinungsbild der Mitochondrien, einer verminderten Produktion von ROS, einem intakten Membranpotenzial und physiologischen ATP-Spiegeln zeigte. Außerdem verhinderte PFTα den Tod der HT-22 Zellen, wenn es bis zu vier Stunden nach dem Beginn der Glutamatbehandlung appliziert wurde. Darüber hinaus war PFTα sogar im Stande, HT-22 Zellen mit reduzierten p53-Spiegeln vor der Glutamatschädigung zu schützen.

Diese Ergebnisse bestätigen das große neuroprotektive Potenzial von PFTα und deuten darauf hin, dass der Effekt von PFTα vor oder zum Zeitpunkt der Mitochondrienschädigung zum Tragen kommt. Weiterhin scheinen andere durch PFTα hervorgerufene Effekte unabhängig von der p53-Blockade zum Schutz der Neurone beizutragen.

Im zweiten Teil der Arbeit wurde der Einfluss von PHDs auf den neuronalen Zelltod untersucht. Dafür wurden die verschiedenen PHD-Inhibitoren DFO, DHB, CPO und Oxyquinoline sowie zwei siRNA Sequenzen zur Verminderung der Expression von PHD1 verwendet. Sowohl die pharmakologischen Inhibitoren als auch die gentechnische Reduktion der PHD1-Spiegel schützten die HT-22 Zellen vor dem Zelltod durch Glutamatschädigung sowie der daraus folgenden Lipidperoxidation und Schädigung der Mitochondrien. Die Funktionalität der Mitochondrien wurde durch Untersuchungen der mitochondrialen Atmung sowie des Membranpotenzials und der ATP-Spiegel nachgewiesen. Außerdem führten beide Ansätze zur Hemmung der PHDs zu einer verminderten Produktion von ROS in den Mitochondrien und verhinderten die durch oxidativen Stress hervorgerufene Fragmentierung der Mitochondrien. Auch wenn die Effekte der PHD1 siRNA signifikant geringer waren als

die der pharmakologischen Inhibitoren, deuten diese Ergebnisse insgesamt darauf hin, dass sowohl die selektive Hemmung der PHD1 Expression als auch die pharmakologische Inhibition aller PHD Isoformen zu einem Schutz der Mitochondrien und damit zur Neuroprotektion beitragen.

Um den Wirkungsmechanismus von Oxyquinoline aufzuklären, wurde die Expression und Regulation von ATF4 näher untersucht, da frühere Arbeiten gezeigt haben, dass PHDs über eine Interaktion mit ATF4 Zelltodmechanismen beeinflussen können. Messungen der Proteinexpression nach Oxyquinoline-Behandlung zeigten, dass dieser PHD-Inhibitor den Abfall der ATF4-Spiegel nach der Glutamatschädigung verhindern konnte. Allerdings schützte Oxyquinoline auch solche Zellen, in denen die ATF4 Expression durch siRNA blockiert war. Daher wurde die schützende Wirkung von Oxyquinoline offenbar nicht allein über ATF4 vermittelt und der zugrundeliegende Mechanismus der Protektion bedarf weiterer Untersuchungen.

In einem letzten Schritt wurde das Konzept der PHD-Inhibition auch im Modell der Ferroptose überprüft. Sowohl die pharmakologischen PHD-Inhibitoren als auch die verminderte Expression von PHD1 führten zu einer Protektion der HT-22 Zellen gegenüber Erastin, was die Bedeutung der PHDs für den neuronalen Zelltod unterstreicht und sie als vielversprechende Zielstruktur in der Behandlung neurodegenerativer Erkrankungen hervorhebt.

7 Abbreviations

Abbreviation	Full text
Aβ	Amyloid beta
ACD	Accidental cell death
ACSF2	Acyl-CoA synthethase family member 2
AD	Alzheimer's disease
AIF	Apoptosis inducing factor
ANT	Adenine nucleotide translocase
Apaf1	Apoptosis-protease activating factor 1
APP	Amyloid precursor protein
APS	Ammonium persulfate
ATF4	Activating transcription factor 4
ATM	Ataxia telangiectasia mutated
ATP	Adenosine triphosphate
AV/PI	FITC conjugated AnnexinV/ propidium iodide
BCA	Bicinchoninic acid assay
Bak	Bcl-2 antagonist/ killer 1
Bax	Bcl-2-associated x protein
Bcl-xL	B-cell lymphoma-extra large
Bid	BH3 interacting-domain death agonist
Bim	Bcl-2-like protein 11
CAD	Caspase-activated DNase

CDK	Cyclin-dependent kinase
Chk	Checkpoint kinase
CI	Cell index
CPO	Ciclopirox
CS	Citrate synthase
CuZnSOD	Copper and zinc superoxide dismutase
CypD	Cyclophilin D
Cyt c	Cytochrome c
DAPI	4′,6-diamidin-2-phenylindol
DCF	5,6-chloromethyl-2',7'-dichlorodihydrofluorescein diacetate acetyl ester
DD	Death domain
DED	Death effector domain
DHB	Ethyl-3,4-dihydroxybenzoate
DISC	Death inducing signalling complex
DFO	Deferoxamine
DMEM	Dulbecco’s modified eagle’s medium
DMSO	Dimethyl sulfoxide
DNA	Deoxyribonucleic acid
DRP1	Dynamin-related protein 1
DTNB	5,5’-dithio-bis-(2-nitrobenzoic acid)
DTT	Dithiothreitol
E. coli	Escherichia coli

EDTA	Ethylenediaminetetraacetic acid
EGLN	Egg-laying defective nine homolog
EGTA	Ethylene glycol tetraacetic acid
Endo G	Endonuclease G
EPO	Erythropeotin
ERK	Extracellular signal-related kinases
ETC	Electron transport chain
FACS	Fluorescent activated cell sorting
FADD	Fas-associated death domain
$FADH_2$	Reduced flavine adenine dinucleotide
FASL	FAS/CD95 ligand
FCCP	Carbonyl cyanide-4-(trifluoromethoxy)phenylhydrazone
FCS	Fetal calf serum
Fis1	Mitochondrial fission 1 protein
GAPDH	Glyceraldehyde 3-phosphate dehydrogenase
GpX4	Glutathione peroxidase-4
GSH	Glutathione
HD	Huntington’s disease
HCl	Hydrogen chloride
HIF	Hypoxia-inducible factor
H_2O_2	Hydrogen peroxide
IAP	Inhibitor of apoptosis
ICAD	Inhibitor of caspase-activated DNase

ICH	Intracerebral haemorrhage
IMM	Inner mitochondrial membrane
IMS	Mitochondrial intermembrane space
JNK	c-jun NH_2-terminal kinases
LOX	Lipoxygenase
LPS	Lipopolysaccharide
mA	Milli ampere
MAPK	Mitogen-activated protein kinase
MCAO	Middle cerebral artery occlusion
MDM2	Mouse double minute 2 homolog
MEF	Mouse embryo fibroblast
Mfn	Mitofusin
MMP	Mitochondrial membrane potential
MnSOD	Superoxide dismutase 2, mitochondrial
MOMP	Mitochondrial outer membrane permeabilization
mRNA	Messenger ribonucleic acid
mtDNA	Mitochondrial deoxyribonucleic acid
MTT	3-(4,5-Dimethylthiazol-2-yl)-2,5-diphenyltetrazolium bromide
NaCl	Sodium chloride
NADH	Reduced nicotinamide adenine nucleotide
NF-κB	Nuclear factor kappa-light-chain-enhancer of activated B-cells
NGF	Nerve growth factor

NO	Nitric oxide
OCR	Oxygen consumption rate
ODD	Oxygen degradation domain
OGDH	2-oxoglutarate dehydrogenase
Omi/HrtA2	High temperature acquired protein A2
OMM	Outer mitochondrial membrane
Opa1	Optic atrophy 1
Oxy	Oxyquinoline
PARP	Poly (ADP-ribose) polymerase
PBS	Phosphate buffered saline
PCD	Programmed cell death
PCR	Polymerase chain reaction
PD	Parkinson’s disease
PDH	Pyruvate dehydrogenase
PFA	Paraformaldehyde
PFTα	Pifithrin-α
PFTμ	Pifithrin-μ
PHD	HIF-prolyl-4-hydroxylase
PI	Propidium iodide
PS	Phospholipid phosphatidylserine
PTPC	Permeability transition pore complex
PUMA	p53 upregulated modulator of apoptosis
PVDF	Polyvinylidene fluoride

PVL	Periventricular leukomalacia
qs	Quantum satis
RCD	Regulated cell death
RIP	Ribonucleic acid
ROS	Reactive oxygen species
Rpb1	Large subunit of RNA polymerase II
rpm	Revolutions per minute
RT	Room temperature
RT-PCR	Reverse transcriptase polymerase chain reaction
SD	Standard deviation
SDS	Sodium dodecyl sulfate
SDS-PAGE	Sodium dodecyl sulfate polyacrylamide gel electrophoresis
siRNA	Small interfering RNA
SK2/K_{Ca}2.2	Small conductance calcium-activated potassium
Smac/DIABLO	Second mitochondria-derived activator of caspases
tBid	truncated Bid
TAE	TRIS-acetate-EDTA
TBI	Traumatic brain injury
TBS	Tris-buffered saline
TCA	Tricarboxylic acid
TE	Trypsin-EDTA
TEMED	Tetramethylethylenediamine
TIF-IA	Transcription initiation factor IA

TNB	5-thio-2-nitiorbenzoic acid
TNFα	Tumor necrosis factor α
TNFR1	TNFα receptor 1
TMRE	Tetramethylrhodamine ethyl ester
TRADD	TNF receptor-associated death domain
TRAIL	TNF-related apoptosis inducing ligand
TRAILR	TRAIL receptor
Tris	Tris(hydroxymethyl)aminomethane
V	Volt
VDAC	Voltage-dependent anion channel
VHL	von-Hippel-Lindau protein
VEGF	Vascular endothelial growth factor
X_c^-	Cystine/glutamate antiporter system
XIAP	X-chromosomal-linked inhibitor of apoptosis

8 References

1. Galluzzi, L. *et al.* Essential versus accessory aspects of cell death: recommendations of the NCCD 2015. *Cell death and differentiation* **22**, 58–73 (2015).
2. Fulda, S., Gorman, A.M., Hori, O. & Samali, A. Cellular stress responses: cell survival and cell death. *International journal of cell biology* **2010**, 214074 (2010).
3. Zimmermann, K.C., Bonzon, C. & Green, D.R. The machinery of programmed cell death. *Pharmacology & therapeutics* **92**, 57–70 (2001).
4. Culmsee, C. & Landshamer, S. Molecular insights into mechanisms of the cell death program: role in the progression of neurodegenerative disorders. *Curr Alzheimer Res* **3**, 269–283 (2006).
5. Mattson, M.P. Apoptosis in neurodegenerative disorders. *Nature reviews. Molecular cell biology* **1**, 120–129 (2000).
6. Fayaz, S.M., Suvanish Kumar, V S & Rajanikant, G.K. Necroptosis: who knew there were so many interesting ways to die? *CNS & neurological disorders drug targets* **13**, 42–51 (2014).
7. Dekkers, Martijn P J, Nikoletopoulou, V. & Barde, Y.-A. Cell biology in neuroscience: Death of developing neurons: new insights and implications for connectivity. *The Journal of cell biology* **203**, 385–393 (2013).
8. Galluzzi, L. *et al.* Molecular definitions of cell death subroutines: recommendations of the Nomenclature Committee on Cell Death 2012. *Cell death and differentiation* **19**, 107–120 (2012).
9. Kerr, J.F., Wyllie, A.H. & Currie, A.R. Apoptosis: a basic biological phenomenon with wide-ranging implications in tissue kinetics. *British journal of cancer* **26**, 239–257 (1972).
10. Elmore, S. Apoptosis: a review of programmed cell death. *Toxicologic pathology* **35**, 495–516 (2007).
11. Schulze-Osthoff, K., Ferrari, D., Los, M., Wesselborg, S. & Peter, M.E. Apoptosis signaling by death receptors. *Eur J Biochem* **254**, 439–459 (1998).
12. Wajant, H. The Fas signaling pathway: more than a paradigm. *Science (New York, N.Y.)* **296**, 1635–1636 (2002).
13. Hsu, H., Shu, H.B., Pan, M.G. & Goeddel, D.V. TRADD-TRAF2 and TRADD-FADD interactions define two distinct TNF receptor 1 signal transduction pathways. *Cell* **84**, 299–308 (1996).

14. Broughton, Brad R S, Reutens, D.C. & Sobey, C.G. Apoptotic mechanisms after cerebral ischemia. *Stroke; a journal of cerebral circulation* **40**, e331-9 (2009).
15. Asahi, M. *et al.* Expression of interleukin-1 beta converting enzyme gene family and bcl-2 gene family in the rat brain following permanent occlusion of the middle cerebral artery. *Journal of cerebral blood flow and metabolism : official journal of the International Society of Cerebral Blood Flow and Metabolism* **17**, 11–18 (1997).
16. Rami, A., Sims, J., Botez, G. & Winckler, J. Spatial resolution of phospholipid scramblase 1 (PLSCR1), caspase-3 activation and DNA-fragmentation in the human hippocampus after cerebral ischemia. *Neurochemistry international* **43**, 79–87 (2003).
17. Sakahira, H., Enari, M. & Nagata, S. Cleavage of CAD inhibitor in CAD activation and DNA degradation during apoptosis. *Nature* **391**, 96–99 (1998).
18. Kitazumi, I. & Tsukahara, M. Regulation of DNA fragmentation: the role of caspases and phosphorylation. *The FEBS journal* **278**, 427–441 (2011).
19. Li, H., Zhu, H., Xu, C.J. & Yuan, J. Cleavage of BID by caspase 8 mediates the mitochondrial damage in the Fas pathway of apoptosis. *Cell* **94**, 491–501 (1998).
20. Luo, X., Budihardjo, I., Zou, H., Slaughter, C. & Wang, X. Bid, a Bcl2 interacting protein, mediates cytochrome c release from mitochondria in response to activation of cell surface death receptors. *Cell* **94**, 481–490 (1998).
21. Stefanis, L. Caspase-dependent and -independent neuronal death: two distinct pathways to neuronal injury. *The Neuroscientist : a review journal bringing neurobiology, neurology and psychiatry* **11**, 50–62 (2005).
22. Mattson, M.P., Gleichmann, M. & Cheng, A. Mitochondria in neuroplasticity and neurological disorders. *Neuron* **60**, 748–766 (2008).
23. Guan, Q.-H., Pei, D.-S., Zong, Y.-Y., Xu, T.-L. & Zhang, G.-Y. Neuroprotection against ischemic brain injury by a small peptide inhibitor of c-Jun N-terminal kinase (JNK) via nuclear and non-nuclear pathways. *Neuroscience* **139**, 609–627 (2006).
24. Jin, H.-O. *et al.* Up-regulation of Bak and Bim via JNK downstream pathway in the response to nitric oxide in human glioblastoma cells. *Journal of cellular physiology* **206**, 477–486 (2006).
25. Galluzzi, L., Blomgren, K. & Kroemer, G. Mitochondrial membrane permeabilization in neuronal injury. *Nat Rev Neurosci* **10**, 481–494 (2009).

26. Culmsee, C. & Plesnila, N. Targeting Bid to prevent programmed cell death in neurons. *Biochem. Soc. Trans.* **34**, 1334–1340 (2006).
27. Uo, T., Kinoshita, Y. & Morrison, R.S. Neurons exclusively express N-Bak, a BH3 domain-only Bak isoform that promotes neuronal apoptosis. *The Journal of biological chemistry* **280**, 9065–9073 (2005).
28. Kroemer, G., Galluzzi, L. & Brenner, C. Mitochondrial membrane permeabilization in cell death. *Physiological reviews* **87**, 99–163 (2007).
29. Sims, N.R. & Muyderman, H. Mitochondria, oxidative metabolism and cell death in stroke. *Biochimica et biophysica acta* **1802**, 80–91 (2010).
30. Pastorino, J.G. & Hoek, J.B. Regulation of hexokinase binding to VDAC. *Journal of bioenergetics and biomembranes* **40**, 171–182 (2008).
31. O'Gorman, E., Beutner, G., Wallimann, T. & Brdiczka, D. Differential effects of creatine depletion on the regulation of enzyme activities and on creatine-stimulated mitochondrial respiration in skeletal muscle, heart, and brain. *Biochimica et biophysica acta* **1276**, 161–170 (1996).
32. Giorgio, V. *et al.* Dimers of mitochondrial ATP synthase form the permeability transition pore. *Proceedings of the National Academy of Sciences of the United States of America* **110**, 5887–5892 (2013).
33. Bonora, M. *et al.* Role of the c subunit of the FO ATP synthase in mitochondrial permeability transition. *Cell cycle (Georgetown, Tex.)* **12**, 674–683 (2013).
34. Fernandez-Sanz, C. *et al.* Altered FoF1 ATP synthase and susceptibility to mitochondrial permeability transition pore during ischaemia and reperfusion in aging cardiomyocytes. *Thrombosis and haemostasis* **113** (2015).
35. Li, P. *et al.* Cytochrome c and dATP-dependent formation of Apaf-1/caspase-9 complex initiates an apoptotic protease cascade. *Cell* **91**, 479–489 (1997).
36. Zou, H., Henzel, W.J., Liu, X., Lutschg, A. & Wang, X. Apaf-1, a human protein homologous to C. elegans CED-4, participates in cytochrome c-dependent activation of caspase-3. *Cell* **90**, 405–413 (1997).
37. Verhagen, A.M., Coulson, E.J. & Vaux, D.L. Inhibitor of apoptosis proteins and their relatives: IAPs and other BIRPs. *Genome biology* **2**, REVIEWS3009 (2001).
38. Zhu, C. *et al.* Involvement of apoptosis-inducing factor in neuronal death after hypoxia-ischemia in the neonatal rat brain. *Journal of neurochemistry* **86**, 306–317 (2003).

39. Zhu, C. *et al.* Apoptosis-inducing factor is a major contributor to neuronal loss induced by neonatal cerebral hypoxia-ischemia. *Cell death and differentiation* **14**, 775–784 (2007).
40. Vande Walle, L. *et al.* Proteome-wide Identification of HtrA2/Omi Substrates. *Journal of proteome research* **6**, 1006–1015 (2007).
41. Murphy, T.H., Miyamoto, M., Sastre, A., Schnaar, R.L. & Coyle, J.T. Glutamate toxicity in a neuronal cell line involves inhibition of cystine transport leading to oxidative stress. *Neuron* **2**, 1547–1558 (1989).
42. Tan, S., Schubert, D. & Maher, P. Oxytosis: A novel form of programmed cell death. *Curr Top Med Chem* **1**, 497–506 (2001).
43. Landshamer, S. *et al.* Bid-induced release of AIF from mitochondria causes immediate neuronal cell death. *Cell Death Differ.* **15**, 1553–1563 (2008).
44. Fukui, M., Song, J.-H., Choi, J., Choi, H.J. & Zhu, B.T. Mechanism of glutamate-induced neurotoxicity in HT22 mouse hippocampal cells. *Eur. J. Pharmacol.* **617**, 1–11 (2009).
45. Sato, H., Tamba, M., Ishii, T. & Bannai, S. Cloning and expression of a plasma membrane cystine/glutamate exchange transporter composed of two distinct proteins. *The Journal of biological chemistry* **274**, 11455–11458 (1999).
46. Tan, S., Sagara, Y., Liu, Y., Maher, P. & Schubert, D. The regulation of reactive oxygen species production during programmed cell death. *J. Cell Biol.* **141**, 1423–1432 (1998).
47. Dringen, R. & Hirrlinger, J. Glutathione pathways in the brain. *Biological chemistry* **384**, 505–516 (2003).
48. Aoyama, K. & Nakaki, T. Impaired glutathione synthesis in neurodegeneration. *International journal of molecular sciences* **14**, 21021–21044 (2013).
49. Tobaben, S. *et al.* Bid-mediated mitochondrial damage is a key mechanism in glutamate-induced oxidative stress and AIF-dependent cell death in immortalized HT-22 hippocampal neurons. *Cell Death Differ.* **18**, 282–292 (2011).
50. Seiler, A. *et al.* Glutathione peroxidase 4 senses and translates oxidative stress into 12/15-lipoxygenase dependent- and AIF-mediated cell death. *Cell Metab.* **8**, 237–248 (2008).
51. Grohm, J. *et al.* Inhibition of Drp1 provides neuroprotection in vitro and in vivo. *Cell Death Differ.* **19**, 1446–1458 (2012).

52. Li, Y., Maher, P. & Schubert, D. Requirement for cGMP in nerve cell death caused by glutathione depletion. *The Journal of cell biology* **139**, 1317–1324 (1997).
53. Zhang, Y. & Bhavnani, B.R. Glutamate-induced apoptosis in neuronal cells is mediated via caspase-dependent and independent mechanisms involving calpain and caspase-3 proteases as well as apoptosis inducing factor (AIF) and this process is inhibited by equine estrogens. *BMC neuroscience* **7**, 49 (2006).
54. Polster, B.M., Basañez, G., Etxebarria, A., Hardwick, J.M. & Nicholls, D.G. Calpain I induces cleavage and release of apoptosis-inducing factor from isolated mitochondria. *The Journal of biological chemistry* **280**, 6447–6454 (2005).
55. Tan, S., Wood, M. & Maher, P. Oxidative stress induces a form of programmed cell death with characteristics of both apoptosis and necrosis in neuronal cells. *Journal of neurochemistry* **71**, 95–105 (1998).
56. Culmsee, C. *et al.* Apoptosis-inducing factor triggered by poly(ADP-ribose) polymerase and Bid mediates neuronal cell death after oxygen-glucose deprivation and focal cerebral ischemia. *J. Neurosci.* **25**, 10262–10272 (2005).
57. Stanciu, M. *et al.* Persistent activation of ERK contributes to glutamate-induced oxidative toxicity in a neuronal cell line and primary cortical neuron cultures. *J. Biol. Chem.* **275**, 12200–12206 (2000).
58. Satoh, T. *et al.* Neuroprotection by MAPK/ERK kinase inhibition with U0126 against oxidative stress in a mouse neuronal cell line and rat primary cultured cortical neurons. *Neurosci. Lett.* **288**, 163–166 (2000).
59. Suh, H.-W., Kang, S. & Kwon, K.-S. Curcumin attenuates glutamate-induced HT22 cell death by suppressing MAP kinase signaling. *Mol. Cell. Biochem.* **298**, 187–194 (2007).
60. Cardoso, A L C *et al.* siRNA delivery by a transferrin-associated lipid-based vector: a non-viral strategy to mediate gene silencing. *J Gene Med* **9**, 170–183 (2007).
61. Son, Y. *et al.* Mitogen-Activated Protein Kinases and Reactive Oxygen Species: How Can ROS Activate MAPK Pathways? *Journal of signal transduction* **2011**, 792639 (2011).
62. Barho, M.T. *et al.* N-acyl derivatives of 4-phenoxyaniline as neuroprotective agents. *ChemMedChem* **9**, 2260–2273 (2014).

63. Oppermann, S. *et al.* Novel N-phenyl-substituted thiazolidinediones protect neural cells against glutamate- and tBid-induced toxicity. *J. Pharmacol. Exp. Ther.* **350**, 273–289 (2014).
64. Öxler, E.-M., Dolga, A. & Culmsee, C. AIF depletion provides neuroprotection through a preconditioning effect. *Apoptosis* **17**, 1027–1038 (2012).
65. Behl, C., Hovey, L., Krajewski, S., Schubert, D. & Reed, J.C. BCL-2 prevents killing of neuronal cells by glutamate but not by amyloid beta protein. *Biochemical and biophysical research communications* **197**, 949–956 (1993).
66. Dolga, A.M. *et al.* Mitochondrial small conductance SK2 channels prevent glutamate-induced oxytosis and mitochondrial dysfunction. *The Journal of biological chemistry* **288**, 10792–10804 (2013).
67. Ratan, R.R., Murphy, T.H. & Baraban, J.M. Oxidative stress induces apoptosis in embryonic cortical neurons. *Journal of neurochemistry* **62**, 376–379 (1994).
68. Neitemeier, S., Ganjam, G.K., Diemert, S. & Culmsee, C. Pifithrin-α provides neuroprotective effects at the level of mitochondria independently of p53 inhibition. *Apoptosis : an international journal on programmed cell death* **19**, 1665–1677 (2014).
69. Reuther, C., Ganjam, G.K., Dolga, A.M. & Culmsee, C. The serine protease inhibitor TLCK attenuates intrinsic death pathways in neurons upstream of mitochondrial demise. *Apoptosis* (2014).
70. Kang, Y., Tiziani, S., Park, G., Kaul, M. & Paternostro, G. Cellular protection using Flt3 and PI3Kα inhibitors demonstrates multiple mechanisms of oxidative glutamate toxicity. *Nat Commun* **5**, 3672 (2014).
71. Grohm, J., Plesnila, N. & Culmsee, C. Bid mediates fission, membrane permeabilization and peri-nuclear accumulation of mitochondria as a prerequisite for oxidative neuronal cell death. *Brain Behav. Immun.* **24**, 831–838 (2010).
72. Pallast, S., Arai, K., Wang, X., Lo, E.H. & van Leyen, K. 12/15-Lipoxygenase targets neuronal mitochondria under oxidative stress. *J. Neurochem.* **111**, 882–889 (2009).
73. Vanden Berghe, T., Linkermann, A., Jouan-Lanhouet, S., Walczak, H. & Vandenabeele, P. Regulated necrosis: the expanding network of non-apoptotic cell death pathways. *Nature reviews. Molecular cell biology* **15**, 135–147 (2014).
74. Dixon, S.J. *et al.* Ferroptosis: an iron-dependent form of nonapoptotic cell death. *Cell* **149**, 1060–1072 (2012).

75. Dixon, S.J. & Stockwell, B.R. The role of iron and reactive oxygen species in cell death. *Nat. Chem. Biol.* **10**, 9–17 (2014).
76. Yagoda, N. *et al.* RAS-RAF-MEK-dependent oxidative cell death involving voltage-dependent anion channels. *Nature* **447**, 864–868 (2007).
77. Dixon, S.J. *et al.* Pharmacological inhibition of cystine-glutamate exchange induces endoplasmic reticulum stress and ferroptosis. *eLife* **3**, e02523 (2014).
78. Yang, W.S. *et al.* Regulation of ferroptotic cancer cell death by GPX4. *Cell* **156**, 317–331 (2014).
79. Yang, W.S. & Stockwell, B.R. Synthetic lethal screening identifies compounds activating iron-dependent, nonapoptotic cell death in oncogenic-RAS-harboring cancer cells. *Chemistry & biology* **15**, 234–245 (2008).
80. Wolpaw, A.J. *et al.* Modulatory profiling identifies mechanisms of small molecule-induced cell death. *Proceedings of the National Academy of Sciences of the United States of America* **108**, E771-80 (2011).
81. Skouta, R. *et al.* Ferrostatins inhibit oxidative lipid damage and cell death in diverse disease models. *J. Am. Chem. Soc.* **136**, 4551–4556 (2014).
82. Linkermann, A. *et al.* Synchronized renal tubular cell death involves ferroptosis. *Proceedings of the National Academy of Sciences of the United States of America* **111**, 16836–16841 (2014).
83. Friedmann Angeli, Jose Pedro *et al.* Inactivation of the ferroptosis regulator Gpx4 triggers acute renal failure in mice. *Nature cell biology* **16**, 1180–1191 (2014).
84. Toledo, F. & Wahl, G.M. Regulating the p53 pathway: in vitro hypotheses, in vivo veritas. *Nat. Rev. Cancer* **6**, 909–923 (2006).
85. Vousden, K.H. & Prives, C. Blinded by the Light: The Growing Complexity of p53. *Cell* **137**, 413–431 (2009).
86. Murray-Zmijewski, F., Lane, D.P. & Bourdon, J.-C. p53/p63/p73 isoforms: an orchestra of isoforms to harmonise cell differentiation and response to stress. *Cell death and differentiation* **13**, 962–972 (2006).
87. van Heemst, D., den Reijer, P M & Westendorp, R G J. Ageing or cancer: a review on the role of caretakers and gatekeepers. *European journal of cancer (Oxford, England : 1990)* **43**, 2144–2152 (2007).
88. Matoba, S. *et al.* p53 regulates mitochondrial respiration. *Science (New York, N.Y.)* **312**, 1650–1653 (2006).

89. Bensaad, K. *et al.* TIGAR, a p53-inducible regulator of glycolysis and apoptosis. *Cell* **126**, 107–120 (2006).
90. Bensaad, K., Cheung, E.C. & Vousden, K.H. Modulation of intracellular ROS levels by TIGAR controls autophagy. *The EMBO journal* **28**, 3015–3026 (2009).
91. Vousden, K.H. & Lane, D.P. p53 in health and disease. *Nature reviews. Molecular cell biology* **8**, 275–283 (2007).
92. Tomasevic, G., Shamloo, M., Israeli, D. & Wieloch, T. Activation of p53 and its target genes p21WAF1/Cip1 and PAG608/Wig-1 in ischemic preconditioning. *Molecular Brain Research* **70**, 304–313 (1999).
93. Culmsee, C. & Mattson, M.P. p53 in neuronal apoptosis. *Biochem. Biophys. Res. Commun.* **331**, 761–777 (2005).
94. Plesnila, N. *et al.* Delayed neuronal death after brain trauma involves p53-dependent inhibition of NF-kappaB transcriptional activity. *Cell Death Differ.* **14**, 1529–1541 (2007).
95. Checler, F. & Alves da Costa, Cristine. p53 in neurodegenerative diseases and brain cancers. *Pharmacol. Ther.* **142**, 99–113 (2014).
96. Culmsee, C. *et al.* A synthetic inhibitor of p53 protects neurons against death induced by ischemic and excitotoxic insults, and amyloid beta-peptide. *J. Neurochem.* **77**, 220–228 (2001).
97. Bae, B.-I. *et al.* p53 mediates cellular dysfunction and behavioral abnormalities in Huntington's disease. *Neuron* **47**, 29–41 (2005).
98. Culmsee, C. *et al.* Reciprocal inhibition of p53 and nuclear factor-kappaB transcriptional activities determines cell survival or death in neurons. *J. Neurosci.* **23**, 8586–8595 (2003).
99. Xiang, H. *et al.* Evidence for p53-mediated modulation of neuronal viability. *J. Neurosci.* **16**, 6753–6765 (1996).
100. Crumrine, R.C., Thomas, A.L. & Morgan, P.F. Attenuation of p53 expression protects against focal ischemic damage in transgenic mice. *J. Cereb. Blood Flow Metab.* **14**, 887–891 (1994).
101. Vaseva, A.V. *et al.* p53 opens the mitochondrial permeability transition pore to trigger necrosis. *Cell* **149**, 1536–1548 (2012).
102. Morrison, R.S., Kinoshita, Y., Johnson, M.D., Guo, W. & Garden, G.A. p53-dependent cell death signaling in neurons. *Neurochemical research* **28**, 15–27 (2003).

103. Keramaris, E., Hirao, A., Slack, R.S., Mak, T.W. & Park, D.S. Ataxia telangiectasia-mutated protein can regulate p53 and neuronal death independent of Chk2 in response to DNA damage. *The Journal of biological chemistry* **278**, 37782–37789 (2003).

104. Sancar, A., Lindsey-Boltz, L.A., Unsal-Kaçmaz, K. & Linn, S. Molecular mechanisms of mammalian DNA repair and the DNA damage checkpoints. *Annual review of biochemistry* **73**, 39–85 (2004).

105. Morris, E.J. *et al.* Cyclin-dependent kinases and P53 pathways are activated independently and mediate Bax activation in neurons after DNA damage. *The Journal of neuroscience : the official journal of the Society for Neuroscience* **21**, 5017–5026 (2001).

106. Mielke, K. & Herdegen, T. JNK and p38 stresskinases--degenerative effectors of signal-transduction-cascades in the nervous system. *Progress in neurobiology* **61**, 45–60 (2000).

107. Beckerman, R. & Prives, C. Transcriptional regulation by p53. *Cold Spring Harb Perspect Biol* **2**, a000935 (2010).

108. Xiang, H. *et al.* Bax involvement in p53-mediated neuronal cell death. *The Journal of neuroscience : the official journal of the Society for Neuroscience* **18**, 1363–1373 (1998).

109. Nakano, K. & Vousden, K.H. PUMA, a novel proapoptotic gene, is induced by p53. *Mol. Cell* **7**, 683–694 (2001).

110. Niizuma, K., Endo, H., Nito, C., Myer, D.J. & Chan, P.H. Potential role of PUMA in delayed death of hippocampal CA1 neurons after transient global cerebral ischemia. *Stroke* **40**, 618–625 (2009).

111. Fortin, A. *et al.* APAF1 is a key transcriptional target for p53 in the regulation of neuronal cell death. *The Journal of cell biology* **155**, 207–216 (2001).

112. Semont, A. *et al.* Involvement of p53 and Fas/CD95 in murine neural progenitor cell response to ionizing irradiation. *Oncogene* **23**, 8497–8508 (2004).

113. Miyashita, T., Harigai, M., Hanada, M. & Reed, J.C. Identification of a p53-dependent negative response element in the bcl-2 gene. *Cancer research* **54**, 3131–3135 (1994).

114. Haupt, Y., Rowan, S., Shaulian, E., Vousden, K.H. & Oren, M. Induction of apoptosis in HeLa cells by trans-activation-deficient p53. *Genes & development* **9**, 2170–2183 (1995).

115. Green, D.R. & Kroemer, G. Cytoplasmic functions of the tumour suppressor p53. *Nature* **458**, 1127–1130 (2009).

116. Moll, U.M., Wolff, S., Speidel, D. & Deppert, W. Transcription-independent pro-apoptotic functions of p53. *Current opinion in cell biology* **17**, 631–636 (2005).

117. Endo, H., Saito, A. & Chan, P.H. Mitochondrial translocation of p53 underlies the selective death of hippocampal CA1 neurons after global cerebral ischaemia. *Biochemical Society transactions* **34**, 1283–1286 (2006).

118. Endo, H., Kamada, H., Nito, C., Nishi, T. & Chan, P.H. Mitochondrial translocation of p53 mediates release of cytochrome c and hippocampal CA1 neuronal death after transient global cerebral ischemia in rats. *The Journal of neuroscience : the official journal of the Society for Neuroscience* **26**, 7974–7983 (2006).

119. Bonini, P. *et al.* Oxidative stress induces p53-mediated apoptosis in glia: p53 transcription-independent way to die. *Journal of neuroscience research* **75**, 83–95 (2004).

120. Strom, E. *et al.* Small-molecule inhibitor of p53 binding to mitochondria protects mice from gamma radiation. *Nat. Chem. Biol.* **2**, 474–479 (2006).

121. Nijboer, C.H. *et al.* Targeting the p53 pathway to protect the neonatal ischemic brain. *Ann. Neurol.* **70**, 255–264 (2011).

122. Gilman, C.P. *et al.* p53 is present in synapses where it mediates mitochondrial dysfunction and synaptic degeneration in response to DNA damage, and oxidative and excitotoxic insults. *Neuromolecular Med.* **3**, 159–172 (2003).

123. McBride, H.M., Neuspiel, M. & Wasiak, S. Mitochondria: more than just a powerhouse. *Current biology : CB* **16**, R551-60 (2006).

124. Wallace, D.C. A mitochondrial paradigm of metabolic and degenerative diseases, aging, and cancer: a dawn for evolutionary medicine. *Annual review of genetics* **39**, 359–407 (2005).

125. Galluzzi, L. *et al.* Mitochondrial liaisons of p53. *Antioxidants & redox signaling* **15**, 1691–1714 (2011).

126. Chan, D.C. Mitochondria: dynamic organelles in disease, aging, and development. *Cell* **125**, 1241–1252 (2006).

127. Chen, H. & Chan, D.C. Mitochondrial dynamics--fusion, fission, movement, and mitophagy--in neurodegenerative diseases. *Human molecular genetics* **18**, R169-76 (2009).

128. Chen, H., Chomyn, A. & Chan, D.C. Disruption of fusion results in mitochondrial heterogeneity and dysfunction. *The Journal of biological chemistry* **280**, 26185–26192 (2005).

129. Pich, S. *et al.* The Charcot-Marie-Tooth type 2A gene product, Mfn2, up-regulates fuel oxidation through expression of OXPHOS system. *Human molecular genetics* **14**, 1405–1415 (2005).

130. Lin, M.T. & Beal, M.F. Mitochondrial dysfunction and oxidative stress in neurodegenerative diseases. *Nature* **443**, 787–795 (2006).

131. Anandatheerthavarada, H.K., Biswas, G., Robin, M.-A. & Avadhani, N.G. Mitochondrial targeting and a novel transmembrane arrest of Alzheimer's amyloid precursor protein impairs mitochondrial function in neuronal cells. *The Journal of cell biology* **161**, 41–54 (2003).

132. Kawamoto, Y., Ito, H., Kobayashi, Y., Suzuki, Y. & Takahashi, R. Localization of HtrA2/Omi immunoreactivity in brains affected by Alzheimer's disease. *Neuroreport* **21**, 1121–1125 (2010).

133. Park, H.-J., Seong, Y.-M., Choi, J.-Y., Kang, S. & Rhim, H. Alzheimer's disease-associated amyloid beta interacts with the human serine protease HtrA2/Omi. *Neuroscience letters* **357**, 63–67 (2004).

134. Martin, L.J. *et al.* Parkinson's disease alpha-synuclein transgenic mice develop neuronal mitochondrial degeneration and cell death. *The Journal of neuroscience : the official journal of the Society for Neuroscience* **26**, 41–50 (2006).

135. Holmström, K.M. & Finkel, T. Cellular mechanisms and physiological consequences of redox-dependent signalling. *Nature reviews. Molecular cell biology* **15**, 411–421 (2014).

136. Ott, M., Gogvadze, V., Orrenius, S. & Zhivotovsky, B. Mitochondria, oxidative stress and cell death. *Apoptosis : an international journal on programmed cell death* **12**, 913–922 (2007).

137. Murphy, M.P. How mitochondria produce reactive oxygen species. *The Biochemical journal* **417**, 1–13 (2009).

138. Fukui, M. & Zhu, B.T. Mitochondrial superoxide dismutase SOD2, but not cytosolic SOD1, plays a critical role in protection against glutamate-induced oxidative stress and cell death in HT22 neuronal cells. *Free radical biology & medicine* **48**, 821–830 (2010).

139. Fleury, C., Mignotte, B. & Vayssière, J.-L. Mitochondrial reactive oxygen species in cell death signaling. *Biochimie* **84**, 131–141 (2002).

140. Martinou, J.-C. & Youle, R.J. Mitochondria in apoptosis: Bcl-2 family members and mitochondrial dynamics. *Developmental cell* **21**, 92–101 (2011).

141. Epstein, A.C. *et al.* C. elegans EGL-9 and mammalian homologs define a family of dioxygenases that regulate HIF by prolyl hydroxylation. *Cell* **107**, 43–54 (2001).

142. Speer, R.E. *et al.* Hypoxia-inducible factor prolyl hydroxylases as targets for neuroprotection by "antioxidant" metal chelators: From ferroptosis to stroke. *Free Radic. Biol. Med.* **62**, 26–36 (2013).

143. Rabinowitz, M.H. Inhibition of hypoxia-inducible factor prolyl hydroxylase domain oxygen sensors: tricking the body into mounting orchestrated survival and repair responses. *Journal of medicinal chemistry* **56**, 9369–9402 (2013).

144. Patel, S.A. & Simon, M.C. Biology of hypoxia-inducible factor-2alpha in development and disease. *Cell death and differentiation* **15**, 628–634 (2008).

145. Zaman, K. *et al.* Protection from oxidative stress-induced apoptosis in cortical neuronal cultures by iron chelators is associated with enhanced DNA binding of hypoxia-inducible factor-1 and ATF-1/CREB and increased expression of glycolytic enzymes, p21(waf1/cip1), and erythropoietin. *The Journal of neuroscience : the official journal of the Society for Neuroscience* **19**, 9821–9830 (1999).

146. Kim, J.-w., Tchernyshyov, I., Semenza, G.L. & Dang, C.V. HIF-1-mediated expression of pyruvate dehydrogenase kinase: a metabolic switch required for cellular adaptation to hypoxia. *Cell metabolism* **3**, 177–185 (2006).

147. Scortegagna, M. *et al.* HIF-2alpha regulates murine hematopoietic development in an erythropoietin-dependent manner. *Blood* **105**, 3133–3140 (2005).

148. Bruick, R.K. & McKnight, S.L. A conserved family of prolyl-4-hydroxylases that modify HIF. *Science (New York, N.Y.)* **294**, 1337–1340 (2001).

149. Siddiq, A., Aminova, L.R. & Ratan, R.R. Hypoxia inducible factor prolyl 4-hydroxylase enzymes: center stage in the battle against hypoxia, metabolic compromise and oxidative stress. *Neurochemical research* **32**, 931–946 (2007).

150. Berra, E. *et al.* HIF prolyl-hydroxylase 2 is the key oxygen sensor setting low steady-state levels of HIF-1alpha in normoxia. *The EMBO journal* **22**, 4082–4090 (2003).

151. Flamme, I. *et al.* Mimicking hypoxia to treat anemia: HIF-stabilizer BAY 85-3934 (Molidustat) stimulates erythropoietin production without hypertensive effects. *PloS one* **9**, e111838 (2014).

152. Smirnova, N.A. *et al.* Utilization of an in vivo reporter for high throughput identification of branched small molecule regulators of hypoxic adaptation. *Chemistry & biology* **17**, 380–391 (2010).

153. Nagel, S. *et al.* Neuroprotection by dimethyloxalylglycine following permanent and transient focal cerebral ischemia in rats. *Journal of cerebral blood flow and metabolism : official journal of the International Society of Cerebral Blood Flow and Metabolism* **31**, 132–143 (2011).

154. Ogle, M.E., Gu, X., Espinera, A.R. & Wei, L. Inhibition of prolyl hydroxylases by dimethyloxaloylglycine after stroke reduces ischemic brain injury and requires hypoxia inducible factor-1α. *Neurobiology of disease* **45**, 733–742 (2012).

155. Siddiq, A. *et al.* Hypoxia-inducible factor prolyl 4-hydroxylase inhibition. A target for neuroprotection in the central nervous system. *The Journal of biological chemistry* **280**, 41732–41743 (2005).

156. Wu, Y. *et al.* Neuroprotection of deferoxamine on rotenone-induced injury via accumulation of HIF-1 alpha and induction of autophagy in SH-SY5Y cells. *Neurochemistry international* **57**, 198–205 (2010).

157. Chinta, S.J., Rajagopalan, S., Ganesan, A. & Andersen, J.K. A possible novel anti-inflammatory mechanism for the pharmacological prolyl hydroxylase inhibitor 3,4-dihydroxybenzoate: implications for use as a therapeutic for Parkinson's disease. *Parkinson's disease* **2012**, 364684 (2012).

158. Niatsetskaya, Z. *et al.* HIF prolyl hydroxylase inhibitors prevent neuronal death induced by mitochondrial toxins: therapeutic implications for Huntington's disease and Alzheimer's disease. *Antioxidants & redox signaling* **12**, 435–443 (2010).

159. Ritchie, C.W. *et al.* Metal-protein attenuation with iodochlorhydroxyquin (clioquinol) targeting Abeta amyloid deposition and toxicity in Alzheimer disease: a pilot phase 2 clinical trial. *Archives of neurology* **60**, 1685–1691 (2003).

160. Siddiq, A. *et al.* Selective inhibition of hypoxia-inducible factor (HIF) prolyl-hydroxylase 1 mediates neuroprotection against normoxic oxidative death via HIF- and CREB-independent pathways. *J. Neurosci.* **29**, 8828–8838 (2009).

161. Li, D., Bai, T. & Brorson, J.R. Adaptation to moderate hypoxia protects cortical neurons against ischemia-reperfusion injury and excitotoxicity independently of HIF-1α. *Experimental neurology* **230**, 302–310 (2011).

162. Durán, R.V. *et al.* HIF-independent role of prolyl hydroxylases in the cellular response to amino acids. *Oncogene* **32**, 4549–4556 (2013).

163. Mikhaylova, O. *et al.* The von Hippel-Lindau tumor suppressor protein and Egl-9-Type proline hydroxylases regulate the large subunit of RNA polymerase II in response to oxidative stress. *Molecular and cellular biology* **28**, 2701–2717 (2008).

164. Zhang, Q. *et al.* Control of cyclin D1 and breast tumorigenesis by the EglN2 prolyl hydroxylase. *Cancer cell* **16**, 413–424 (2009).

165. Hiwatashi, Y. *et al.* PHD1 interacts with ATF4 and negatively regulates its transcriptional activity without prolyl hydroxylation. *Experimental cell research* **317**, 2789–2799 (2011).

166. Köditz, J. *et al.* Oxygen-dependent ATF-4 stability is mediated by the PHD3 oxygen sensor. *Blood* **110**, 3610–3617 (2007).

167. Masuoka, H.C. & Townes, T.M. Targeted disruption of the activating transcription factor 4 gene results in severe fetal anemia in mice. *Blood* **99**, 736–745 (2002).

168. Harding, H.P. *et al.* An integrated stress response regulates amino acid metabolism and resistance to oxidative stress. *Molecular cell* **11**, 619–633 (2003).

169. Lange, P.S. *et al.* ATF4 is an oxidative stress-inducible, prodeath transcription factor in neurons in vitro and in vivo. *The Journal of experimental medicine* **205**, 1227–1242 (2008).

170. Ord, D., Meerits, K. & Ord, T. TRB3 protects cells against the growth inhibitory and cytotoxic effect of ATF4. *Experimental cell research* **313**, 3556–3567 (2007).

171. Karuppagounder, S.S. & Ratan, R.R. Hypoxia-inducible factor prolyl hydroxylase inhibition: robust new target or another big bust for stroke therapeutics? *J. Cereb. Blood Flow Metab.* **32**, 1347–1361 (2012).

172. Lieb, M.E., Menzies, K., Moschella, M.C., Ni, R. & Taubman, M.B. Mammalian EGLN genes have distinct patterns of mRNA expression and regulation.

Biochemistry and cell biology = Biochimie et biologie cellulaire **80**, 421–426 (2002).

173. Metzen, E. *et al.* Intracellular localisation of human HIF-1 alpha hydroxylases: implications for oxygen sensing. *Journal of cell science* **116**, 1319–1326 (2003).

174. Tian, Y.-M., Mole, D.R., Ratcliffe, P.J. & Gleadle, J.M. Characterization of different isoforms of the HIF prolyl hydroxylase PHD1 generated by alternative initiation. *The Biochemical journal* **397**, 179–186 (2006).

175. Takeda, K. *et al.* Placental but not heart defects are associated with elevated hypoxia-inducible factor alpha levels in mice lacking prolyl hydroxylase domain protein 2. *Molecular and cellular biology* **26**, 8336–8346 (2006).

176. Aragonés, J. *et al.* Deficiency or inhibition of oxygen sensor Phd1 induces hypoxia tolerance by reprogramming basal metabolism. *Nature genetics* **40**, 170–180 (2008).

177. Chen, R.-L. *et al.* Roles of individual prolyl-4-hydroxylase isoforms in the first 24 hours following transient focal cerebral ischaemia: insights from genetically modified mice. *The Journal of physiology* **590**, 4079–4091 (2012).

178. Adluri, R.S. *et al.* Disruption of hypoxia-inducible transcription factor-prolyl hydroxylase domain-1 (PHD-1-/-) attenuates ex vivo myocardial ischemia/reperfusion injury through hypoxia-inducible factor-1α transcription factor and its target genes in mice. *Antioxidants & redox signaling* **15**, 1789–1797 (2011).

179. Schneider, M. *et al.* Loss or silencing of the PHD1 prolyl hydroxylase protects livers of mice against ischemia/reperfusion injury. *Gastroenterology* **138**, 1143-54.e1-2 (2010).

180. Ndubuizu, O.I., Chavez, J.C. & LaManna, J.C. Increased prolyl 4-hydroxylase expression and differential regulation of hypoxia-inducible factors in the aged rat brain. *American journal of physiology. Regulatory, integrative and comparative physiology* **297**, R158-65 (2009).

181. Appelhoff, R.J. *et al.* Differential function of the prolyl hydroxylases PHD1, PHD2, and PHD3 in the regulation of hypoxia-inducible factor. *The Journal of biological chemistry* **279**, 38458–38465 (2004).

182. Minamishima, Y.A. *et al.* Somatic inactivation of the PHD2 prolyl hydroxylase causes polycythemia and congestive heart failure. *Blood* **111**, 3236–3244 (2008).

183. Takeda, K. *et al.* Regulation of adult erythropoiesis by prolyl hydroxylase domain proteins. *Blood* **111**, 3229–3235 (2008).

184. Takeda, K., Cowan, A. & Fong, G.-H. Essential role for prolyl hydroxylase domain protein 2 in oxygen homeostasis of the adult vascular system. *Circulation* **116**, 774–781 (2007).

185. Natarajan, R., Salloum, F.N., Fisher, B.J., Kukreja, R.C. & Fowler, A.A. Hypoxia inducible factor-1 activation by prolyl 4-hydroxylase-2 gene silencing attenuates myocardial ischemia reperfusion injury. *Circulation research* **98**, 133–140 (2006).

186. Kunze, R. *et al.* Neuron-specific prolyl-4-hydroxylase domain 2 knockout reduces brain injury after transient cerebral ischemia. *Stroke; a journal of cerebral circulation* **43**, 2748–2756 (2012).

187. Rohrbach, S., Simm, A., Pregla, R., Franke, C. & Katschinski, D.M. Age-dependent increase of prolyl-4-hydroxylase domain (PHD) 3 expression in human and mouse heart. *Biogerontology* **6**, 165–171 (2005).

188. Cervera, A.M. *et al.* An alternatively spliced transcript of the PHD3 gene retains prolyl hydroxylase activity. *Cancer letters* **233**, 131–138 (2006).

189. Bishop, T. *et al.* Abnormal sympathoadrenal development and systemic hypotension in PHD3-/- mice. *Molecular and cellular biology* **28**, 3386–3400 (2008).

190. Xie, L. *et al.* Depletion of PHD3 protects heart from ischemia/reperfusion injury by inhibiting cardiomyocyte apoptosis. *Journal of molecular and cellular cardiology* **80C**, 156–165 (2015).

191. Oriowo, B. *et al.* Targeted gene deletion of prolyl hydroxylase domain protein 3 triggers angiogenesis and preserves cardiac function by stabilizing hypoxia inducible factor 1 alpha following myocardial infarction. *Current pharmaceutical design* **20**, 1305–1310 (2014).

192. Straub, J.A., Lipscomb, E.A., Yoshida, E.S. & Freeman, R.S. Induction of SM-20 in PC12 cells leads to increased cytochrome c levels, accumulation of cytochrome c in the cytosol, and caspase-dependent cell death. *Journal of neurochemistry* **85**, 318–328 (2003).

193. Lipscomb, E.A., Sarmiere, P.D. & Freeman, R.S. SM-20 is a novel mitochondrial protein that causes caspase-dependent cell death in nerve growth

factor-dependent neurons. *The Journal of biological chemistry* **276**, 5085–5092 (2001).

194. Schlisio, S. *et al.* The kinesin KIF1Bbeta acts downstream from EglN3 to induce apoptosis and is a potential 1p36 tumor suppressor. *Genes & development* **22**, 884–893 (2008).

195. Morimoto, B.H. & Koshland, D.E. Excitatory amino acid uptake and N-methyl-D-aspartate-mediated secretion in a neural cell line. *Proc. Natl. Acad. Sci. U.S.A.* **87**, 3518–3521 (1990).

196. Davis, J.B. & Maher, P. Protein kinase C activation inhibits glutamate-induced cytotoxicity in a neuronal cell line. *Brain research* **652**, 169–173 (1994).

197. Maher, P. & Davis, J.B. The role of monoamine metabolism in oxidative glutamate toxicity. *The Journal of neuroscience : the official journal of the Society for Neuroscience* **16**, 6394–6401 (1996).

198. Mattson, M.P. Modification of ion homeostasis by lipid peroxidation: roles in neuronal degeneration and adaptive plasticity. *Trends Neurosci.* **21**, 53–57 (1998).

199. Berridge, M.V., Tan, A.S., McCoy, K.D. & RUI WANG. BIOCHEMICA_96_4_p14-19.

200. Diemert, S. *et al.* Impedance measurement for real time detection of neuronal cell death. *J. Neurosci. Methods* **203**, 69–77 (2012).

201. Schutte, B., Nuydens, R., Geerts, H. & Ramaekers, F. Annexin V binding assay as a tool to measure apoptosis in differentiated neuronal cells. *Journal of Neuroscience Methods* **86**, 63–69 (1998).

202. Hermeking, H. *et al.* 14-3-3 sigma is a p53-regulated inhibitor of G2/M progression. *Mol. Cell* **1**, 3–11 (1997).

203. Galluzzi, L., Kepp, O., Krautwald, S., Kroemer, G. & Linkermann, A. Molecular mechanisms of regulated necrosis. *Semin. Cell Dev. Biol.* (2014).

204. Rieker, C. *et al.* Nucleolar disruption in dopaminergic neurons leads to oxidative damage and parkinsonism through repression of mammalian target of rapamycin signaling. *J. Neurosci.* **31**, 453–460 (2011).

205. Yonekura, I., Takai, K., Asai, A., Kawahara, N. & Kirino, T. p53 potentiates hippocampal neuronal death caused by global ischemia. *J. Cereb. Blood Flow Metab.* **26**, 1332–1340 (2006).

206. Kreiner, G. *et al.* A neuroprotective phase precedes striatal degeneration upon nucleolar stress. *Cell Death Differ.* **20**, 1455–1464 (2013).

207. Komarov, P.G. *et al.* A chemical inhibitor of p53 that protects mice from the side effects of cancer therapy. *Science* **285**, 1733–1737 (1999).

208. Rocha, S., Campbell, K.J., Roche, K.C. & Perkins, N.D. The p53-inhibitor pifithrin-alpha inhibits firefly luciferase activity in vivo and in vitro. *BMC Mol. Biol.* **4**, 9 (2003).

209. Diemert, S. *The role of p53 and CYLD in mitochondrial death pathways and mechanisms of neuronal necroptosis.* Dissertation (Marburg, 2011).

210. Racay, P., Tatarkova, Z., Drgova, A., Kaplan, P. & Dobrota, D. Effect of ischemic preconditioning on mitochondrial dysfunction and mitochondrial p53 translocation after transient global cerebral ischemia in rats. *Neurochemical research* **32**, 1823–1832 (2007).

211. Vousden, K.H. p53: death star. *Cell* **103**, 691–694 (2000).

212. Hoagland, M.S., Hoagland, E.M. & Swanson, H.I. The p53 inhibitor pifithrin-alpha is a potent agonist of the aryl hydrocarbon receptor. *J. Pharmacol. Exp. Ther.* **314**, 603–610 (2005).

213. Komarova, E.A. *et al.* p53 inhibitor pifithrin alpha can suppress heat shock and glucocorticoid signaling pathways. *J. Biol. Chem.* **278**, 15465–15468 (2003).

214. Kim, E.Y. *et al.* Proteomic analysis of oxidative stress-induced neuronal cell death by using two-dimensional fluorescence difference gel electrophoresis. *Int. J. Mol. Med.* **26**, 829–835 (2010).

215. Li, Z. *et al.* ROS leads to MnSOD upregulation through ERK2 translocation and p53 activation in selenite-induced apoptosis of NB4 cells. *FEBS letters* **584**, 2291–2297 (2010).

216. Lee, D.W. *et al.* Inhibition of prolyl hydroxylase protects against 1-methyl-4-phenyl-1,2,3,6-tetrahydropyridine-induced neurotoxicity: model for the potential involvement of the hypoxia-inducible factor pathway in Parkinson disease. *The Journal of biological chemistry* **284**, 29065–29076 (2009).

217. Lee, S. *et al.* Neuronal apoptosis linked to EglN3 prolyl hydroxylase and familial pheochromocytoma genes: developmental culling and cancer. *Cancer cell* **8**, 155–167 (2005).

218. Lewerenz, J. *et al.* Mutation of ATF4 mediates resistance of neuronal cell lines against oxidative stress by inducing xCT expression. *Cell Death Differ* **19**, 847–858 (2011).

219. Yukawa, K., Tanaka, T., Tsuji, S. & Akira, S. Regulation of transcription factor C/ATF by the cAMP signal activation in hippocampal neurons, and molecular interaction of C/ATF with signal integrator CBP/p300. *Brain research. Molecular brain research* **69**, 124–134 (1999).

220. Lewerenz, J. & Maher, P. Basal Levels of eIF2 Phosphorylation Determine Cellular Antioxidant Status by Regulating ATF4 and xCT Expression. *Journal of Biological Chemistry* **284**, 1106–1115 (2009).

221. Henke, N. *et al.* The plasma membrane channel ORAI1 mediates detrimental calcium influx caused by endogenous oxidative stress. *Cell death & disease* **4**, e470 (2013).

222. Liu, Y., Fiskum, G. & Schubert, D. Generation of reactive oxygen species by the mitochondrial electron transport chain. *Journal of neurochemistry* **80**, 780–787 (2002).

223. Pfeiffer, A. *et al.* Mitochondrial function and energy metabolism in neuronal HT22 cells resistant to oxidative stress. *British journal of pharmacology* **171**, 2147–2158 (2014).

224. Yin, X.-M. Bid, a BH3-only multi-functional molecule, is at the cross road of life and death. *Gene* **369**, 7–19 (2006).

225. Grohm, J. *Molecular regulation of mitochondrial dynamics by dynamin-related protein 1 (Drp1) and Bid in model systems of neuronal cell death.* Dissertation (Marburg, 2011).

226. Wang, D.B., Kinoshita, C., Kinoshita, Y. & Morrison, R.S. p53 and mitochondrial function in neurons. *Biochim. Biophys. Acta* (2014).

227. Vousden, K.H. & Vande Woude, G F. The ins and outs of p53. *Nature cell biology* **2**, E178-80 (2000).

228. Steckley, D. *et al.* Puma is a dominant regulator of oxidative stress induced Bax activation and neuronal apoptosis. *The Journal of neuroscience : the official journal of the Society for Neuroscience* **27**, 12989–12999 (2007).

229. Engel, T. *et al.* Reduced hippocampal damage and epileptic seizures after status epilepticus in mice lacking proapoptotic Puma. *FASEB J.* **24**, 853–861 (2010).

230. Stambolsky, P. *et al.* Regulation of AIF expression by p53. *Cell death and differentiation* **13**, 2140–2149 (2006).

231. Guo, X. *et al.* Inhibition of mitochondrial fragmentation diminishes Huntington's disease-associated neurodegeneration. *The Journal of clinical investigation* **123**, 5371–5388 (2013).

232. Sax, J.K. *et al.* BID regulation by p53 contributes to chemosensitivity. *Nature cell biology* **4**, 842–849 (2002).

233. Yu, J., Wang, Z., Kinzler, K.W., Vogelstein, B. & Zhang, L. PUMA mediates the apoptotic response to p53 in colorectal cancer cells. *Proc. Natl. Acad. Sci. U.S.A.* **100**, 1931–1936 (2003).

234. Yu, J. & Zhang, L. The transcriptional targets of p53 in apoptosis control. *Biochem. Biophys. Res. Commun.* **331**, 851–858 (2005).

235. Leker, R.R., Aharonowiz, M., Greig, N.H. & Ovadia, H. The role of p53-induced apoptosis in cerebral ischemia: effects of the p53 inhibitor pifithrin alpha. *Exp. Neurol.* **187**, 478–486 (2004).

236. Kelly, K.J. P53 Mediates the Apoptotic Response to GTP Depletion after Renal Ischemia-Reperfusion: Protective Role of a p53 Inhibitor. *Journal of the American Society of Nephrology* **14**, 128–138 (2003).

237. Murphy, Patrick J M *et al.* Pifithrin-alpha inhibits p53 signaling after interaction of the tumor suppressor protein with hsp90 and its nuclear translocation. *J. Biol. Chem.* **279**, 30195–30201 (2004).

238. Sohn, D. *et al.* Pifithrin-α protects against DNA damage-induced apoptosis downstream of mitochondria independent of p53. *Cell Death Differ* **16**, 869–878 (2009).

239. Ali, S.H. & DeCaprio, J.A. Cellular transformation by SV40 large T antigen: interaction with host proteins. *Seminars in cancer biology* **11**, 15–23 (2001).

240. Chou, J., Greig, N.H., Reiner, D., Hoffer, B.J. & Wang, Y. Enhanced survival of dopaminergic neuronal transplants in hemiparkinsonian rats by the p53 inactivator PFT-α. *Cell Transplant* **20**, 1351–1359 (2011).

241. Zhu, X. *et al.* Novel p53 Inactivators with Neuroprotective Action: Syntheses and Pharmacological Evaluation of 2-Imino-2,3,4,5,6,7-hexahydrobenzothiazole and 2-Imino-2,3,4,5,6,7-hexahydrobenzoxazole Derivatives ⊥. *J. Med. Chem.* **45**, 5090–5097 (2002).

242. Duan, W. *et al.* p53 inhibitors preserve dopamine neurons and motor function in experimental parkinsonism. *Ann. Neurol.* **52**, 597–606 (2002).

243. Yang, L.-Y. *et al.* Post-trauma administration of the pifithrin-α oxygen analog improves histological and functional outcomes after experimental traumatic brain injury. *Experimental neurology* **269**, 56–66 (2015).

244. Mendjargal, A. *et al.* Pifithrin-α, a pharmacological inhibitor of p53, downregulates lipopolysaccharide-induced nitric oxide production via impairment of the MyD88-independent pathway. *Int. Immunopharmacol.* **15**, 671–678 (2013).

245. Kim, G.W., Kondo, T., Noshita, N. & Chan, P.H. Manganese superoxide dismutase deficiency exacerbates cerebral infarction after focal cerebral ischemia/reperfusion in mice: implications for the production and role of superoxide radicals. *Stroke; a journal of cerebral circulation* **33**, 809–815 (2002).

246. Copin, J.C., Gasche, Y. & Chan, P.H. Overexpression of copper/zinc superoxide dismutase does not prevent neonatal lethality in mutant mice that lack manganese superoxide dismutase. *Free radical biology & medicine* **28**, 1571–1576 (2000).

247. Morrison, R.S. *et al.* Loss of the p53 tumor suppressor gene protects neurons from kainate-induced cell death. *The Journal of neuroscience : the official journal of the Society for Neuroscience* **16**, 1337–1345 (1996).

248. Jansson, M. *et al.* Arginine methylation regulates the p53 response. *Nat. Cell Biol.* **10**, 1431–1439 (2008).

249. Schödel, J. *et al.* HIF-prolyl hydroxylases in the rat kidney: physiologic expression patterns and regulation in acute kidney injury. *The American journal of pathology* **174**, 1663–1674 (2009).

250. Wottawa, M., Köditz, J. & Katschinski, D.M. Normoxic destabilization of ATF-4 depends on proteasomal degradation. *Acta physiologica (Oxford, England)* **198**, 457–463 (2010).

251. Tan, S., Somia, N., Maher, P. & Schubert, D. Regulation of antioxidant metabolism by translation initiation factor 2alpha. *The Journal of cell biology* **152**, 997–1006 (2001).

252. Ameri, K. & Harris, A.L. Activating transcription factor 4. *The international journal of biochemistry & cell biology* **40**, 14–21 (2008).

253. Andersen, H.H., Johnsen, K.B. & Moos, T. Iron deposits in the chronically inflamed central nervous system and contributes to neurodegeneration. *Cellular and molecular life sciences : CMLS* **71**, 1607–1622 (2014).

254. Laino, V. *Bid links ferroptosis to mitochondrial demise and intrinsic pathways of cell death.* Bachelor thesis (Perugia, 2014).

9 Publications

9.1 Original papers

Neitemeier S, Ganjam GK, Diemert S, Culmsee C: Pifithrin-α provides neuroprotective effects at the level of mitochondria independently of p53 inhibition, Apoptosis, 19: 1665-1677, 2014

Karuppagounder S, Alim I, Khim S, Bourassa M, Sleiman S, John R, Thinnes C, Yeh T, Demetriades M, **Neitemeier S**, Cruz D, Gazaryan I, Killilea D, Morgenstern L, Xi G, Keep R, Schallert T, Tappero R, Zhong J, Cho S, Maxfiel F, Holman T, Culmsee C, Fong G, Cave J, Schofield C, Colbourne F, Coppola G, Ratan R: Adaptaquin is an inhibitor of oxygen-sensing prolyl-hydroxylase domain enzymes that abrogates ATF4-dependent death and improves outcomes from brain hemorrhage, submitted

Neitemeier S[#], Oppermann S[#], Laino V[#], Jelinek A, Ganjam GK, Dolga AM, Culmsee C: Bid links ferroptosis to mitochondrial cell death pathways in neurons, submitted

[#] contributed equally

9.2 Books

Dolga AM, Oppermann S, Richter M, Honrath B, **Neitemeier S**, Jelinek A, Ganjam GK, Culmsee C: 'Molecular mechanisms underlying oxytosis' in 'Apoptosis and Beyond: the way cells die, Springer (submitted)

9.3 Poster presentations

2014

Neitemeier S, Dolga AM, Karuppagounder S, Ratan R, Culmsee C: Inhibitors of HIF-proly-4-hydroxylases (HIF-PHD) mediate mitochondrial protection and prevent oxytosis in neuronal cells. Society for Neuroscience Annual Meeting, Neuroscience 2014, Washington, USA, 15.-19.11.2014

Ganjam GK, Dolga AM, **Neitemeier S**, Bolte K, Höllerhage M, Oertel WE, Hoeglinger GU, Culmsee C: Caspase inhibition mitigates alpha synuclein cytotoxicity and mitochondrial demise in human dopaminergic neurons. Society for Neuroscience Annual Meeting, Neuroscience 2014, Washington, USA, 15.-19.11.2014

Neitemeier S, Diemert S, Ganjam GK, Culmsee C: Sustained neuroprotective effects after pharmacological inhibition of p53 compared to siRNA-mediated p53 silencing. DPhG Jahrestagung 2014, Frankfurt, Germany, 24.-26.09.2014

Neitemeier S, Laino V, Oppermann S, Ganjam GK, Dolga AM, Culmsee C: Bid links ferroptosis to mitochondrial cell death pathways in neurons. DPhG Jahrestagung 2014, Frankfurt, Germany, 24.-26.09.2014

Ganjam GK, Dolga AM, **Neitemeier S**, de Andrade A, Bolte K, Oertel W, Höglinger GU, Culmsee C: Human dopaminergic neurons as a model system for Parkinson's disease. 8th International Symposium on Neuroprotection and Neurorepair, Magdeburg, Germany, 09.-12.04.2014

2013

Dolga AM, de Andrade A, **Neitemeier S**, Ganjam GK, Höglinger G, Culmsee C: Protective effects of SK/K_{Ca}2 channel activators in human dopaminergic neurons. 11th International Conference on Alzheimer's and Parkinson's Diseases, Florence, Italy, 06.-10.03.2013

Neitemeier S, Diemert S, Ganjam GK, Culmsee C: Neuroprotective effects through inhibition of p53. Tag der Wissenschaft, Marburg, Germany, 22.02.2013

10 Danksagung

Die Danksagung enthält persönliche Angaben und ist nicht Bestandteil der elektronischen Ausgabe.

11 Curriculum vitae

Der CV enthält persönliche Angaben und ist nicht Bestandteil der elektronischen Ausgabe.